THE MESSENGER

EL MENSAJERO

ESO

Munich

La Silla
La Serena
Santiago

No. 38—December 1984

Visit of STC to Possible Sites for the VLT in Northern Chile

D. Enard, ESO

The STC (Scientific Technical Committee) met at La Silla the 8th and 9th of October. Following the meeting, a 3-day-long trip to northern Chile brought the STC members (Fig. 1) to and above a few sites which have been picked up as potentially interesting spots by A. Ardeberg during his exploratory survey of 1983/84.

One of the most promising sites is Cerro Paranal, located at about 150 km south of Antofagasta and 15 km from the coast (Fig. 2). The elevation is 2,650 m. This site is attractive because of its relatively easy access, its dryness and photometric quality. Its proximity to the coast raises hope that the atmosphere is little disturbed by neighbouring mountains and that consequently seeing is excellent. As noted by a few STC members, the site suffers from its relative narrowness and although the space available would be quite sufficient for the VLT, there would be little space for other telescopes. Other summits in the neighbourhood could however be used.

Another close-by mountain, Cerro Armazonas, 3,100 m high, has also been visited. It is much larger than Paranal but, further inland by about 22 km, it may not be as good as Paranal, though only an objective comparison could ascertain this.

The region close to the Bolivian border, north-east of San Pedro d'Atacama, is rich of very high elevation volcanos; a 3-hour ride from San Pedro brought courageous STC members up to one of the few accessible volcanos, the Apogado at 5,650 m elevation. As shown in Fig. 1, (some) STC members felt still very comfortable, although even slight efforts were painfully experienced. Locating an observatory at such an elevation would probably be quite adventurous, but the fundamental problem remains the determination of the value of such sites with respect to La Silla and other excellent sites such as Mauna Kea.

There are many sites in Chile which, with elevations of about 4,000 m, would represent a good compromise between the desire to go as high as possible and the necessity to offer bearable working conditions. Experience at Hawaii suggests that 4,200 m is still acceptable from the human point of view. Such sites can be found in the vicinity of the high volcanos, in the central chain west of San Pedro, and also east of La Silla. None of those mountains appears completely isolated and access is rather difficult, but they would probably deserve attention, especially if the other lower elevation sites would prove to be unsatisfactory either from a seeing or humidity point of view.

After the completion of the initial exploratory survey, started in 1983 by Arne Ardeberg, a larger scale programme of investigation is being defined.

A dedicated working group composed of European experts in the field has been set up and will issue recommendations. Automatic meteorologic stations have already been installed at Paranal and at La Silla; a third station will be installed at one

Fig. 1: *Pierre Charvin and Gustav Tammann looking still very comfortable at Volcano Apagado at 5650 m altitude. This volcano is one of the very few high summits easily accessible by car.*

Fig. 2: *Aerial view of Cerro Paranal. The elevation is close to 2,700 m and the coast is only at 15 km distance. The white spot at the right hand of the summit is a shelter used by the two persons who monitor the site. The ridge is facing the prevailing wind direction and is about 400 m long.*

high elevation site in December. They will provide easy processable data that will complement the data collected since September 1983. A tethered balloon will also permit to measure the turbulence as well as other meteorologic parameters, between 0 and 800 m above sites. This equipment is easily transportable and should permit a preliminary investigation of the local contribution to seeing. More permanent equipment, such as fast thermal sensors, acoustic radars and seeing monitors, is planned for 1985 at Paranal (and La Silla in view of an absolute calibration with existing telescopes).

The importance of seeing for the new large telescope projects as well as the perspective for improving the image quality through adaptive correction have raised up considerable efforts by several groups to better understand the causes of seeing deterioration, and possibly find cures. Despite the difficulty of comparing quantitatively results obtained by different methods at different places, it is hoped that within 2 to 3 years an agreement could be reached on a few vital questions such as "what makes a site really good?", or "how important is it to set a telescope at a high site?". Those questions are indeed of paramount importance for the ESO VLT.

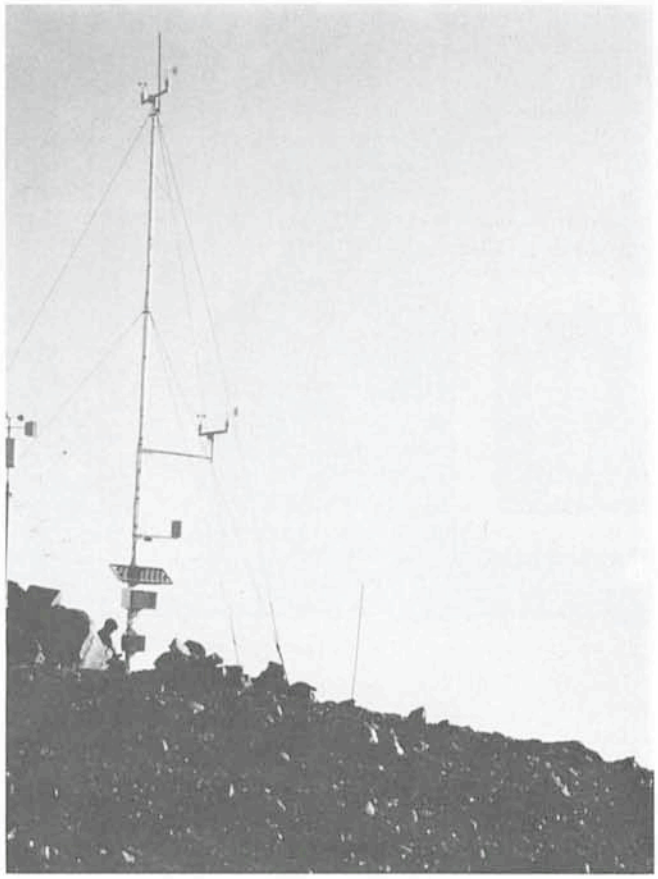

Fig. 3: *A new automatic meteorologic station at Cerro Paranal. Another station is installed at La Silla on a 30 m high mast. A third one will be installed on a high elevation site.*

Blue Compact Galaxies: Infants of the Universe?

N. Bergvall and K. Olofsson, Astronomical Observatory, Uppsala

1. What is a Blue Compact Galaxy?

Shortly after the completion of the 48″ Palomar Observatory Schmidt telescope in the beginning of the 1950s, a great number of stellar objects with fuzzy images were discovered on photographic plates obtained with the instrument. Subsequent spectroscopic observations revealed that these so-called "stars" actually were of extragalactic nature. In the 1960s Fritz Zwicky established this new fascinating type of objects as a separate morphological type, the "compact galaxies", CGs, defining them by their stellar appearance and by demanding that their surface luminosity should be brighter than 20^{m}arcsec^{-2}. Examples of three such cases, which we are presently investigating, are given in Fig. 1.

Historically it is interesting to note that while Zwicky thought that many compact galaxies represented one of the final stages in the life of a galaxy, closely related to what he called "OBJECT HADES", supposed to be "ultimate objects of greatest compactness", most work today is done on compact galaxies that have properties more typical of newly formed galaxies.

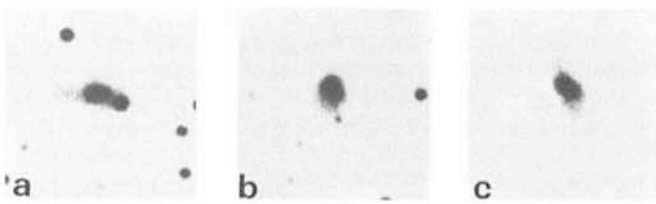

Fig. 1: *Three blue compact galaxies as seen on the ESO Quick Blue Survey plates obtained with the ESO 1 m Schmidt telescope: (a) ESO 338-IG04, (b) ESO 400-G43, (c) ESO 480-IG12 (1 arcmin = 17 mm). Top is north, east is to the left.*

At an early stage Zwicky realized that CGs as a group contained such diverse creatures as giant HII regions, quasars, and stripped-off dwarf ellipticals. This heterogeneous nature of the CGs is reflected in a colour-colour diagram, where they disperse rather much, as is shown in Fig. 2. Here we have plotted positions of 52 CGs in the southern hemisphere, all observed by the Uppsala group. The majority are gathered within the rectangular box where "normal galaxies" are found. However, some of these galaxies show colours that are unusually blue (up and towards the left in the diagram). By far the bluest in our sample is ESO 338–IG04 (B–V = –0.08, U–B = –0.62, extinction corrected). In fact, this object proves to be one of the bluest galaxies ever found.

Two decades ago little was known about these extreme cases. Therefore, a new branch of extragalactic astronomy was developed: the study of blue compact galaxies (BCGs). The blue light is a consequence of the high proportion of young stars in the galaxies, and in some cases no old stars at all can be definitely detected. Among other properties of the BCGs are their richness in gas and their strong deficiency of elements heavier than helium, when compared to galactic HII regions. Therefore, a fundamental question is whether these galaxies are truly young. Alternatively, they may be old galaxies which occasionally go through short bursts of intense star formation. Such a situation is predicted by the stochastic star formation theory (Gerola et al., 1980, *Astrophysical Journal* **242,** 517), provided that the galaxies are sufficiently small. Indeed, the BCGs typically have small sizes. We shall discuss these intricate processes of star formation further in section 4.

In Uppsala, we are now in the process of studying a sample of the bluest compacts by means of observations in the wavelength region from the ultraviolet to the infrared. Besides the already mentioned photometry, we have, for a large sample, obtained spectra of the central regions, mainly by use of the Image Dissector Scanner at La Silla. These show emission-lines and resemble spectra of HII regions superposed on an underlying stellar population. The availability of CCD detectors during the last years has brought new insights into the mystery of BCGs and has revealed peculiarities within these objects that we never would have been able to discover through traditional observational methods. Parallel to the

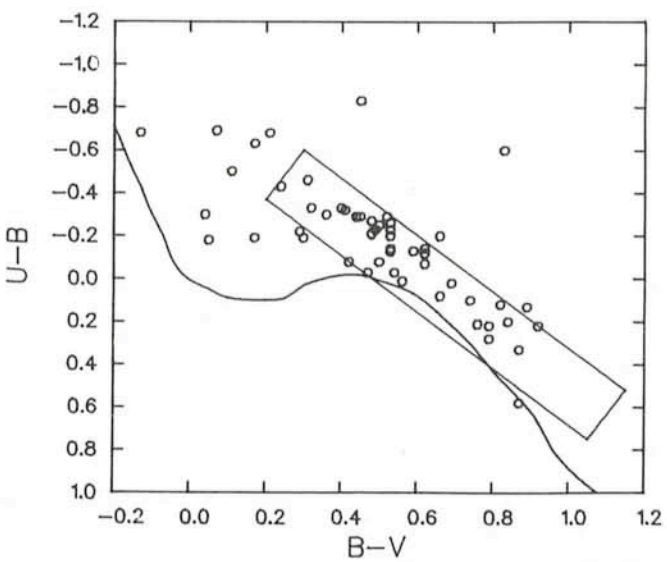

Fig. 2: *U-B/B-V diagram (Johnson system) for a sample of compact galaxies observed with the ESO 1 m telescope at La Silla, by the Uppsala group. Except for a few cases, the aperture covers most of the galaxy. No corrections for galactic extinction have been applied. For comparison, the positions of normal galaxies (box) and galactic main-sequence stars (curve) have been indicated.*

through traditional observational methods. Parallel to the observations we are also developing synthetic models of colour evolution of galaxies as a function of time, based on evolutionary tracks of stars of low metallicity. The purpose is to compare our observed colours with those obtained from the models and thus be able to determine the age of the observed BCGs (for at least the ongoing burst) and to derive information about their stellar mass function. These models will be further discussed below.

2. Breaking Through the Compact Crust . . .

The compact appearance of a BCG is mainly a consequence of its relatively small apparent dimensions and its high surface brightness, which produce overexposed images on the photographic survey plates. Using larger instruments one can resolve the images of these objects and begin to see some very interesting structures.

Fig. 3a shows the appearance of ESO 338–IG04 (see also Fig. 1a) on a short-exposed photographic plate that registers the blue light of the galaxy. The knots surrounding the central "blob" may be giant HII regions or star clusters. A much larger dynamical range is available if one uses a CCD camera as in Fig. 3b and c. The first image (Fig. 3b) shows the result of a division between two CCD frames, one obtained through a broadband filter centred on Hα and the other through an infrared filter centred on ~ 8000 Å (Fig. 3c). Since the "Hα-image" contains light from both gas and stars, while the infrared image is entirely dominated by starlight, the resulting image will show, mainly through the strength of Hα as compared to the stellar continuum, regions where the gaseous emission, and thus probably also the star-forming activity, is most intense. As we can see, a very interesting structure appears, consisting of three hot spots of star formation enclosing the centre. We also see a structure reminding of a spiral arm, stretching out towards the east. It is tempting to interpret the observations in terms of a collapsing agglomeration of HI clouds which are being shocked on their way towards the gravitational centre, thereby triggering the spectacular burst of star formation we are now witnessing. This is what a young galaxy should look like!

The infrared image, however, looks strikingly different with its regular isophotes, more reminding of an old galaxy. It also has a luminosity profile which is typical of old stellar systems. We expect that the time it would take for a galaxy to obtain such a relaxed structure would be of the order of a few 10^8 years.

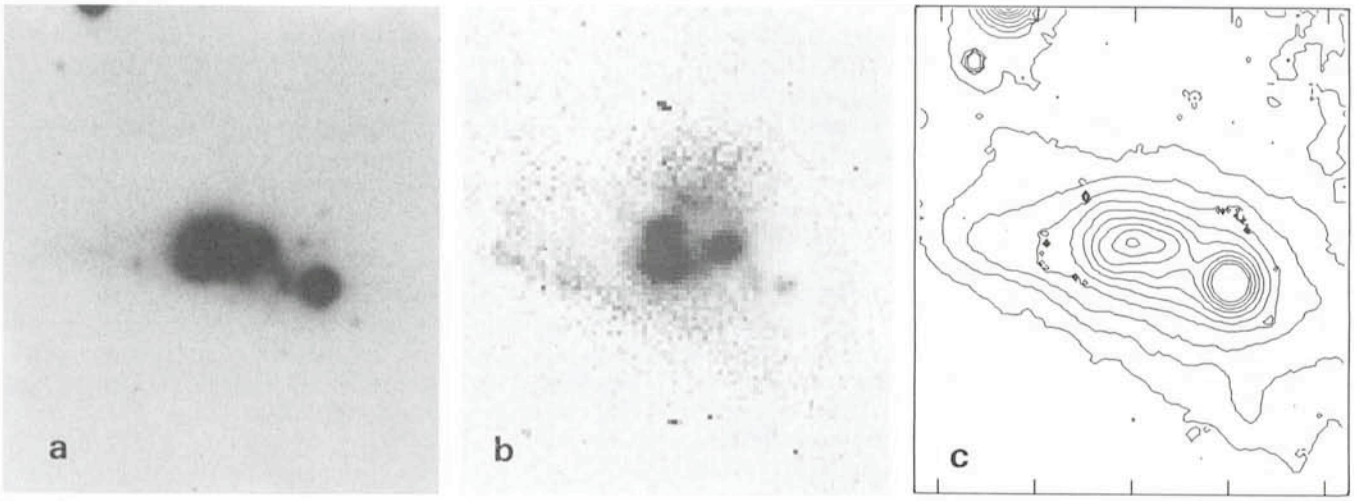

Fig. 3: *Prime focus images of ESO 338-IG04 obtained with the ESO 3.6 m telescope. Top is north, east is to the left. Scale: 0.9″ mm^{-1}. A bright star is superposed on the south-west part of the galaxy. (a) Baked IIIa-J +GG385 filter. Exposure time: 20 minutes. This blue image shows the distribution of the youngest stars in the galaxy. (b) CCD exposure through a broadband ($\Delta\lambda \simeq 120$ Å) filter centred on Hα, divided by the following infrared image. This image shows regions where the equivalent width of Hα is large. These regions are likely to contain the hottest stars. (c) Infrared CCD image obtained through a Gunn I filter centred on ~8000 Å.*

The conclusion we draw from these observations is that the burst we now observe in ESO 338-IG04 is probably not the first one to appear in the history of the galaxy.

3. . . . Heading for the Nebulous Core . . .

If we equip our telescope with a good spectrograph and turn it towards the centre of ESO 338-IG04, we obtain the result shown in Fig. 4. This spectrum is quite typical of BCGs. It is dominated by strong emission lines, emitted by a hot gas of low density, which is mixed with, and ionized by, young massive stars. Although we cannot see much of the spectrum of the stars themselves in the optical region, spectra in the ultraviolet wavelength region obtained with the IUE satellite confirm the presence of hot OB stars. From the relative intensities of the emission lines we may calculate the density, electron temperature and the chemical abundances of the interstellar medium in the object. In ESO 338-IG04, as well as in other BCGs, the abundances are found to be low. If we start from the assumption that the galaxies are old, the low abundances can be explained if the mean gas-consumption rate has been lower than in the solar neighbourhood, or if the

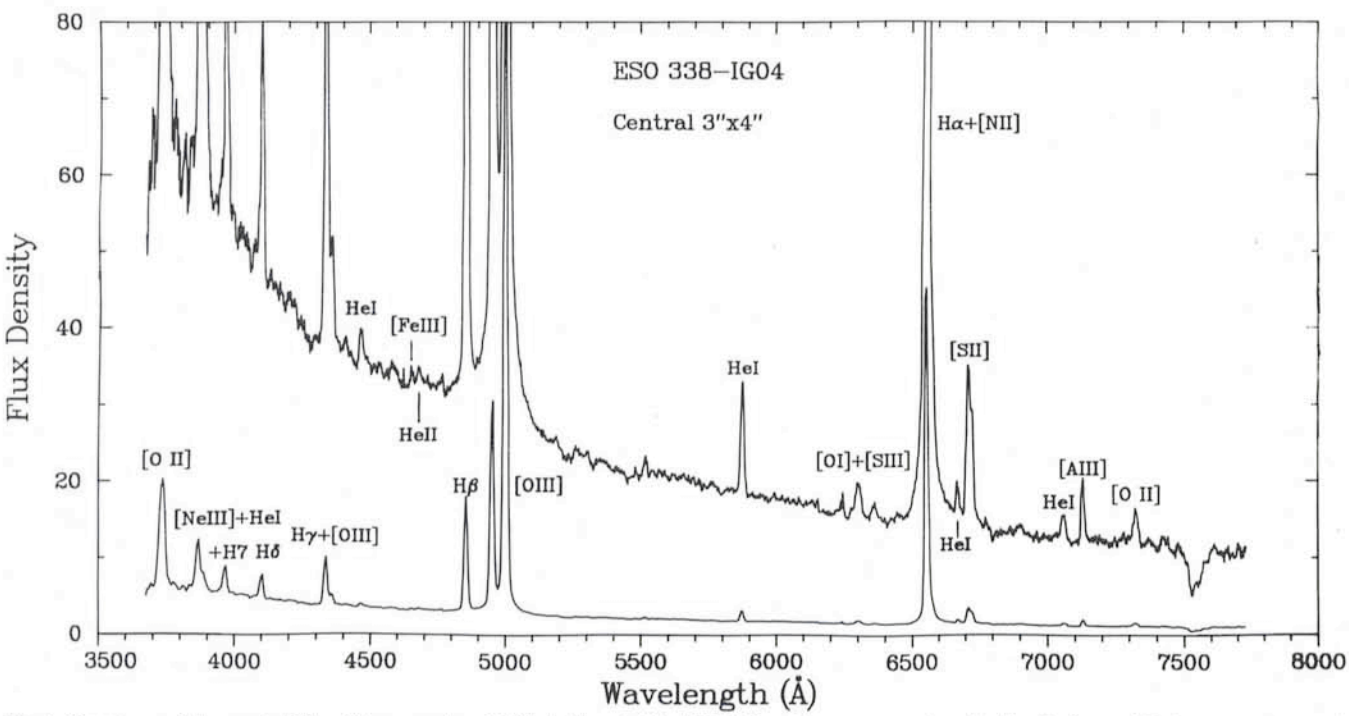

Fig. 4: *Spectrum of the central 3″ x 4″ (pos. angle = 270°) obtained at the ESO 3.6 m telescope equipped with a Boller and Chivens spectrograph and an Image Dissector Scanner. Two versions of the same spectrum are shown. The lower one has been scaled down by a factor of 10. Flux density unit = 1.0 x 10^{-19} Wm^{-2}Å^{-1} for the high amplitude spectrum.*

interstellar gas is steadily being replenished by unprocessed gas, being accreted from the halo. In any case the ongoing burst should be shortlived, in accordance with the stochastic star formation theory.

Alternatively we can speculate over the age of the objects; are they truly young systems? The abundances of the heavy elements should then be biased towards those synthesized in the most massive stars, since they are the first ones to exhaust their nuclear fuel and enrich the interstellar medium through supernovae outbursts. Some support for such a case was found from the C/O abundance in ESO 388-IG04, derived tentatively from an IUE spectrum. On the other hand, Silk (1983, *Mon. Not. Royal Astron. Soc.* **205,** 705) and other workers have found reasons to believe that the mass function for stars in a low-abundant medium is weighted towards the more massive ones. This should produce a similar result and is in line with other results presented below.

Of particular interest is the helium content of the interstellar medium. Like the heavy elements, helium is produced through thermonuclear reactions in the stars. But it is also thought to have been produced within the first minutes following the Big Bang. A good value of the primordial helium content may be determined from analysis of spectra of low-abundant BCGs, since the amount of helium produced in stars is small enough not to influence significantly the determination of the primordial value. This is of course of great interest, since the value is tied to the fundamental cosmological parameters, e.g. the baryon density. The value obtained for ESO 338-IG04, after a careful error analysis, is N(He)/N(H) = 7.4 ± 0.4 %, which is unusually low but still rather typical of BCGs. It indicates that the density of baryons alone is not sufficient to halt the present expansion of the universe. Thus, unless neutrinos or other non-baryonic matter strongly dominate the mass in the universe, we are destined to be travellers with one-way tickets in a forever expanding universe.

4. Colourful Models of Galaxy Evolution

One way of testing the assumption that these galaxies are young is by synthesizing their colour evolution as a function of time, and compare the predicted colours with the observed ones. This is accomplished by utilizing evolutionary tracks of stars. Since we know that BCGs in general have low abundances, we can use metal deficient stars to construct as realistic models as possible. The accuracy of the model results are dependent on our knowledge of how stars of different mass, effective temperature and luminosity evolve as a function of time and metallicity. Present theory of stellar evolution provides us with a fairly detailed description of the life-cycle of a star, at least during most of their lifetimes. Unfortunately the red supergiant phase for stars of low abundances is not very well known.

More important for the model result is the chosen form of the initial mass function (IMF), i.e. the amount of stars formed as a function of their mass, and the star formation rate. The most commonly used form of the IMF is the power law function introduced by Salpeter 1955 (*Astrophysical Journal* **121,** 161) where the slope has the value of $\alpha = 2.35$. Another widely used form of the IMF is the Miller-Scalo mass function, which encounters changes in the slope at 1 and 10 solar masses. In order to illustrate the power of the models, we calculated the evolution of a burst of star formation using two contrasting IMFs, the Miller-Scalo function and a comparatively flat IMF ($\alpha = 1.5$ over the whole mass range). Fig. 5 shows the result. The mass range was 0.5–100 solar masses and the star formation rate was assumed to be constant for 20×10^6 years and was then halted completely.

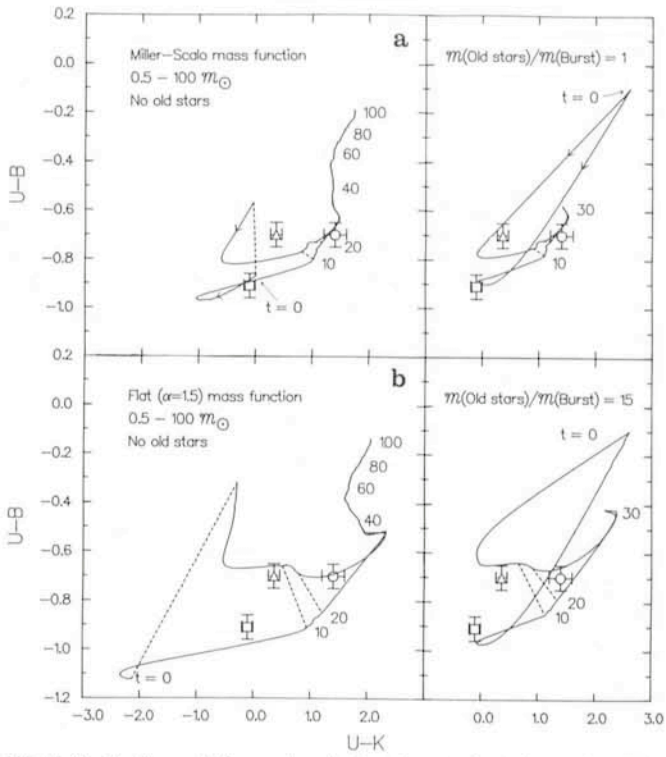

Fig. 5: *Synthetic evolutionary tracks for a burst of star formation. The positions of the three BCGs shown in Fig. 1 are indicated with a square (ESO 338-IG04), a triangle (ESO 480-IG12) and a circle (ESO 400-G43). Bars are mean errors. The U and B magnitudes were obtained with the ESO 1 m telescope, as was the K magnitude for ESO 400-G43. The K magnitude for ESO 480-IG12 was obtained with the ESO 3.6 m telescope while that of ESO 338-IG04 was taken from Gondhalekar et al. (1984,* Mon. Not. R. Astron. Soc. ***209,*** *59). The duration of the burst is 20×10^6 years. The time in 10^6 years is indicated along the evolutionary tracks. The left side of the diagrams shows cases where the galaxy contains no old stars, while on the right old stars have been added. Two tracks are displayed in each diagram, the lower one holds for the pure stellar population in the galaxy, while the upper one includes also the effect of gaseous emission. Two forms of the initial mass function (IMF) were chosen, the Miller-Scalo mass function (a) and a considerably flatter mass function, having an exponent of $\alpha = 1.5$ (b). Evidently the flatter IMF fits better to the observations. A more careful check can be made by comparing other colour indices and the predicted line intensities, obtained from the model, with the observed ones.*

For each IMF, two cases are shown, one which encounters its first burst of star formation, and one with a burst superposed on an underlying older stellar population. Plotted are also positions of three BCGs observed by the Uppsala group. Note that the abscissa gives the broadband colour U–K. This we regard as a more decisive choice when compared to the traditionally more used UBV colours. We see that, in general, model and theory coincide very well, especially for the flat mass function. Our model can also provide us with predicted values of fluxes of the gaseous emission lines. They may be used in order to narrow the range of the free parameters in the models. As regards the youth hypothesis, we see that one cannot rule out the possibility that a large proportion of the mass of the galaxy may be in the form of old stars. Even if we include other colour indices, or predicted emission line fluxes, in the comparison, this frustrating situation does not change much. Today our observations and our models are too crude to permit us to make a conclusive distinction between a young stellar population and a mixed one.

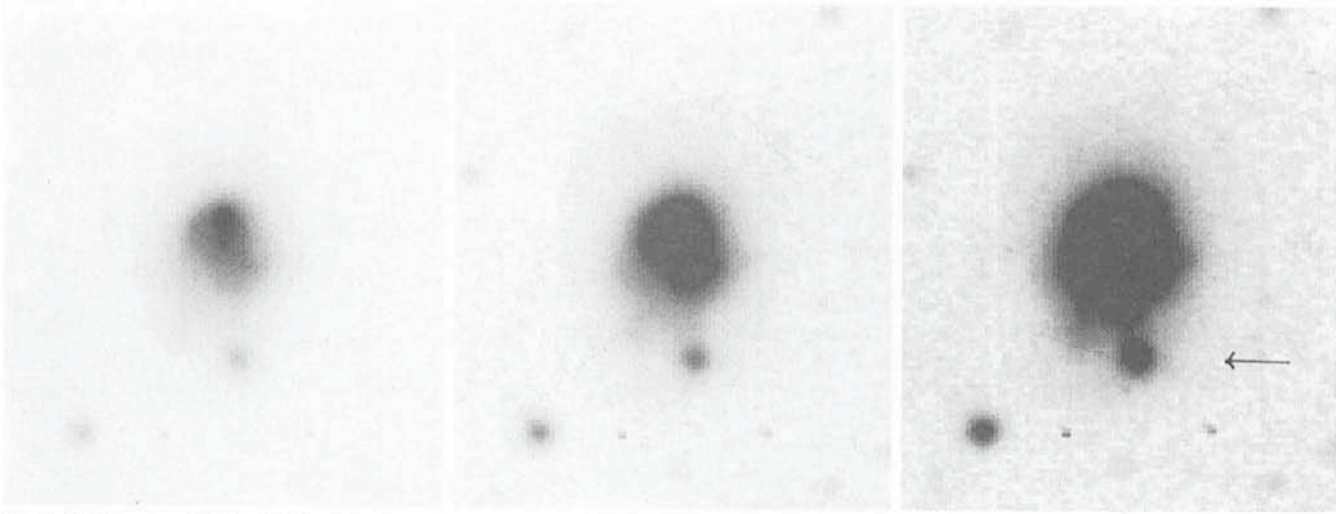

Fig. 6: *CCD image of ESO 400-G43 obtained with the ESO 3.6 m telescope, showing the galaxy as seen in the visual wavelength region. Three different representations of the same exposure are shown in order to let the structural details appear more clearly. The compact object indicated by the arrow is part of the galaxy and shows strong emission lines.*

5. Epilogue

From the preceding discussion we understand that much is still to be learnt about blue compact galaxies. Are they young or are they galaxies that have experienced several bursts of star formation? The answer at this stage has to be yes and no, a diplomatic but still logical answer since we cannot rule out any of these two possibilities. One way of getting ahead is by combining credible spectral synthesis models with carefully planned observations within a broad wavelength region. Results from such work will also be valuable when studying how the IMF and the chemical abundances are related and how they vary across the face of a galaxy. We are now extending our models by implementing spectra of metal-poor stars to the models already presented. More observations in different colours with a CCD camera attached to a large telescope would give us valuable information about the sub-structure within the objects. Is it complex like in the case of ESO 338-IG04? Do all BCGs have a relaxed structure in the infrared? We note that CCD observations of ESO 400-G43 (Fig. 6) show a smooth (although not symmetrical) structure surrounding the compact core also in the visual. And what is the nature of the peculiar emission-line object situated immediately south of the main body (arrow)? We are facing an exciting future in the exotic work of BCGs!

A Complete Optical Survey of Candidate Quasars Down to B = 22.0 with the ESO 3.6 m Telescope

B. Marano[1], G. Zamorani[2] and V. Zitelli[1]

[1] *Dipartimento di Astronomia, Università di Bologna*
[2] *Istituto di Radioastronomia, CNR, Bologna*

The study of the number-magnitude relationship of quasars, together with the statistical analysis of redshift and luminosity distributions of complete samples of quasars at different limiting magnitudes, provides the best tool to investigate the problem of the cosmological evolution of such objects. A summary of the present knowledge on the optical number counts of quasars can be found in recent reviews (see, for example, Woltjer and Setti 1982; Véron 1983). Moreover, after the Einstein X-Ray Observatory provided definitive evidence that quasars are strong X-ray emitters (Tananbaum et al. 1979; Zamorani et al. 1981), the observed optical number counts of quasars have often been used to estimate the overall contribution of this population to the soft X-ray background (Setti and Woltjer 1982; Zamorani 1982). One of the most important sources of uncertainty in this estimate is represented by the still relatively poor knowledge of the detailed behaviour of the number counts relationship for faint ($B > 19.5$) quasars. In fact, it has been shown that, given the observed flattening at faint magnitudes of the number-magnitude relationship, most of the quasars' contribution to the X-ray background is expected from objects in the magnitude range 20–22 (Bonoli et al. 1980).

Two main methods have been successfully applied to the optical selection of quasars:

(1) The ultraviolet excess (UVX) method (see, for example, Braccesi et al. 1980), based on the observational evidence that almost all the known quasars with $z < 2.2$ show $U-B < -0.40$. Since high galactic latitude stars with this colour are rare objects, especially at faint magnitudes, this method provides quite complete and reasonably uncontaminated samples of candidate quasars with $z < 2.2$.

(2) The search for emission-line objects and/or objects with blue continuum on deep "grism" plates. This method is highly efficient in finding high redshift quasars, and, in fact, almost all the radio quiet quasars with redshift larger than 3 have been found by this technique. However, its level of completeness

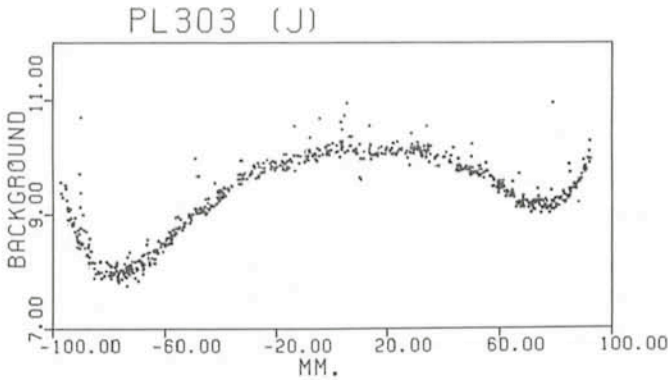

Fig. 1: *Typical behaviour of the linearized background in a slice across a triplet plate.*

(both in terms of limiting magnitude and emission line equivalent width) is very difficult to assess (Clowes 1981).

The characteristics of the two methods are such that they are most effective when applied at the same time on the same field in order to increase the combined level of completeness, as recently also discussed in this journal by Cristiani (1984).

We give here a still preliminary account of the optical search for faint quasars we are performing with the ESO 3.6 m telescope. So far we have applied a colour selection method, which represents an extension of the UVX method (see Koo and Kron 1982 and below), to a high galactic latitude field centred at RA = 03h 10m and $\delta = -55°$ (b = −50°); in the current months we will perform grism and first spectroscopic observations on the same field.

Various sets of deep exposures have been obtained in the passbands U(IIIa-J + UG1), J(IIIa–J + GG385) and F(IIIa–F + GG495). The triplet corrector at the prime focus of the ESO 3.6 m telescope gives a corrected, unvignetted field of about 60 arcminutes in diameter. This represents a very important performance in a programme aiming to extract, by colour measurements, a population of faint objects having low surface density. On each plate the whole useful field was scanned with the ESO PDS micro-densitometer. We adopted an aperture of 50 x 50 microns (0.9 x 0.9 arcsec), which represented a compromise between resolution and number of pixels to be stored and analyzed. An automatic procedure was then applied to extract position and fluxes for all the objects brighter than a given percentage of the local background. Due to the large variations of the background across the triplet useful field (Fig. 1), the sensitivity of the method changes with the position. For the present purposes the selection cut-off was set in such a way to ensure that all the objects brighter than J = 23.0 were extracted and measured. Calibration spots were used to linearize fluxes. This procedure can run as a MIDAS subprogramme as well as an independent programme. Analysis of a whole plate scan (12 million pixels) takes approximately 45 minutes of CPU on a VAX 11/780 computer. J and F magnitude scales were calibrated by using a few CCD exposures obtained at the Danish 1.5 m telescope on La Silla by R. Buonanno and F. Fusi-Pecci on the globular cluster NGC1261, which lies on the border of the field. U, J, F triplet plates with photometric wedge have also been obtained, but, as yet, they have not been fully used for calibration purposes. At the present stage of data reduction a systematic offset as large as 0.20 magnitudes in each band cannot be excluded.

All the objects brighter than J = 22.5 were then separated into stars and galaxies according to the value of the moment of the image (Kron 1980), measured after linearization and background subtraction. Fig. 2 shows the weighted mean of the moments obtained from six plates (two for each bandpass)

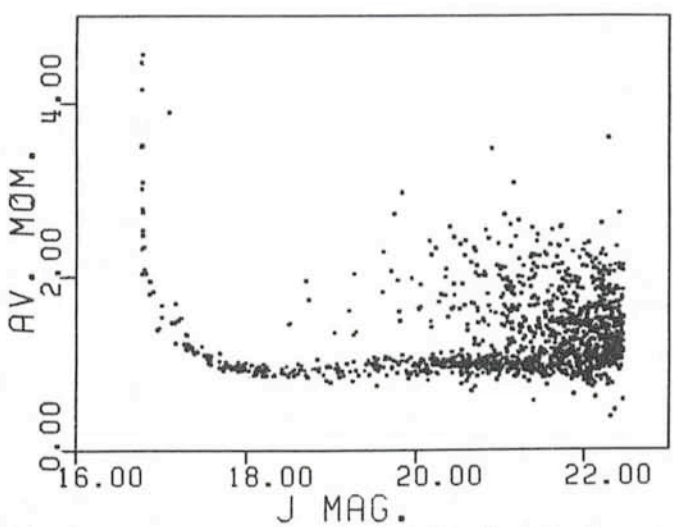

Fig. 2: *Weighted mean of the moments obtained from the six considered plates versus J magnitude. Only 20 % of the objects are shown, in order to avoid overcrowding of points.*

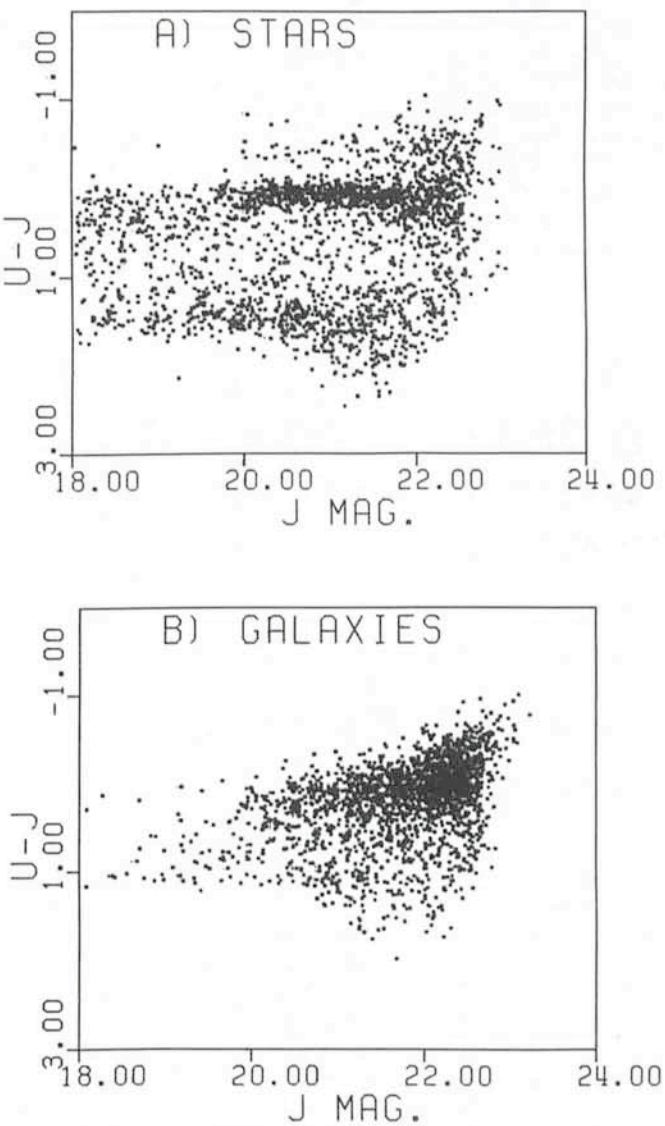

Fig. 3: *U–J versus J for "stars" (a) and "galaxies" (b), as obtained by averaging two plates for each passband.*

versus the J magnitude. Stellar objects populate a well-defined domain in the lower part of the diagram, while galaxies are spread on a large area, corresponding to higher values of the moment. The bright star domain bends towards higher moments because of the plate saturation, which gives a flat top to the images. The adopted method leaves only a few objects brighter than J = 22 with an uncertain classification. However, the number of objects with dubious classification increases very rapidly at fainter magnitudes.

Fig. 3 shows the U–J versus J diagram for stars (a) and galaxies (b), as obtained by averaging two plates for each passband. As typical of high galactic latitude fields, stars are clearly splitted in two main families, hot subdwarfs and M dwarfs. The colour of galaxies undergoes a systematic change with magnitude and a large number of ultraviolet excess galaxies appears at magnitudes fainter than J = 22. This last fact, together with the increasing difficulty in separating faint compact galaxies from true "stellar" objects, sets the most important limit to the reliability of the UVX method in selecting quasars at extremely faint magnitudes. For these reasons we limit our present search to objects brighter than J = 22 and, within this magnitude limit, we define as quasar candidates all the star-like objects lying outside the domain of galactic stars on the U–J vs J–F diagram.

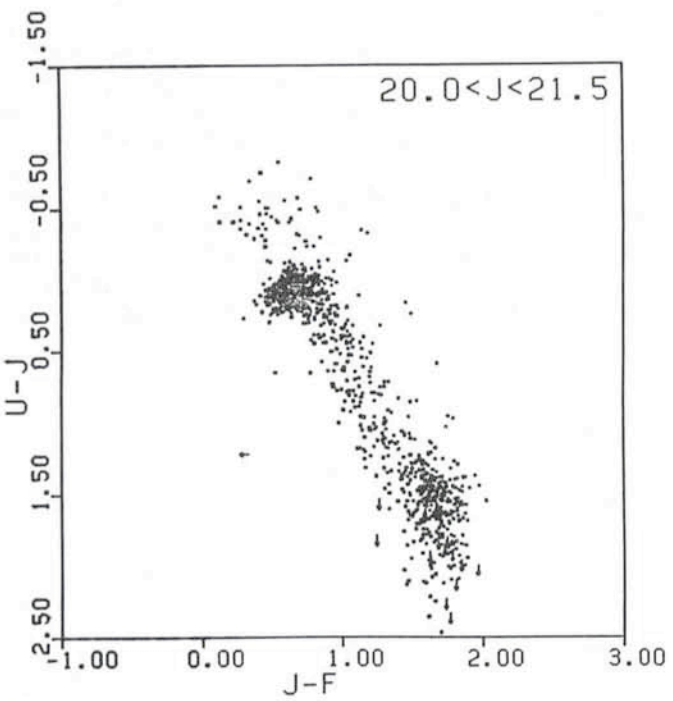

Fig. 4: *U–J versus J–F for all the "stellar" objects in the magnitude range 20.0 < J < 21.5.*

The uncertainties in the zero points of the U, J and F magnitudes do not affect the selection of the QSO candidates, which is based only on the relative position of the objects with respect to galactic stars. Fig. 4 shows the colour-colour diagram that we obtain for the "stellar" objects in the magnitude range J = 20.0–21.5. The data represent the average of two plates for each coulor. The two clumps of hot subdwarf stars and M dwarf stars are clearly visible. Most of the objects lying outside the "normal stars locus" are ultraviolet excess objects. A few objects with "J–F" excess but no ultraviolet excess are also present. They could be high redshift quasars (as well as photometric errors . . .). In any case, these objects with anomalous colours do not appear to contribute in a significant way to the total counts in this magnitude range.

From the present data, in an area of 0.69 square degrees, we obtain a surface density of 84 "non star" stellar images per square degree brighter than J = 21.5 and 185 brighter than J = 22.0, in very good agreement with the results obtained by Koo and Kron (1982) in the Selected Area 68. The comparison of our counts at J = 20 with the results obtained by Braccesi et al. (1980) in the 13h+36 field is less satisfactory. They found a density of about 27 UVX candidate quasars per square degree at B = 20.0, corresponding to J = 19.9. A spectroscopic follow-up of these objects yielded a density of about 20 confirmed quasars per square degree brighter than B = 19.8. According to this result, about 20 objects brighter than J = 20 would then be expected in our field, whilst we found 8. Due to the poor statistics, this discrepancy is at present only suggestive of a real effect. It is possible that statistical fluctuations, together with zero point errors in the J magnitude, can give full account of the different densities. However, considering also recent Koo's results (1983) (16 quasars per square degree with 19.5 < J < 20.5), it seems possible to conclude that there is a tendency, in recent deep optical counts, to find, around J = 20, a lower surface density of UVX objects than that found by Braccesi et al. This, if confirmed by future work with better statistics, would produce a softer bending in the counts than previously assumed for studying evolutionary models and estimating the QSOs contribution to the X-ray background.

Acknowledgements

The authors acknowledge the precious help they got from H. E. Schuster (who obtained also some plates) and H. Helborn at La Silla, and from P. Grosbøl and D. Ponz during part of the reduction work in Garching.

References

Bonoli, F., Braccesi, A., Marano, B., Merighi, R. and Zitelli, V.: 1980, *Astronomy and Astrophysics,* **90,** L10.

Braccesi, A., Zitelli, V., Bonoli, F. and Formiggini, L.: 1980, *Astronomy and Astrophysics,* **85,** 80.

Clowes, R.G.: 1981, *M.N.R.A.S.,* **197,** 731.

Cristiani, S.: 1984, *The Messenger,* **35,** 13.

Koo, D.C.: 1983, Proceedings 24th Liège International Astrophysical Symposium on "Quasars and Gravitational Lenses", p. 240.

Koo, D.C. and Kron, R.G.: 1982, *Astronomy and Astrophysics,* **105,** 107.

Kron, R.G.: 1980, *Astrophysical Journal* Suppl., **43,** 305.

Setti, G., and Woltjer, L.: 1982, "Astrophysical Cosmology", Proceedings of the Vatican Study Week on Cosmology and Fundamental Physics, H.A. Bruck, G.V. Coyne, and M.S. Longair (eds.), Pontificia Academia Scientiarum, p. 315.

Tananbaum, H., Avni, Y., Branduardi, G., Elvis, M., Fabbiano, G., Feigelson, E., Giacconi, R., Henry, J.P., Pye, J.P., Soltan, A., and Zamorani, G.: 1979, *Astrophysical Journal* Letters, **234,** L9.

Véron, P.: 1983, Proceedings 24th Liège International Astrophysical Symposium on "Quasars and Gravitational Lenses", p. 210.

Woltjer, L. and Setti, G.: 1982, "Astrophysical Cosmology", Proceedings of the Vatican Study Week on Cosmology and Fundamental Physics, H.A. Bruck, G.V. Coyne, and M.S. Longair (eds.), Pontificia Academia Scientiarum, p. 293.

Zamorani, G.: 1982, "Progress in Cosmology", Proceedings of the Oxford International Symposium, A.W. Wolfendale (ed.), p. 203.

Zamorani, G.: Henry, J.P., Maccacaro, T., Tananbaum, H., Soltan, A., Avni, Y., Liebert, J., Stocke, J., Strittmatter, P.A., Weymann, R.J., Smith, M.G. and Condon, J.J.: 1981, *Astrophysical Journal,* **245,** 357.

The ESO Faint Object Spectrograph and Camera (EFOSC)

B. Buzzoni, B. Delabre, H. Dekker, S. D'Odorico, D. Enard, P. Focardi, B. Gustafsson, W. Nees, J. Paureau and R. Reiss, ESO

History

In the year 1981, the Instrumentation Group, then unter the direction of D. Enard, started a design study for a Low Dispersion Spectrograph for the ESO 3.6 m telescope. In September 1982, a decision was taken for a Focal Reducer type instrument at the Cassegrain focus. Prestudies, including flexure analysis and optical design, were completed early in 1983. Integration tests started in Garching in the beginning of 1984; a first telescope test was performed successfully in June 1984.

H. Dekker was project manager. S. D'Odorico, who became Head of the Optical Instrumentation Group in 1983, provided the overall guidance in the integration and astronomical test phases. B. Delabre was responsible for the optical design. J. Paureau and G. Hess designed the mechanics and the structure and W. Nees and B. Gustafsson were responsible for electronics and control software. During the test phase, B. Buzzoni did the integration and R. Reiss installed and tuned the CCD. P. Focardi helped reducing and assessing the quality of the test observations.

The instrument will be available for general use in low dispersion spectroscopy and direct imaging modes from April 1985. Manuals are in preparation and will be available at this date (1), (2). Multiple object spectroscopy will probably be offered six months later.

Design Options

The goal of the study was to find a very efficient instrument configuration with which low dispersion spectroscopy (down to 100 Å/mm) and field spectroscopy could be done. A capability for direct imaging was thought to be essential, both for the acquisition of very faint objects and for photometry. It was intended to use a thin, back-illuminated RCA CCD with 512 x 320 pixels of 30 μm. Initial solutions were investigated based on concave gratings in the primary focus. However, it appeared that it is presently not yet possible to make efficient F/3 concave gratings, either holographic or ruled. Also, the prime focus is more difficult to access and offers rather limited space. An advantage is obviously the single reflection in the telescope.

For the Cassegrain, a simple, compact and very efficient configuration was found, consisting of a focal reducer, converting the F/8 telescope beam to F/2.5. A parallel beam space was foreseen in which grisms of filters can be inserted. This solution was finally adopted. Enard and Delabre discuss the different optical design options in more detail in (3).

Design

As always in the design of an astronomical instrument, an important question to answer is the projected pixel size on the sky. As a compromise between the requirements for direct imaging and spectroscopy and taking into account the average seeing at the 3.6 m, we finally fixed the camera speed to F/2.5, giving a pixel size of .67″ for the RCA chip we use.

The other key parameter is the camera focal length which determines the dispersion attainable with a given grism. Scaling the instrument up rapidly increases the complexity of optics and mechanics. A focal length of 100 mm provides dispersions of up to 120 Å/mm. (The active grating area is still only 40 mm in diameter which keeps grating costs down.)

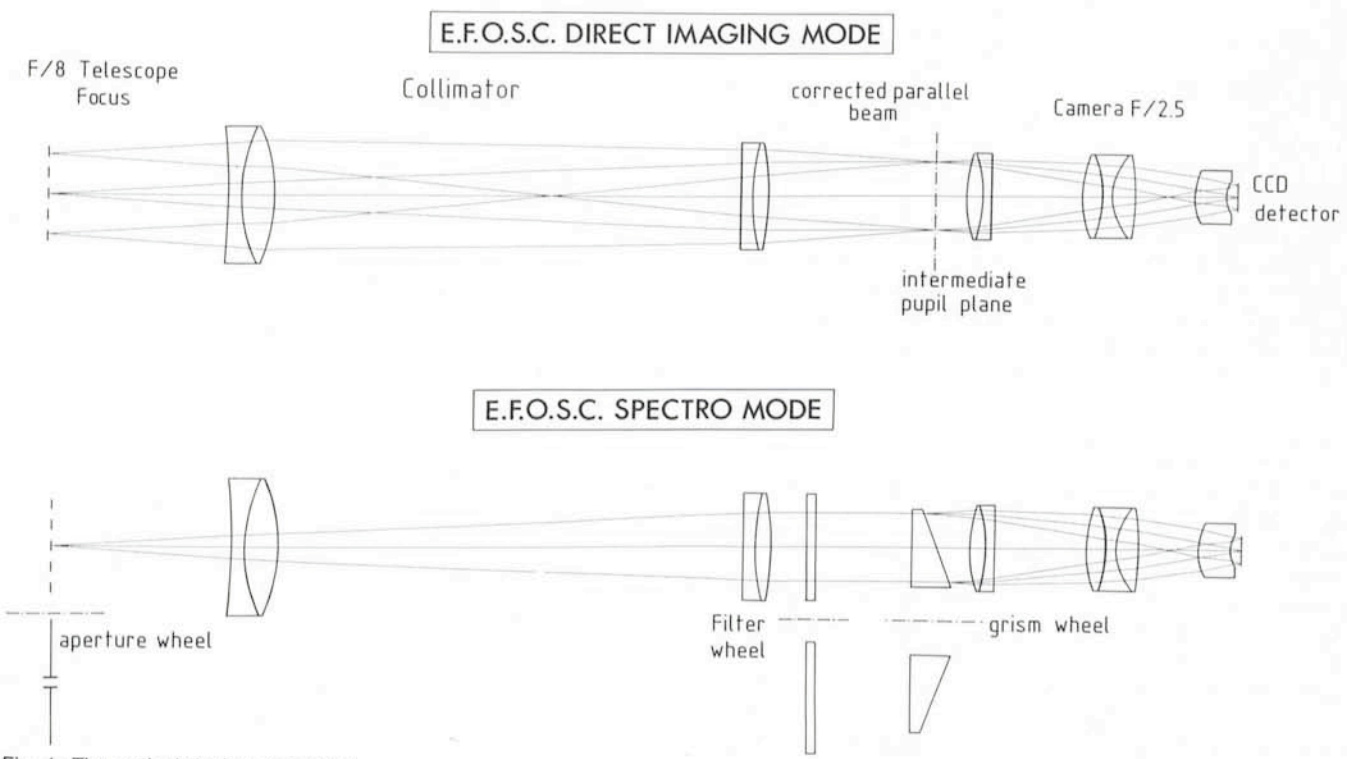

Fig. 1: *The optical design of EFOSC.*

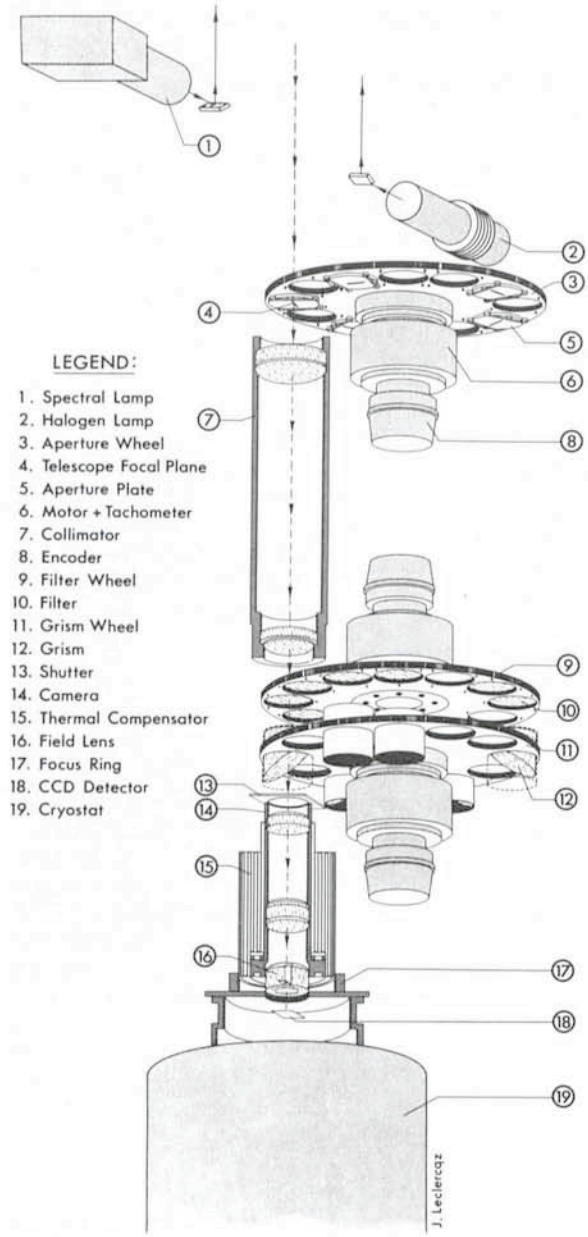

Fig. 2: *EFOSC layout.*

The focal reducer is totally based on lens combinations; it has no mirrors and presents no vignetting or central obscuration. Its main elements are a collimator, consisting of 2 lens groups, and a camera consisting of 3 lens groups (see Fig. 1). The collimator produces an image of the telescope entrance pupil just in front of the camera. The aspheric camera field lens also serves as a cryostat window. Up till now, fully dioptric spectrographs were rather unusual in astronomy, they are now conceivable because of new developments in glasses, optical design programmes, high-efficiency coatings and dispersing elements (grisms).

The image quality – characterized by the diameter which encircles 80 % of the geometrical energy – of this design is quite good; in white light (3500–10000 Å) imaging, the image quality in the central 10 mm of the field is better than .3", in the corners the quality is about .5". This result could only be reached by using a new glass (Schott type FK54) which allows excellent secondary coulour correction, while at the same time its blue transmission is still quite acceptable, unusual for a glass of this type. It also has disadvantages, notably its very high coefficient of expansion (twice that of a normal glass) and local glass homogeneity problems (schlieren) which are however not a limiting factor for the relatively small lenses of EFOSC. The difference in thermal expansion coefficient requires care in the cementing of the lenses and in the handling.

A slight disadvantage of this type of design is the so-called sky concentration, also known from wide-field telescope correctors. It appears as a diffuse spot, 5–10 % above the background in the centre of the image. It is caused by light which is back-reflected by the chip into the camera and returned by some optical surface. Optically, it can be seen as the superposition of several demagnified out-of-focus images of the CCD, each image corresponding to an optical surface. The largest contributions come from the field lens. Our experience indicates that flat-fielding will correct this effect to better than 1 %.

Fig. 2 gives a view of the instrument. It is equipped with 3 wheels, each with 12 positions. Table 1 lists the currently available slits and filters. Note that all filters must have image quality over the full 50 mm used – an important consideration for users bringing their own filters. The grism wheel holds up to 9 grisms, providing different dispersions and wavelength coverage. Two positions are reserved for Hartmann screens, to be used for focusing.

The camera is mounted in a thermal compensator, a unit which automatically moves the camera lenses with temperature to maintain the focus. The user needs only to focus the telescope.

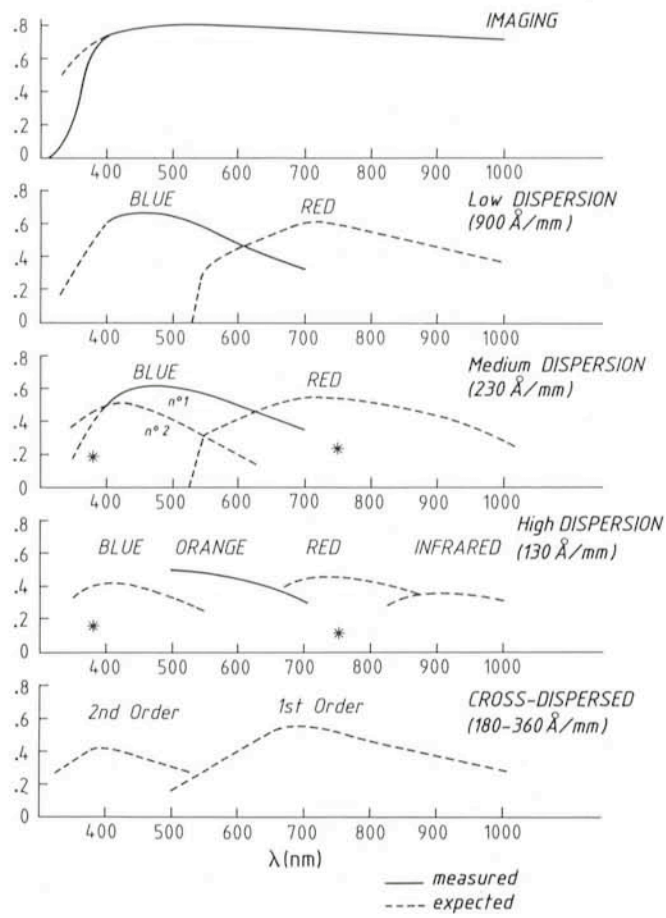

Fig. 3: *Efficiency and wavelength coverage in imaging and spectroscopic modes. Full lines represent actual measurements, dotted lines are values expected for components which were not yet received. The lenses are being recemented because of problems with the UV transmission of the previously used cement. The stars represent the efficiency of the Boller and Chivens spectrograph at comparable dispersions.*

Above the aperture wheel, four calibration lamps are mounted, one halogen and three spectral lamps.

The only useful coating available for the very large wavelength range is a quarter-wave MgF2 layer, paeked at about 5000 Å. The average optical troughput between 3500 and 10000 Å is 75 %, with a maximum of 82 % at 5500 Å. In Fig. 3, the overall optical efficiency is shown in direct imaging and spectroscopic modes.

The structure was designed for high rigidity and is shaped as a box, closed on three sides. The fourth side is open for easy access. All units are pinned for reproducible mounting. Flanges at both ends attach to the telescope and to the CCD cryostat (see Fig. 4). Flexure tests (1) have shown that image movement is negligible (< 0.1 pixel) for a 30 degree attitude change, corresponding to an exposure time of 2 hours.

The 3 wheels are driven by direct-drive DC motors with the wheels, tacho and encoder mounted directly on the motor axis. This eliminates backlash which is always a problem when gearboxes are used. The encoders have a resolution of .001 degree; the absolute positioning accuracy of the servo loop is better than .005 degree. The HP 1000 computer sends its motor position command to microprocessor controlled CAMAC modules which provide the position and velocity servo control.

The software consists of three main programmes. With the user interface programme, softkey menus can be chosen and forms filled in; the instrument control programme takes care of the CAMAC communication and the CCD programme sends control commands to the detector and reads out and stores the images on disk. The user interface also provides access to the IHAP image processing programme. For more information about the software see [4].

Operation and Maintenance

In EFOSC, a large number of filters and grisms with different dispersions can be mounted at the same time. This allows a high degree of flexibility in the scientific programmes which can be carried out. Switching from imaging to the spectroscopic mode is accomplished in a few seconds.

Pointing in the spectroscopic mode is done by inserting the mirror mounted in the aperture wheel and centring the object with the slit viewer. If it is too faint to be seen on the TV, a short exposure has to be taken. With an exposure of a few minutes it is possible to reach 23rd magnitude which is about the present limit for spectroscopy. From the image, the offsets to be given to the telescope to centre the object on the slit are computed with a standard batch programme.

Guiding in imaging and spectroscopic modes is done on an offset star. An auto-guider should also be available at the 3.6 m at the beginning of 1985.

The multiple object spectroscopy mode requires a CCD frame of the field to be taken to measure the positions of the objects to be observed. The following morning, an aperture plate is prepared in the La Silla workshop and mounted in the instrument. This procedure has been tested successfully in June and it will be illustrated in detail in a forthcoming article.

EFOSC is a very simple instrument, requiring little maintenance. From time to time, however, checks must be done on the alignment and position of the slits, of the grisms, etc. For this purpose, the instrument control programme can make a series of test exposures during daytime. The resulting images are subsequently automatically analyzed by an IHAP batch programme and the result printed out. A complete self-test sequence will last approximately 2 hours; the print-out documents the condition of the instrument and indicates if corrections must be applied.

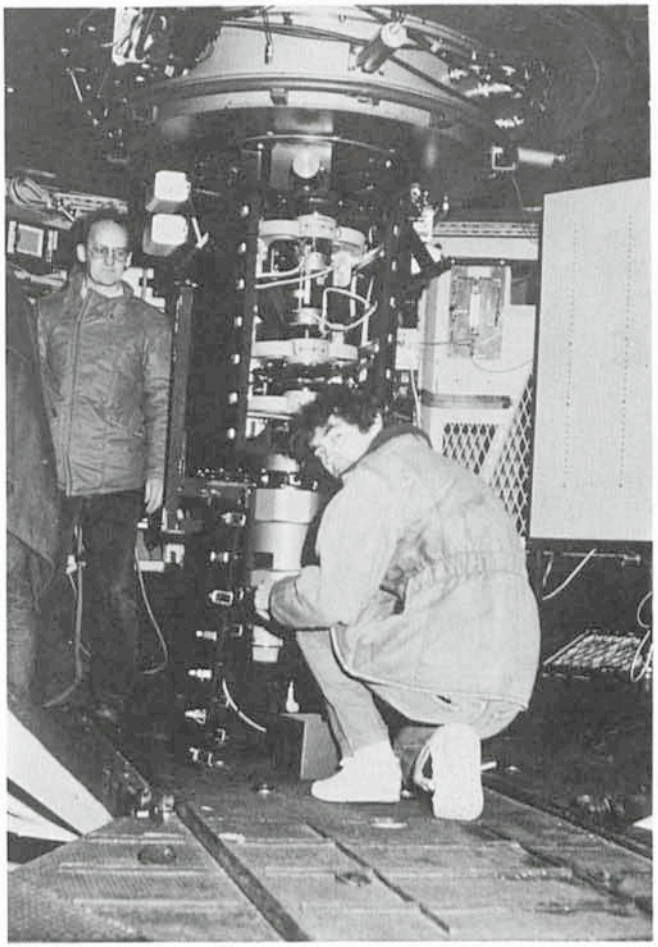

Fig. 4: *The instrument on the telescope. A door in the light-tight enclosure has been removed to exchange filters. On the upper flange, calibration lamps and electronics box are mounted.*

First Results at the Telescope

During the test period at the 3.6 m telescope we checked the different modes of operation and the limiting performance of the instrument. The overall results were quite satisfactory even if the astronomical observations were restricted to two nights in bright moon time due to the poor weather.

An RCA back-illuminated CCD with 40 e rms read-out noise and a peak quantum efficiency of 80 % was used as a detector. The spectrograph, the control programme and the detector worked smoothly throughout the test period. Spectroscopic observations of two QSOs of 17th and 20th magnitude at 7 Å/pixel have already been published (5). From these we estimate the actual efficiency of the spectrograph and detector to be .47. The value predicted from the measured transmission of the optics and the detector characteristics is .50. At 7 Å/pixel and with the present detector the limiting magnitude is about 22 for a 90-minute exposure.

Because of the moon, we obtained only a few photometric data in the direct imaging mode. In the R band stars of 22 magnitude are well detected in a 3-minute exposure. The efficiency of EFOSC can also be judged from the deep view of the Kepler supernova remnant which is shown in Fig. 5.

Observers will also be interested in the flat-fielding and data reduction procedure. For the flat-fielding of the images and of the spectra and for wavelength calibration a reflecting screen was mounted on the top of the telescope sky baffle. Dimension and central obscuration match those of the primary mirror and

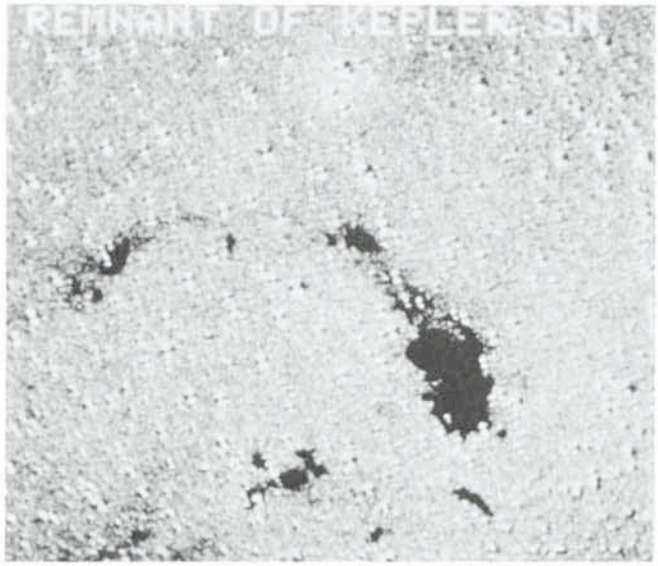

Fig. 5: *A deep image of the remnant of the Kepler supernova (1604 AD) was obtained by subtracting a continuum exposure from one taken through a 60 Å interferential filter centred at 6562 Å. Exposure times were 15 minutes. It is the first time that the optical shell, which has well defined radio and optical counterparts, is seen so clearly.*

it can be inserted remotely in the optical path to reflect the light from the calibration lamps. The calibration procedure is very rapid and it works very well for the spectra. In direct imaging the results are satisfactory (see Fig. 6).

As for data reduction, images are obviously in the same format as e.g. the CCD data with the 2.2 m direct camera with which many ESO observers are familiar. They can be reduced at ESO Garching either with the IHAP or MIDAS systems. The spectra with the standard apertures are in the same format as data from the Boller and Chivens + CCD. They can be fully reduced with IHAP. Some further software development is required for the analysis of "direct" grism images and for multiaperture spectroscopy.

Conclusions

From the first tests at the telescope, EFOSC proved to be a valuable and docile instrument. It is not only the most efficient ESO low dispersion spectrograph but – we like to think – one of the best worldwide in its category. It has a versatile deep imaging capability. We certainly hope it will produce a lot of good data for those programmes which require observations of faint objects.

A Word of Thanks

As is evident from the list of authors, a large team contributed to the development of this instrument in Garching. We want to express our thanks to the staff in La Silla for their excellent assistance during the installation and test on the telescope. A particular thanks goes to L. Baudet and G. Ihle.

References

(1) EFOSC Technical Report, in preparation.
(2) EFOSC Operating Manual, in preparation.
(3) D. Enard, B. Delabre, 1982, Two design approaches for high efficiency, low resolution spectroscopy. Proceedings SPIE **445,** 522.

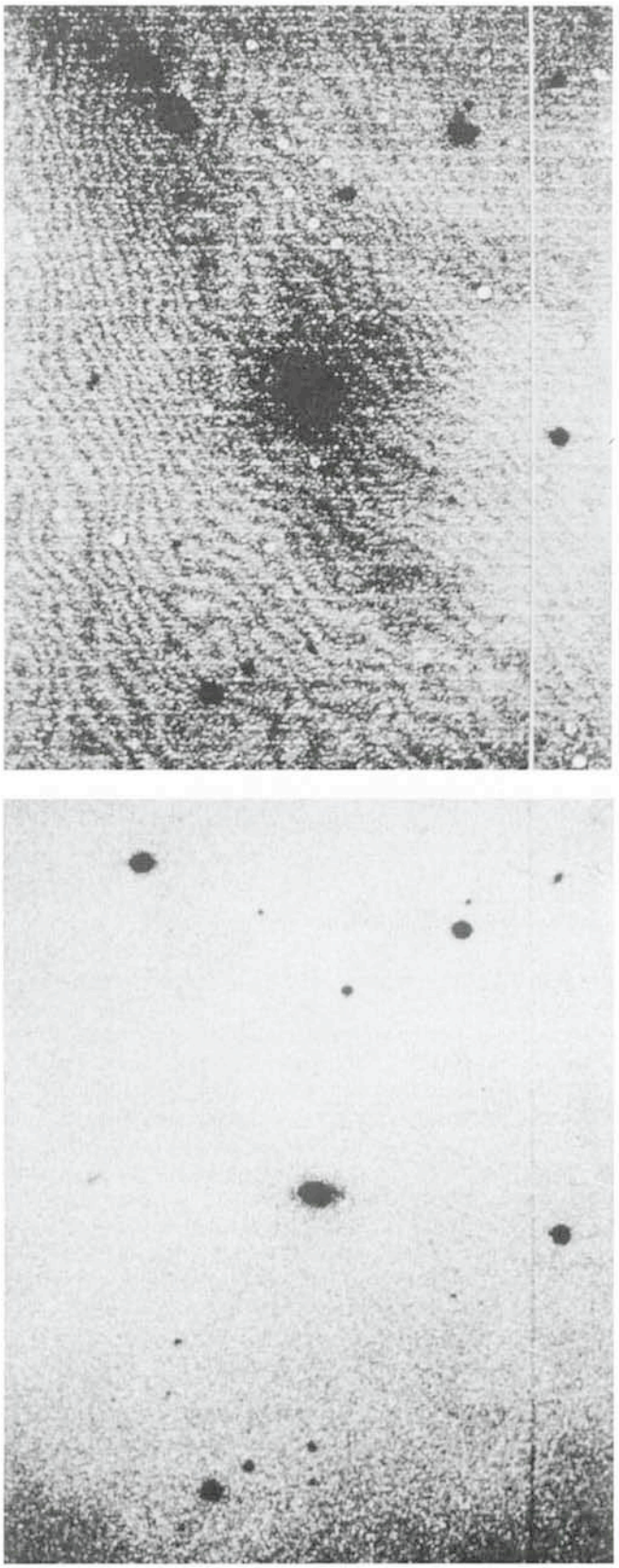

Fig. 6: *(a) An EFOSC 15-minute exposure of the radio galaxy PKS 2158-380 through a 60 Å wide interferential filter centred at 5007 Å. The peak-to-peak intensity of the fringes is at most 5 %. The "sky concentration" at the centre has about the same intensity. (b) The same image after division by the flat field obtained by illumination of a screen inserted in the optical path of the telescope with a calibration lamp. Fringes and sky concentration are corrected to better than 2 %. A uniform gradient of amplitude 5 % is introduced at one edge of the image by the flat-field image which is not fully uniform. While this effect does not prevent accurate photometry to be done, we hope to eliminate it by modifying the lamp support.*

(4) P. Biereichel, B. Gustafsson, G. Raffi, 1983, The New Data Acquisition System for ESO Instrumentation, *The Messenger* **34**, 35.
(5) H. Dekker and S. D'Odorico, 1984, First QSO Spectra with EFOSC, *The Messenger* **37**, 7.

Table 1. Available filters and standard apertures.

In the filter wheel, up to 11 filters may be mounted. The aperture wheel will hold up to 10 standard or special (multi-hole) aperture plates; one position is reserved for an inclined mirror for use with the slit viewer, one position must be free for direct imaging. The twin slits are primarily intended to be used with the cross-dispersed grism.

Filters

A set of redshifted Hα and [OIII] interference filters:

Redshift	Centre wavelength/FWHM	
km/sec	[OIII]	Hα
0	5010/66/130	6562/61/142
3000	5060/56	6634/70
6000	5111/55	6693/94
9000	5162/63	6766/68
12000	5211/60	6832/74
15000	5261/54	
18000	5313/55	6956/64
21000	5354/64	7018/64

A set of U, B, V, R filters.

A set of Gunn G, R, I, Z filters.

Standard aperture plates:

Slits with a length of 3.6':
.5", .75", 1", 1.5", 2", 2.5", 3", 5", 10".

Twin slits 50" apart, each 5" long:
1", 1.5", 2", 3", 6".

Abundances in LINERs

L. Binette, ESO

Introduction

Ionized gas can be detected in the nucleus of most bright galaxies as shown by the recent surveys of Keel (1), Stauffer (2), Phillips et al. (3) and Heckman et al. (4). In fact, Keel detected nuclear emission in all the spiral galaxies (not edge-on) of his magnitude-limited complete sample. Apart from demonstrating that nuclear emission is a common phenomenon, these surveys also showed that the emission can be broadly divided into three classes: those that bear many similarities with spiral arm HII regions and for which young OB type stars are the likely excitation mechanism; secondly, those that are characterized by low excitation lines such as [NII], [OII], [SII] and [OI], which have been termed LINERs (for Low Ionization Nuclear Emission Regions) by Heckman (5), and, finally, the higher excitation (and rarer) Seyferts galaxies which often reveal an important UV continuum excess. The recognized excitation mechanism for Seyferts is photoionization by a non-stellar object.

In the case of LINERs, the excitation mechanism is still debatable. Because of the predominance of low ionization species in the spectra, excitation by shocks appeared promising at first and has been proposed by Heckman. However, recent work by Ferland and Netzer (6), Halpern and Steiner (7) and Keel (8) shows that photoionization by non-thermal UV spectra more easily reproduces the spectral features of LINERs; the latter are also shown to form a natural sequence with Seyferts or Quasars with the ionization parameter as the connecting variable. In support of this, properties like broad Balmer lines or nuclear X-ray flux which are often associated with Seyferts, are also observed in a substantial fraction of LINERs. Although photoionization is adopted in the analysis that follows, the possibility that both mechanisms may be operating to different degrees in different objects cannot be ruled out (Aldrovandi and Contini (9)).

We here present a project summary on LINERs for which two types of results are available at this stage: first, new diagrams of emission line ratios which reveal tighter correlations when homogeneous data are used, second, a new grid of photoionization calculations which aim at analysing the sensitivity to input parameters like optical thickness, hardness of the ionizing spectrum and distribution of the gas. It is concluded that abundances are more uniform (and solar) than previous work suggested.

New Diagnostic Diagrams for LINERs

Although photoionization models have proved successful in reproducing various correlations in selected diagnostic diagrams, the scatter of the data remained nevertheless substantial. From trying out new combinations of line ratios, however, it has become apparent that this scatter can be significantly reduced if one defines diagrams which are optimized for the type of spectrum that characterises LINERs; as a by-product, these new diagrams also give more compelling evidence in favour of photoionization. For example, there are many advantages in replacing the much in vogue OII/OIII axis which represents the excitation of the gas, by OI/OIII, an equivalent excitation index. (Obviously, this is only possible for classes of objects like LINERs which present a significant [OI] flux). While the previously used OIII/Hβ versus OII/OIII diagram is significantly affected by interstellar extinction or by collisional deexcitation due to high densities, the new diagram proposed in Fig. 1 is quite insensitive to these effects. In fact, the dispersion introduced in Figs. 1 and 2 due to reddening is quite small because the reddening correction (represented by the arrow normalized to E(B-V) = 0.66) runs in about the same direction as the correlation shown by the objects. Similar considerations apply to the effect on the line ratios of collisional deexcitation. For instance, the dispersion introduced by varying the densities is no more than 0.24 dex if these are below 4.0×10^6 cm^{-3} (this result is born out of computations of models such as those described below). Another factor favouring Fig. 1 is that it is quite insensitive to geometrical parameters defining the gas distribution as has been shown using spatially "integrated" models. Unfortunately, one parameter – optical thickness – could pose a serious problem for any diagram involving [OI] but, as it turns out, the ionized condensations appear to be optically thick at least in the majority of the objects. This is indicated by the scatter which should otherwise be larger than observed in Fig. 1. The possibility of optical thinness is further discussed in Binette (10).

A set of spectral data on LINERs larger than available to Ferland and Netzer or Halpern and Steiner is plotted in Figs. 1 and 2; it includes data from both Keel (8) and Stauffer (11). (A few ellipticals have been added by Keel to the subset). These data are represented by squares except for the higher excitation objects of Stauffer for which diamonds are used. These latter objects would not strictly be classified as LINERs if Heckman's criterion concerning the relative strength of [OIII] is

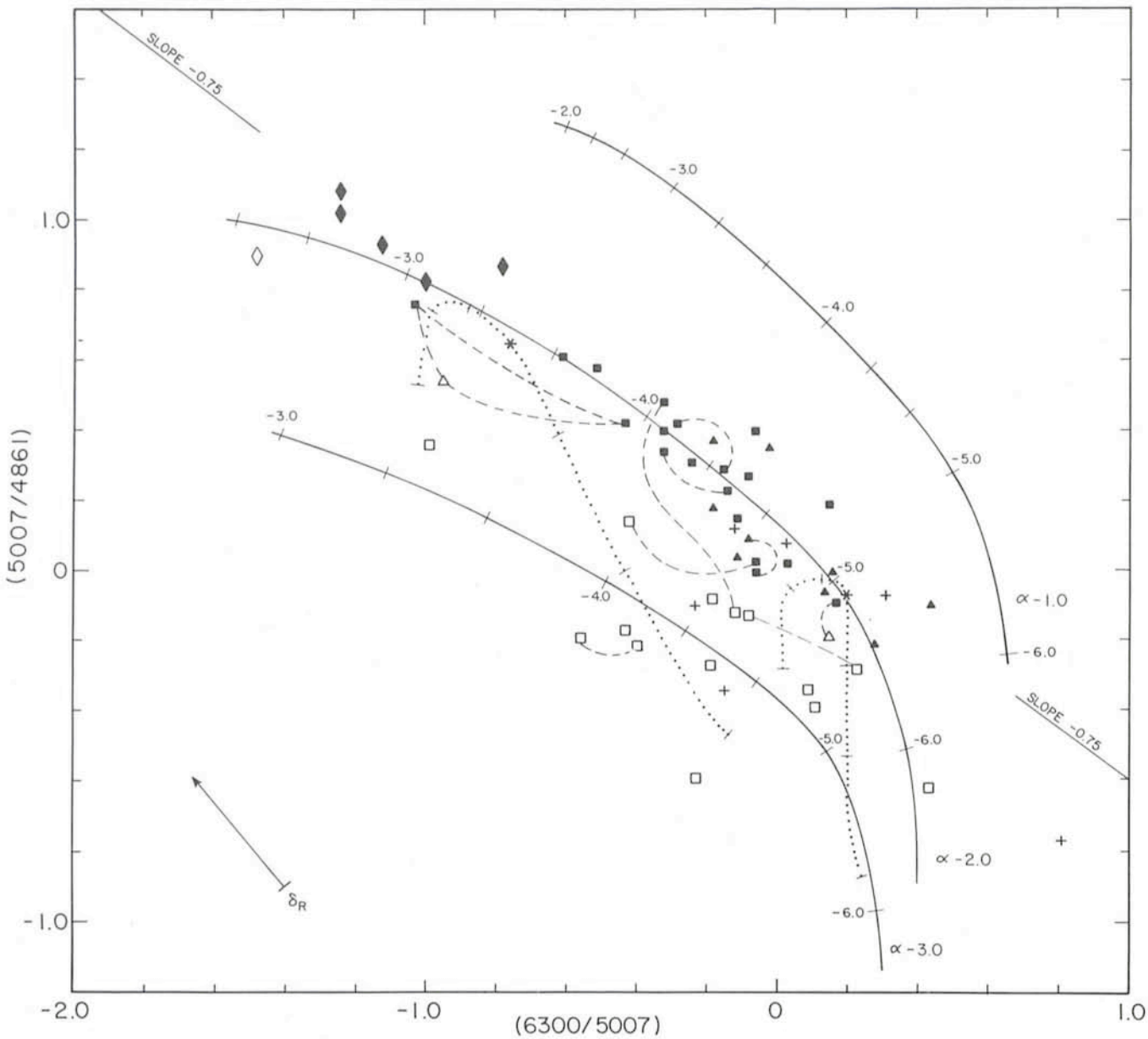

Fig. 1: *[OIII]/Hβ versus [OI]/[OIII] diagram for models; for the sample galaxies, the ordinate is [OIII]/(Hα/3). Squares represent objects from Stauffer (11) and Keel (8). Diamonds distinguish the higher excitation objects from Stauffer. Triangles are allocated to the sample of Heckman et al. (4) as listed in Ferland and Netzer (6). Open figures characterize objects which are more than 0.17 dex below the straight line (or envelope) of slope −0.75. Broken lines join multiple measurements of the same object. Continuous lines represent the locus of "integrated" models (with α = −1,−2,−3) while asterisks and dotted lines refer to individual calculations at various abundances (here α = −2).*

invoked. On the other hand, one can doubt of its relevance in the context of surveys where unnecessary preselection could hide meaningful trends across classes. One must also bear in mind that Stauffer discovered these objects following the same systematic procedure as for the LINERs and even though they could be labelled Seyferts, they are at least of a very underluminous sort and quite homogeneous in spectral properties. This is seen in Figs. 1 and 2 where diamonds appear simply as an extension to LINERs, which suggests that these objects represent a difference in degree and not in class. However, this is a point requiring further confirmation since the statistics are rather limited. Finally, to complete the data base, the LINERs from the list given in Ferland and Netzer (6) that correspond to the magnitude-limited survey of Heckman et al. (4) are included and represented by the triangles. It should be noted that no correction for reddening has been applied to the data shown and that the Hβ flux used in ordinate of Fig. 1 was always derived from the Hα measurement, using: Hβ = Hα/3.0.

One of the most significant results from Fig. 1 is that three quarters of the objects taken from *complete magnitude-limited samples* can be contained in a linear band 0.3 dex wide only (the range in OI/OIII covers 1.7 dex). Inspection of Fig. 1 suggests that the objects' distribution is characterized by an "upper envelope" towards which the objects tend to concentrate. The latter is empirically defined as a straight line of slope −0.75 and intercept (0.0, 0.2). Filled symbols in both figures correspond to objects which fall within 0.17 dex of the line and, conversely, the open symbols are assigned to the more distant objects below the envelope. It is remarkable, and certainly not fortuitous, that most survey objects are confined to a relatively narrow band. This shows that a sample of emission galaxies not biased towards high luminosity emission line objects (as is the case for objective prism detection surveys, for example) has relatively homogeneous spectral properties. Incidentally, LINERs from ill-defined samples such as those listed in Ferland and Netzer (which complements the subset of Heck-

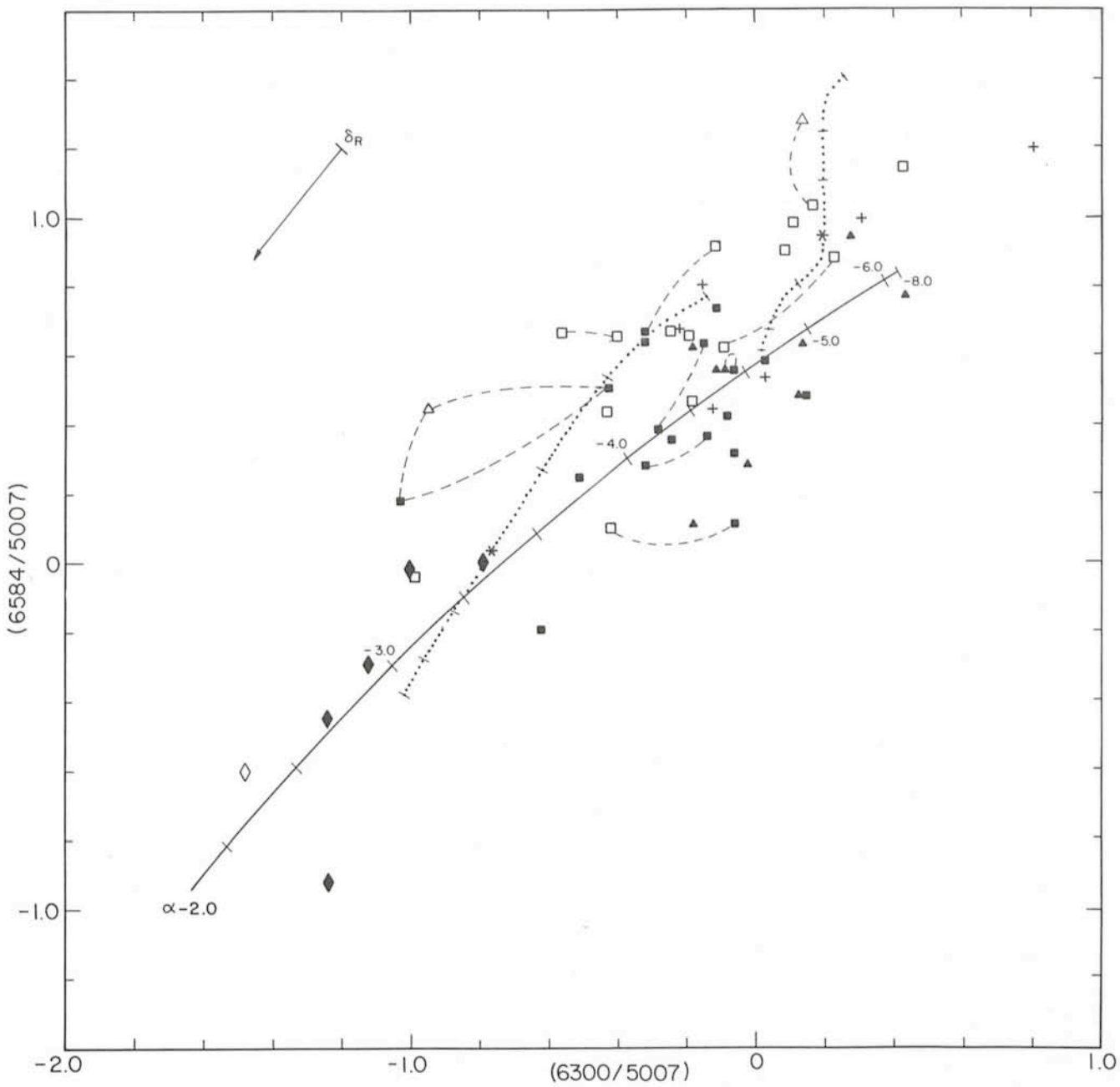

Fig. 2: *[NII]/[OIII] versus [OI]/[OIII] diagram. Symbols have the same meaning as in Fig. 1.*

man et al.), if included, considerably increase the scatter in the diagrams. They also have a clear tendency to appear significantly below the envelope. The explanation for this as well as for the particular position of open-symbol objects is probably that the clouds are optically thin or, alternatively, that these objects have superimposed nuclear HII regions besides the LINER phenomenon, as discussed in Binette (10). Metallicity variations are apparently not relevant here since a correlation exists between line luminosity of an object and its distance in Fig. 1 from the upper envelope. For this reason, we will concentrate on filled-symbol objects in the following discussion on abundances.

Photoionization Calculations

The smaller scatter in the new diagrams can be used to set some interesting limits on the variations of abundances from object to object. To determine, on the other hand, what these abundances are relative to hydrogen is a more difficult problem since the electronic temperature is unknown and some assumptions must be made concerning the shape of the UV ionizing spectrum which is responsible for the heating as well as for the ionization balance. As in Ferland and Netzer (6), the shape adopted here will be a power-law of index α ($F_\nu = k\nu^{\alpha}$) with no cutoff or extinction. The effect of varying α is illustrated in Fig. 1 for three sequences of models. The calculations were performed using the multipurpose code MAPPINGS (Binette (12)). All significant charge transfer reactions involving hydrogen or helium have been included and the effects of X-ray ionization on the ionic and thermal balance have been fully accounted for.

Previous photoionization calculations assumed only discrete values of the ionization parameter U (which expresses the density of impinging ionizing photons relative to the cloud's density). The present calculations on the other hand (the loci of which are shown as continuous lines) were

obtained by summing up the contributions of clouds at different distances from the ionizing source. This is justified since the emission in LINERs is spatially resolved and known to cover hundreds of parsecs in diameter. Because most spectrophotometric data were obtained through circular or square apertures, the spectrum likely represents a mixture of high and low ionization lines emitted at different radii, an effect taken into account in the present models. The filling factor (or number) of ionized clouds has been assumed to decrease exponentially with distance from a centrally located ionizing source; the cloud density was fixed at 400 cm^{-3}. It was assumed that the clouds were individually optically thick but because the observed filling factor is very small, the covering factor of (intervening) clouds was always considered negligible. This method, described in more detail in ref. 10, is obviously applicable to the gas-limited geometries thought to prevail in LINERs (cf. Keel (1)) rather than to radiation-limited geometries. Adopting a spherical distribution of clouds, the resulting models will hereafter be labelled "integrated". They are characterized by an effective U_e which is simply a weighted average of the ionization parameter. Fiducial marks along the continuous lines indicate successive values of Log U_e with a step of −0.3 between integer values (e.g. −3.0, −3.3, −3.6 . . .). In order to show the relative position of "non-integrated" models, calculations at values of Log U of −3.0 and −3.6 are represented by asterisks (left and right respectively). It is clear from Fig. 1 that integrated or discrete U sequences overlap quite well but with a systematic shift in the value of U between the two sequences.

The two dotted curves in Figs. 1 and 2 show the effect of varying the abundances (the asterisks are actually part of these curves) and the fiducial marks from left to right correspond to successive increases by factor two of all elements' abundances (except He) relative to hydrogen (from 1/8 to 8 times the reference set). The reference set of abundances was chosen to reflect the observed radial increase in metallicity in spirals as determined by supernova remnants' and HII regions' abundance analysis. Its main characteristics (by number) are as follows: He/H = 0.10, O/H = 0.001, O/N = 3.0 and O/S = 45 (for comparison, solar abundances would give: 0.085, 0.0008, 8 and 41 respectively). A mild depletion of the refractory elements C, Mg, Si has been allowed for.

In Figs. 1 and 2, the index $\alpha = -2.0$ appears the best choice for the objects as a whole and is adopted. In support of this we note that the observed upper envelope in Fig. 1 is probably a consequence of a moderately steep ionizing spectrum since, as shown by the dotted lines, varying abundances only populate a region below the maximum in OIII/Hβ that occurs around solar values. It must be emphasized that with the flatter indices used in previous work, this turnaround in the [OIII] intensity would only occur at very high metallicity so that with reasonable abundances [OIII] is then simply proportional to metallicity. This could explain how previous calculations favoured anomalous abundances of 0.3 solar since otherwise the majority of objects were found to be below the locus of their solar abundances' models.

As for the metallicity of the nuclear interstellar medium, the two dotted lines in Fig. 1 show the filled-symbol objects to be consistent with abundances that are roughly solar with variations in these probably confined to between solar and three times solar. This range of variations is smaller than in Keel (8) who derived an (N+O) abundance index that ranges from 0.88 to 4.7 times solar. Concerning nitrogen, the NII/OIII ratio of Fig. 2 scales almost linearly with the N/O abundance ratio and, therefore, the filled-symbol objects are considered consistent with variations in N/O not exceeding a factor three. It is to be noted that the determined average value (<N/O> = 1/3) is definitely above solar. Since many factors, such as observational errors, differences in the ionizing spectrum or reduced optical thickness, could account for part of the scatter in the figures, it is plausible that abundances are actually even more uniform than suggested here.

References

(1) Keel, W.C.: 1983, *Astrophys. J. Suppl.* **52,** 229.
(2) Stauffer, J.R.: 1982, *Astrophys. J. Suppl.* **50,** 517.
(3) Phillips, M.M., Jenkins, C.J., Dopita, M.A., Sadler, E.M. and Binette, L.: 1985, *Astrophys. J.* (submitted).
(4) Heckman, T., Balick, B. and Crane, P.: 1980, *Astron. Astrophys. Suppl.* **40,** 295.
(5) Heckman, T.: 1980, *Astron. Astrophys.* **87,** 152.
(6) Ferland, G.J. and Netzer, H.: 1983, *Astrophys. J.* **264,** 105.
(7) Halpern, J.P. and Steiner, J.E.: 1983, *Astrophys. J. Lett.* **269,** L37.
(8) Keel, W.C.: 1983, *Astrophys. J.* **269,** 466.
(9) Aldrovandi, S.M.V. and Contini, M.: 1983, *Astron. Astrophys.* **127,** 15.
(10) Binette, L.: 1985, *Astron. Astrophys.* (ESO preprint 350).
(11) Stauffer, J.R.: 1982, *Astrophys. J.* **262,** 66.
(12) Binette, L.: 1982, Ph.D. Thesis, Australian Nat. Univ., Canberra.

Absorption Lines of Interstellar C_2 and CN Molecules

E.F. van Dishoeck, Sterrewacht Leiden, the Netherlands, and
J.H. Black, Steward Observatory, Tucson, USA

Introduction

A considerable part of our knowledge about interstellar clouds stems from observations of their constituent molecules. In particular, diffuse interstellar clouds—i.e. clouds which do not entirely obscure the light from the stars which lie behind them—may be conveniently studied by the resonance absorption lines of the molecules superposed on the spectra of background stars. Already more than 40 years ago, the first three interstellar molecules CH, CH^+ and CN were discovered in this way at visible wavelengths. However, the next discovery of a molecule in the visible, C_2 (Souza and Lutz, 1977, *Astrophysical Journal* **216,** L 49), had to wait for the advent of high-resolution spectrographs with detectors that are very sensitive in the red part of the spectrum. At present, one of the best instruments in the world for these observations is the ESO Coudé Echelle Spectrometer (CES). The instrument has been described previously in the *Messenger* by Enard (**17,** 32 and **26,** 22), and its excellent performance has been demonstrated by the multitude of enthusiastic papers on CES observations in the last few issues of the *Messenger* (see e.g. Ferlet, **30,** 9; Andersen et al., **34,** 26).

Observations of molecules are not only interesting because they provide the abundance of the species in the interstellar

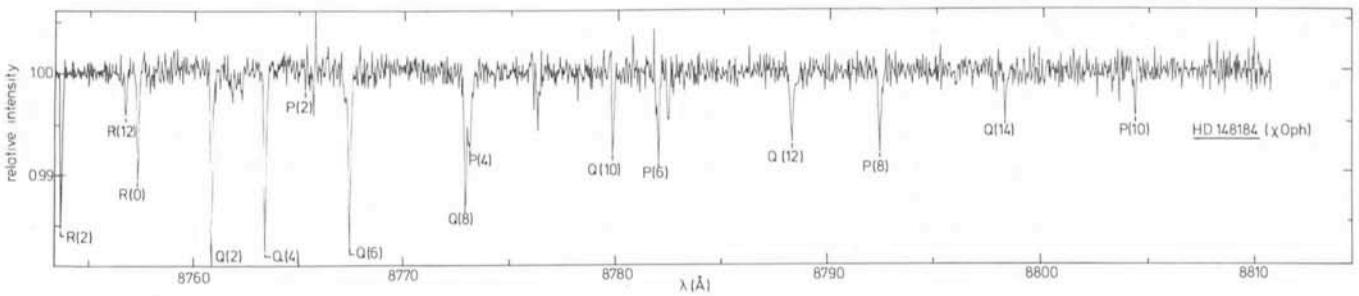

Fig. 1: *The spectrum of χ Oph in the region of the (2,0) Phillips band of C_2, obtained with the ESO CES fed by the CAT telescope. In addition to the lines shown in this figure, the R(4)-R(10) lines also appear shortward of the R(2) line. They are superposed on a broad stellar feature and are therefore not shown. Note that the strongest line absorbs less than 2 % of the starlight at this resolution.*

medium: they also may give valuable information on the physical conditions (such as temperature and density) prevailing in the cloud. C_2 is a particularly interesting molecule in this respect because it is a symmetric species with no permanent dipole moment. As a result, its excited rotational levels have long radiative lifetimes and may be highly populated in interstellar clouds by collisional and radiative processes. In contrast, molecules with a permanent dipole moment (such as CH and CN) are mainly in their ground rotational state.

What is Observed?

Fig. 1 shows part of the spectrum of the star χ Oph (V = 4.4, $A_v \simeq 1$ mag) in the region of the C_2 lines around 8750 Å, obtained with the CES fed by the 1.4 m CAT telescope (van Dishoeck and de Zeeuw, 1984, *M.N.R.A.S.* **206,** 383). A total of 10 hours of integration time at a resolving power of 80,000 was needed to obtain the high signal-to-noise ratio. No fewer than seventeen interstellar C_2 lines can be identified in the spectrum! The lines originate in the various rotational levels J of the ground vibrational state v = 0 of the molecule. They end in the v = 2 vibrational level of the first excited singlet electronic state, the so-called A state, of C_2. From each level J > 0 of the lower state, three different lines can arise, namely those for which the J quantum number in the upper state differs by −1, 0 or 1; they are designated by the P, Q or R lines, respectively. Thus the notation Q (2) indicates the Q line originating from J = 2 of the lower state. Fig. 2 illustrates the energy levels of the molecule involved and several observed transitions. Note that even a line arising in J = 14 has been observed: this level has an excitation energy corresponding to a temperature of more than 500 K — i.e. much larger than the kinetic temperature in the cloud! The equivalent widths of the strongest lines, e.g. the Q(2) line, are about 2 mÅ, those of the weaker observed lines only 0.5 mÅ.

The conversion of equivalent widths into column densities is a simple task for the C_2 lines, since the lines are unsaturated so that there are no curve-of-growth effects. As Fig. 1 shows, for several J values not only the stronger Q line, but also the weaker P and R lines have been detected. Since these lines originate from a common lower level J, they should yield the same column density for that level. In this way we have an excellent independent check on the reliablility of the results.

Interpretation

The column densities N_J indicate the number of C_2 molecules in the various rotational levels J. These populations are a measure of how internal energy is distributed on average within the molecule. In microscopic terms, temperature is a measure of the rate and force with which molecules strike each other in the gas; if the gas is in equilibrium these collisions govern the distribution of internal energy within the molecules as well. In that case, the rotational level populations in C_2 might provide a sort of remote thermometer. When N_J is plotted against the excitation energy E_J of level J, however, it appears that the populations cannot be characterized by a single (rotational) temperature. For χ Oph, the lower levels give $T_{rot} \simeq$ 65 K, while for the higher levels $T_{rot} \simeq$ 150 K. Both of these "internal" temperatures are higher than the kinetic temperature of the gas $T \simeq$ 40 K. Thus some mechanism other than collisions with gas particles is populating the excited J levels, and the C_2 molecules are not in complete equilibrium with the gas.

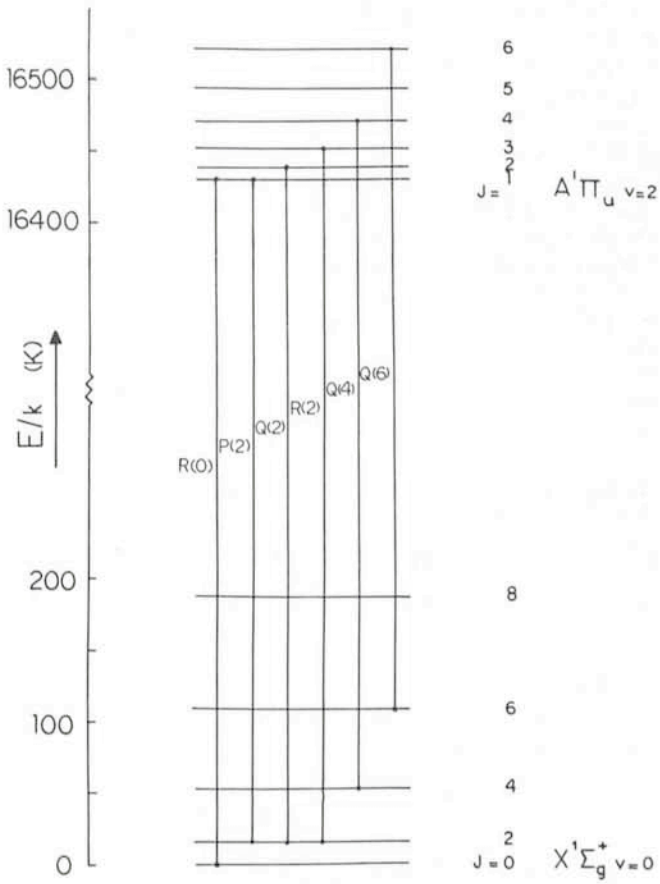

Fig. 2: *Energy level diagram of the A-X (2,0) Phillips band of C_2. Some of the observed transitions are indicated. Note that, because of symmetry considerations, only even J levels exist in the ground state of $^{12}C_2$. The energy scale has been converted to a temperature scale for convenience.*

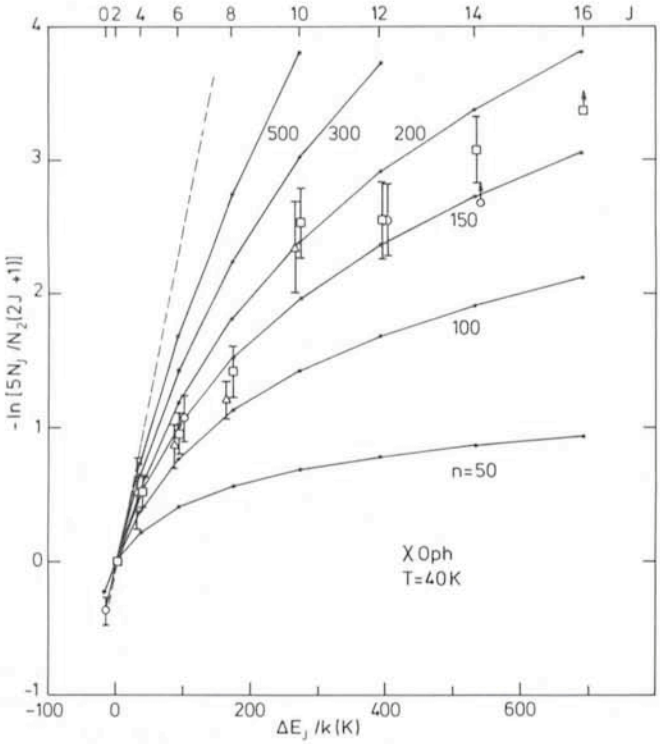

Fig. 3: *The theoretical relative rotational populations of C_2 as functions of the excitation energy (or rotational quantum number J). The solid curves were calculated for a kinetic temperature T = 40 K and several densities n (in cm^{-3}). The dashed line indicates the thermal distribution at 40 K. The observed populations for the cloud in front of χ Oph are indicated by various symbols. △: the column density N_J is obtained from the P line; □: N_J obtained from the Q line; ○: N_J obtained from the R line. Note the good agreement in general between the N_J's obtained from the different lines. Theory and observations are in harmony for T ≃ 40 K and n ≃ 160 cm^{-3}.*

How does this enhanced population arise? A radiative pumping theory has been suggested by Chaffee et al. (*Ap. J.*, 1980, **236,** 474), and developed in detail by the present authors (*Ap. J.*, 1982, **258,** 533). In this mechanism, the C_2 molecules first absorb photons from the interstellar radiation field at a high rate. The absorptions are primarily at wavelengths 8000–12000 Å with excitations into the first excited singlet electronic state, the A state. In Fig. 2, this process has been illustrated for the v=2 vibrational level of the A state (corresponding to the observed absorption lines), but excitations may also occur into v=0, 1, 3, etc. The molecules, however, will not stay long in the excited electronic state, but they will radiate spontaneously back into the various levels of the ground electronic state, the X state. In particular, the spontaneous emission occurs not only back into the levels from which the absorptions originated, but also into higher vibration-rotation levels of the ground state. These excited levels cannot decay subsequently through fast dipole transitions, because the C_2 molecule has no dipole moment. They may, however, cascade down into the rotational levels of the lowest vibrational state through slow quadrupole transitions and through intercombination transitions with a nearby triplet state. These radiative processes, governed by the strength of the interstellar radiation field in the (infra) red part of the spectrum, compete with the collisional (de-)excitation processes, governed by the interstellar temperature and density, in establishing the steady-state populations of the rotational levels J of the ground state. Theoretical rotational populations can thus be calculated for a given temperature, density and radiation field, provided all the molecular parameters entering the analysis (such as oscillator strengths and collisional cross sections) are well known. Unfortunately, even for a simple diatomic molecule as C_2, many of these molecular properties are still poorly determined! However, with the help of modern quantum chemical techniques at least some of the crucial parameters can be computed from first principles (see e.g. van Dishoeck, 1984, thesis Leiden).

Theory vs Observations

Fig. 3 shows the theoretical relative rotational population distribution of C_2 as a function of excitation energy $\Delta E_J/k$, for a kinetic temperature T = 40 K and several densities n (where n = n (H) + n (H_2)). Here ΔE_J is the excitation energy of level J relative to that of J = 2 (the level J = 2 is taken as the reference because its observational uncertainties are less than those for J = 0). The calculations are presented in a logarithmic form, with the statistical weights included, so that in the limit of high densities, where the population distribution becomes thermal, a straight line results. It is easily seen that for low densities, n ≃ 50–500 cm^{-3}—i.e. just the range of densities in diffuse clouds!—the population distribution is far from thermal; indeed, the radiative pumping theory correctly reproduces an enhanced population in the higher levels.

Fig. 3 includes the observed C_2 rotational populations toward χ Oph. The observations agree well with the theory for T ≃ 40 K and n ≃ 150–200 cm^{-3}. In this way, the C_2 observations may be used to extract temperatures and densities in the clouds, information which is still difficult to determine otherwise.

Observational Programme and Results

Until recently, absorption line observations of C_2 had been made in only a few directions, mainly on the northern hemisphere. Since C_2 appears to be such a useful tool for probing the physical conditions in diffuse clouds, we decided to extend the search to stars in the southern sky. For the first observations, only a few bright (V < 6) southern stars with large column densities of foreground interstellar matter (log $N(H_2)$ > 20.5, A_v > 1 mag) were selected. The initial list contained only three stars in Ophiuchus: ζ Oph, χ Oph and ϱ Oph. Beautiful C_2 spectra, such as the one shown in Fig. 1, were readily obtained in these directions (see also Danks and Lambert, 1983, *Astronomy and Astrophysics,* **124,** 188, and an unpublished paper by Charfman and Aardvark: "We two see C_2 too!"), and the physical conditions in the clouds in front of the stars were inferred.

Detection of the C_2 (3,0) Phillips Band

The results of the C_2 analysis (T ≃ 25 K, n ≃ 200 cm^{-3}) for the well-known cloud in front of ζ Oph were of great interest since previous studies had suggested either a much higher temperature T ≃ 65 K, or a much higher density, n > 1000 cm^{-3}. In order to check the C_2 results, we have very recently performed additional observations of ζ Oph, this time not in the region of the C_2 (2,0) Phillips band around 8750 Å, but of the (3,0) band around 7720 Å (van Dishoeck and Black, in preparation). The (first) detection of interstellar C_2 at these wavelengths is shown in Fig. 4, where several C_2 lines, originating from levels up to J = 10, appear. Because of the smaller oscillator strength for the (3,0) band compared with the (2,0) band, the features are very weak, but reliable column densities can be derived from them. The results appear to be in good agreement with those obtained from the (2,0) band observations, and they strongly suggest a low temperature T ≃ 25 K for the bulk of the ζ Oph cloud.

The pattern of the stronger absorption lines in Fig. 4 belongs to molecular oxygen in the Earth's atmosphere. During the

year as the Earth moves in its orbit around the Sun, its velocity relative to ζ Oph changes. Owing to the Doppler effect, this velocity produces a shift in the wavelengths at which the C_2 lines appear, relative to the positions of the stationary oxygen lines. Only at a certain time of year are most of the C_2 lines not directly obscured by oxygen lines: this effect had to be taken into account in preparing our ESO observations request. The second named author, who has a knack for making sign errors in such velocity calculations, was naturally nervous about the prediction, and was greatly relieved when C_2 lines appeared between the oxygen lines as expected.

Observations of Highly-Reddened Stars

Since the C_2 absorption lines lie in the far-red part of the spectrum where the extinction is much smaller than in the blue, they may be observed in thicker interstellar clouds than most other molecules, in particular the H_2 molecule for which only resonance lines in the UV exist. We have therefore extended our search for interstellar C_2 to fainter stars ($V \simeq 8$) with a higher reddening ($A_v \simeq 3$ mag). Such clouds with $A_v \simeq 3$ are very interesting since they are generally dense enough to permit radio observations. They would therefore bridge the gap between the classical diffuse clouds investigated only optically, and the classical dark clouds studied only with radio techniques. The C_2 searches have already been successful for the clouds in front of the stars HD 147889 ($V = 8.1$, $A_v \simeq 3$), HD 29647 ($V = 8.3$, $A_v \simeq 3$) and very recently HD 169454 ($V = 6.6$, $A_v \simeq 3$). The last two clouds appear to be quite cool, $T \simeq 15$ K with $n \simeq 350$ cm^{-3}, in agreement with radio observations. On the other hand, the C_2 data suggest that the HD 147889 cloud is warmer, $T \simeq 70$ K, than the temperature $T \simeq 40$ K, inferred from radio observations. Much remains still to be learned about such clouds.

C_2 Abundances

Apart from the physical conditions, information about the abundance of interstellar C_2 can also be extracted from the observations. For the classical diffuse clouds, such as that in front of ζ Oph, the total C_2 column density is about 2×10^{13} cm^{-2} and its abundance relative to H_2 is about 5×10^{-8}. For thicker clouds, C_2 column densities up to 10^{14} cm^{-2} are found. No comparison with H_2 column densities is possible in these clouds, since the background stars are too faint to permit UV observations of the H_2 lines.

Detection of the Red System of CN

Recent observations of the CN molecule (Federman et al., 1984, ESO preprint no. 336) suggest a very interesting relationship between the abundances of the C_2 and CN molecules. Although ion-molecule reactions are generally thought to control the formation of small interstellar molecules in diffuse clouds, a neutral-neutral reaction must be invoked to explain the observed relationship between the C_2 and CN abundances. Further observational tests of this relationship are clearly needed, especially for denser clouds. So far, all CN observations have been performed in the blue around 3874 Å. However, there also exist resonance lines of CN in the red around 7900 Å, which are more suitable for studying the denser clouds. These lines have been observed extensively in the atmospheres of cool stars and comets, but not previously in the interstellar medium. If the relationship between the C_2 and CN abundances would also hold for the denser clouds with $A_v \simeq 3$ mag, then the clouds which have large C_2 column densities should also show strong CN lines. As a test, we have performed very recently observations (van Dishoeck and Black, in preparation) around 7900 Å toward the star HD 169454, which shows strong interstellar C_2 lines. A two-hour integration produced clearly the strong $R_1(0)$ line of CN with an equivalent width of about 9 mÅ! In addition, the $^RQ_{21}(0)$, $^SR_{21}(0)$, $R_1(1)$ and $^RQ_{21}(1)$ lines have been detected, whereas the $Q_1(1)$ and $^QR_{12}(1)$ lines are lost in atmospheric features. These atmospheric absorptions are due to water vapor; in order that they be as weak as possible, it is advantageous to have a very dry observational site like La Silla (see Brand, *The Messenger* **29,** 20).

This (first) observation of the red system of interstellar CN is not only interesting for the determination of the CN abundance. It may also provide an important tool for measuring the temperature of the cosmic microwave background radiation at 2.64 mm wavelength by comparing the strengths of the lines originating from $J = 0$ and 1. Because CN has a large dipole moment, the population in $J = 1$ is very small and it can only be maintained by absorption of the cosmic background radiation. This analysis of the rotational population of CN has been done previously using lines in the blue system of CN (see e.g. Meyer and Jura, 1983, *Astrophysical Journal,* **276,** L1) with the result $T_b = (2.73 \pm 0.04)$ K, in agreement with a 2.7 K blackbody spectrum. A preliminary analysis of the red system gives $T_b = (2.6 \pm 0.3)$ K. Although this result is not yet as accurate as for the blue system, it provides an independent measure of T_b. Obviously, the data may be improved upon by using longer integration times or by choosing a more suitable background star, such as HD 147889 or HD 29647.

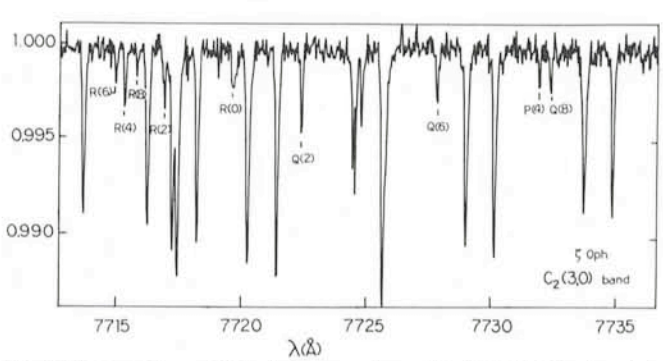

Fig. 4: *The spectrum of ζ Oph in the region of the (3,0) Phillips band of C_2, obtained with the CES. The total integration time was 7 hours. All features without identification are due to molecular oxygen. The C_2 Q(4) line is lost in one of them; the Q(10) line has been detected longward of 7735 Å.*

Concluding Remark

Because the CES affords very high resolution with excellent sensitivity in the far red part of the spectrum, it is now possible to invade the domain of radio astronomers and probe the interior of molecular clouds using optical absorption lines. Because the CES is so convenient to use, it is also possible for theorists like us to masquerade as observers from time to time with some success!

ESO-IRAM-Onsala Workshop on (Sub)mm Astronomy

In the context of the planned installation at La Silla of the 15 m (sub)mm telescope "SEST", a workshop will be held near Onsala from 17 to 20 June 1985. The scientific aspects will be stressed, and in particular the connection with work at other wavelengths. Further information may be obtained from Dr. P. Shaver at ESO in Garching.

Polarization Measurements at La Silla

T. Korhonen[1], V. Piirola[2], and A. Reiz[3]

[1] *Turku University Observatory*
[2] *Helsinki University Observatory*
[3] *Copenhagen University Observatory*

During February this year measurements of interstellar polarization were carried out at La Silla. We used the Danish 1.5 m telescope equipped with a new type of multichannel double beam chopping polarimeter designed by one of us (V.P.). One of the purposes of our mission was to test the polarimeter and matching data acquisition system, and, in doing so, evaluate the performance of the equipment. The polarimeter was built in the shop of the Turku University Observatory under the supervision of T.K. Below, we shall describe the construction of the polarimeter and the aim of the programmes that were executed; we shall also report on some of the results obtained:

The polarimeter, which can easily be changed into a multichannel photometer, is a further development of an earlier design, described by V. Piirola (1973, 1975). The principle of the operation of the instrument is given in Fig. 1. The focal plane diaphragm has two apertures. The light of the observed star passes one of the apertures while the other allows an amount of background, equal to that which traverses the star aperture, to enter the instrument in the photometric mode (Fig. 1a). A rotating chopper alternately closes one of the apertures, leaving the other free, with a chopping frequency of 25 Hz. Thus the photocathode is illuminated alternately by the star and the sky apertures. The field lens forms on the photocathode an image of the telescope mirror, the exit pupil,

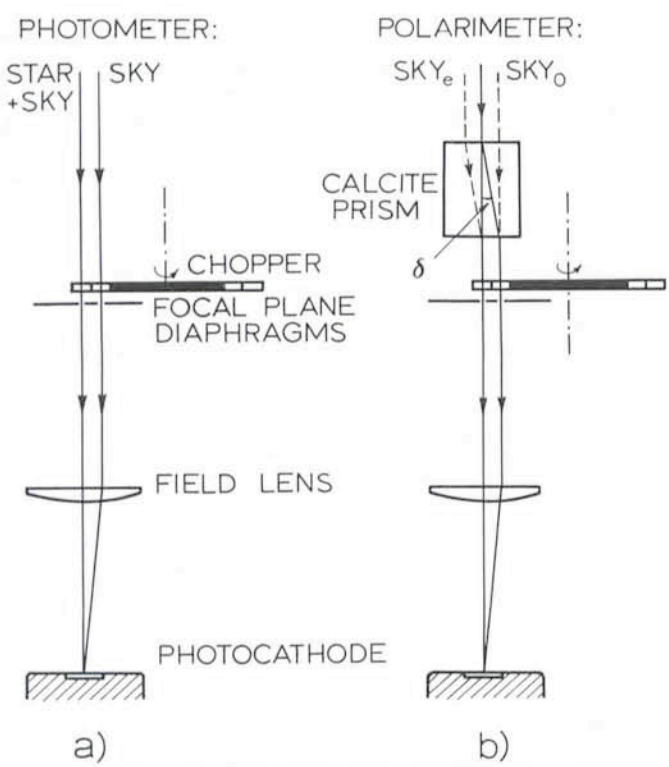

Fig. 1: *Principle of operation of the double beam chopping photometer-polarimeter.*

through which the flux of both the star and the sky passes. Thus the radiation falls always on the same part of the cathode. The chopper also controls the light of two infrared emitting diodes which alternately illuminate two photodiodes. With the help of the signals of the photodiodes the registration electronics is synchronized so as to count pulses corresponding to the star and the background diaphragms separately by means of two counters.

When the instrument is used for polarization observations, a plane parallel calcite plate is inserted in front of the focal plane, Fig. 1b. At the upper boundary the incoming light is divided into two mutually perpendicularly polarized components. The ordinary rays are refracted according to the normal refraction law but the extraordinary rays are deviated by an angle 6°14′. At the lower boundary the extraordinary rays are refracted back to their original direction. The result is a parallel displacement of the extraordinary rays. Hence, two perpendicularly polarized images of a star are formed in the focal plane of the telescope.

The calcite plate is dimensioned and oriented in such a way that when the ordinary image is centred in the star diaphragm the extraordinary image is automatically centred in the background diaphragm. Thus the polarized components are measured like star and sky in photometry and no changes in the equipment, except inserting the calcite plate and refocussing, are necessary. The Stokes parameters of the linearly polarized light are usually computed from measurements made in eight different position angles of the instrument. The construction has another important advantage: As we can see from Fig. 1b, both components of the sky background pass both diaphragms, and polarization of the sky is directly eliminated.

The direct elimination of the sky background polarization has been found especially valuable in the observations of faint stars and in moonlight. If a considerable amount of the background radiation is composed of scattered light, it can be highly polarized and very small relative changes in the sky background could cause large errors in the measured stellar polarization. Also the very small value of systematic errors obtained for brighter stars may be in part the result of the effective cancellation of the background polarization.

A new multichannel version of the polarimeter was put into operation in the Metsähovi Observatory of the University of Helsinki in early 1979. The colour bands (UBVRI) are separated by dichroic filters, which reflect a desired spectral interval and transmit the other wavelengths. By using four such selective beam-splitters the light is directed to five photomultipliers for strictly simultaneous recording. The resulting passbands are close to the standard UBVRI system, with equivalent wavelengths 0.36, 0.44, 0.53, 0.69, and 0.83 μm, respectively. The photomultiplier box is freon cooled to −20° C to reduce the dark current of the gallium arsenide photocathodes of the R and I photomultipliers.

The operation of the polarimeter is controlled by a microprocessor unit which is a modification of the KLT Data Adapter, programmed for the data acquisition and reduction with the chopping polarimeter. The unit is commercially available from KLT Elektroniikka Oy, Linnankatu 1, SF-00160 Helsinki 16, Finland. The present version is capable of counting pulses from five photomultipliers into 2 × 5 registers in the chopping mode. A complete polarimetric observation consists of eight integrations of starlight in different orientations of the polarimeter or the retarder, from which the normalized Stokes

parameters, average intensities and error estimates from photon statistics are computed and printed.

In the automatic mode the processor generates pulses for the stepping motor rotating the retarder in front of the calcite plate. For linear polarization observations a half-wave retarder and for circular polarization a quarter-wave retarder is used. After the eight integrations the results are computed and listed. New observation is started automatically. The background values are stored and updated with desired intervals, usually about every 15 min. In the manual mode each integration is initiated by a start command. This mode is used in the most stringent applications where the whole polarimeter is rotated in steps of 45°.

The instrument is changed to a multichannel sky-chopping photometer by removing the calcite plate from the beam. Conventional (non-chopping) photometry is also possible, as it may be desirable in the case of bright stars and negligible sky intensity, or surface photometry with large diaphragms.

The multichannel polarimeter has been used in 1979–81 in the Metsähovi Observatory, and since 1981 in the Crimean Astrophysical Observatory, mainly for studies of interacting close binaries (see e.g. Piirola and Vilhu, 1982, Piirola et al., 1983, Efimov et al., 1984). The instrument for the present observations at La Silla is practically identical to the aforementioned polarimeter. Some modifications were made in the polarimeter head to enable a remote TV-control with the Danish 1.5 m telescope.

The following three programmes were carried out during the 17 nights allocated:

(i) measurements of polarization of stars with very small polarization, taken from J. Tinbergen's list (Tinbergen, 1979);

(ii) measurements of stars with large polarization, $P \geqq 1\%$, taken from D.S. Mathewson and V.L. Ford (1970), K. Serkowski (1974), and from J.S. Hsu and M. Breger (1982);

(iii) measurement of A and F type, Population II stars, of intermediate and high galactic latitudes for which good Strömgren four-colour and Hβ photometry exist (J. Knude, 1981).

(i) The programme was designed for determining the instrumental polarization, that is the polarization due to telescope and polarimeter. The 35 stars that were measured in the U, B, V spectral regions during two nights are all nearby objects and their interstellar polarization should, therefore, be negligible. Thus the mean values of the observed Stokes parameter, $\overline{P}_x$, $\overline{P}_y$, represent the instrumental polarization by means of which the observed P_x, P_y must be corrected. When subtracting the instrumental polarization each colour was treated separately. In comparing our results with Tinbergen's (1982), denoted by 1/2(I + II) (see his Table 5) we have taken the average of our B and V parameter values. The small difference in effective wavelength, in the sense that ours is shorter, will hardly influence the results. Taking Tinbergen's values as reference, we get the following deviations in units of 10^{-5}:

$$\Delta P_x = -4.3 \pm 1.9$$
$$\Delta P_y = 3.9 \pm 1.5$$

In Table 1 we have listed the differences between Stokes parameter values for three other sources taken from Table 4 in Tinbergen's paper.

TABLE 1

	Schröder Tinbergen	Serkowski Tinbergen	Serkowski et al. Tinbergen	KPR Tinbergen
$\Delta\overline{P}_x$	-5.4 ± 1.5	-3.3 ± 2.9	-8.0 ± 4.3	-4.3 ± 1.9
$\Delta\overline{P}_y$	4.9 ± 1.9	1.2 ± 3.6	-0.7 ± 3.7	3.9 ± 1.5

Taking the weighted arithmetic mean of the first three sets of data, we get –5.2 and 3.3, respectively, in units of 10^{-5}, which differ by less than one unit from our ΔP_x, ΔP_y. It should be kept in mind that the Serkowski and Serkowski et al. data are from observations with a rotatable telescope. We conclude that systematic errors in our polarization values due to instrumental polarization are less than $2 \cdot 10^{-5}$.

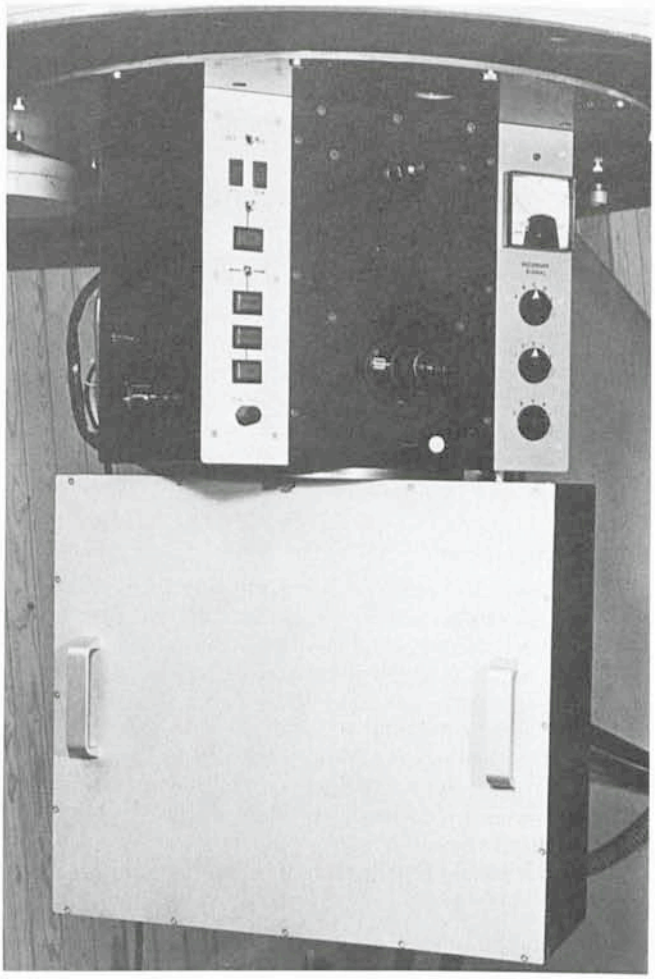

Fig. 2: *The simultaneous five colour photopolarimeter attached to the Danish 1.5 m telescope. The lower box is freon cooled to –20° C and contains five photomultipliers to which light is directed through dichroic filters.*

(ii) Measuring stars with high polarization, $P \geqq 1\%$, would enable us to judge the quality of our material from several points of view. In this category we have observed 5 stars from the list of Hsu and Breger of polarization standard stars. 17 stars are common with those observed by Serkowski et al. for studying the wavelength dependence of interstellar polarization. Additional objects are from the Mathewson and Ford catalogue.

A comparison of our polarization values with those of Serkowski et al. leads to the following regression lines for the U, B, V pass bands:

$$P^U(\mathrm{KPR}) = \underset{\pm.017}{1.073}\, P^U(\mathrm{Serk}) - \underset{\pm.033}{0.097}$$
$$P^B(\mathrm{KPR}) = \underset{\pm.016}{1.015}\, P^B(\mathrm{Serk}) - \underset{\pm.036}{0.084}$$
$$P^V(\mathrm{KPR}) = \underset{\pm.014}{1.043}\, P^V(\mathrm{Serk}) - \underset{\pm.033}{0.077}$$

Not unexpectedly the largest deviations are found in the U channel. These relations should be regarded as preliminary and may be slightly changed by a more refined statistical

treatment. We have done the same excercise comparing our polarization values with those of Mathewson and Ford, measured in the B region. Three stars for which polarizations differ markedly have been omitted. We have made two least square solutions, one where the star HD 160529, P = 7.12 has been omitted

$$P(KPR) = 1.010\ P(MF) - 0.032,\ \text{HD 160529 omitted}$$
$$\pm.0.14 \qquad \pm 0.030$$
$$P(KPR) = 1.010\ P(MF) - 0.031,\ \text{HD 160529 included}$$
$$\pm.010 \qquad \pm 0.024$$

They give identical results. Repeating the solution, assuming errors in both coordinates, we get the values 1.016 and −0.042, respectively.

The same material has been used for examining how well our data fit Serkowski's empirical formula relating the ratio $P(\lambda)/P(\lambda_{max})$ to the corresponding ratio λ_{max}/λ (Serkowski et al., 1975)

$$P(\lambda)/P(\lambda_{max}) = \exp(-K \ln^2 \lambda/\lambda_{max}),\ K = 1.15 \qquad (1)$$

Recent polarization observations in the near infrared by B.A. Wilking et al. (1980, 1982) have led to a revised form of this relation reflecting a linear variation of K with λ_{max}. However, for the optical region in which our observations have been made, the two expressions will give almost identical results.

Even though the material is limited, 37 stars observed in the U, B, V, R spectral regions, most of them during more than 10 nights and none less than two nights, we think that the observations fit the curve calculated from Eq. (1) quite well (Fig. 3). Summing up the results obtained from a preliminary analysis of the large polarization data, we conclude that they show very minor scatter, the systematic errors being at the 10^{-4} level.

(iii) With regard to the third group of stars our plan was to reobserve those A and F Population II objects of intermediate and high galactic latitude for which well determined colour excesses and distances were available (J. Knude, 1981) and for which polarizations had been measured in an earlier run, March 1980. Altogether about 200 stars had been observed in the B spectral region, distributed over 8 areas. The instrument used on that occasion was a prototype of the present double beam chopping polarimeter (Piirola 1973 and 1975).

The purpose of the programme was to study the correlation between polarization and colour excess in an endeavour to determine an upper limit for the ratio between these two quantities and hence a lower limit for the colour excess. Various attempts based on photometric observations have been made in recent years to determine the interstellar reddening in the polar caps (c.f. Appenzeller, 1975). With the exception of Knude's photometric work, using Strömgren four-colour and Hβ photometry in much denser net than before, the results have come out negative or inconclusive. On the other hand accurate polarimetry has demonstrated that light from stars in the galactic polar caps is polarized, and that, therefore, interstellar dust must be present also at high galactic latitudes. It would then be of considerable interest to fix an upper limit for the ratio between polarization and colour excess. In the paper by Serkowski et al. the following upper limit has been derived:

$$P_{max}/E(B-V) \leqq 0.195, \qquad (2)$$

where P_{max} is the maximum interstellar polarization.

This relation, which puts a lower limit on the colour excess, seems to hold for most galactic stars, also for objects in regions where the interstellar reddening law deviates noticeably from its standard form.

Our polarization measurements from the 1984 run are complete for only 4 areas; the number of stars observed is 85,

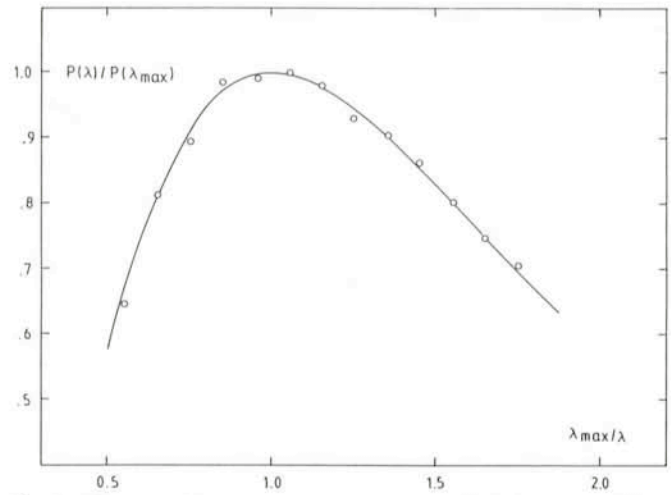

Fig. 3: *The normalized wavelength dependence of interstellar linear polarization derived from observations with the double beam chopping polarimeter at La Silla. The open circles represent mean values of $P(\lambda)/P(\lambda_{max})$ calculated for equidistant arguments of λ_{max}/λ. The solid line represents equation (1). The figure is based on 165 polarization measurements in the UBVRI pass bands.*

of which 70 have reliable colour excesses. During the 1980 run the polarization in the B pass band was recorded for 172 stars for which colour excess and distance were available (Knude, 1981). We have, therefore, resolved to make use of this material. In Table 2 we have given mean values of polarization and colour excess for the 8 areas.

TABLE 2

$\bar{l}$	$\bar{b}$	$\bar{p}$ %	$\bar{E}$(B–V)	$\overline{p/r}\,10^6$	N
23°	82°	0.050	0.019	7 ± 1	23
282	66	.095	.021	14 ± 2	36
38	60	.122	.009	18 ± 2	22
352	60	.363	.029	52 ± 8	16
9	50	.213	.018	23 ± 2	18
232	46	.076	.019	13 ± 2	26
12	38	.492	.053	64 ± 9	13
23	29	.676	.076	96 ± 14	18

Adopting a linear relation between $\bar{P}$ and $\bar{E}$(b–y) we get

$$\bar{P}_m = 0.163\,\bar{E}(B-V) - 0.001, \qquad (3)$$

P_m polarization in magnitudes, where we have used the relation 1.42 E(B–V) = E(b–y) and further assumed that $\bar{P}$ and $\bar{E}$ are both liable to errors. The slope of the regression line, 0.163, is lower than the value 0.195 quoted from Serkowski et al., which refers to the maximum interstellar polarization and the colour excess E(B–V). It lies also below the often cited value 0.18 (see e.g. Mathewson and Ford). As an order of magnitude estimate of the interstellar reddening at the north galactic pole we take from Table 2 $\bar{P}$ = 0.050 %; by means of Eq. (3) we get $E(B-V) \geqq 0.007$ which is lower than the value 0.012, derived from P_{NGP} = 0.0020 given by Appenzeller (1975).

In Table 2 we have also listed mean values of P/r for each of the 8 areas (r is the distance in parsec). There is marked scatter from $7 \cdot 10^{-6}$, which coincides with the value given by Markkanen (1979, 1975) to a value 14 times larger at the galactic latitude ~30°. It should be kept in mind, when comparing these data with those given by Tinbergen (Table 7), that, in our case, the stars for which polarization has been measured have distances ranging from 50 to 650 parsecs with the majority larger than 150 parsecs.

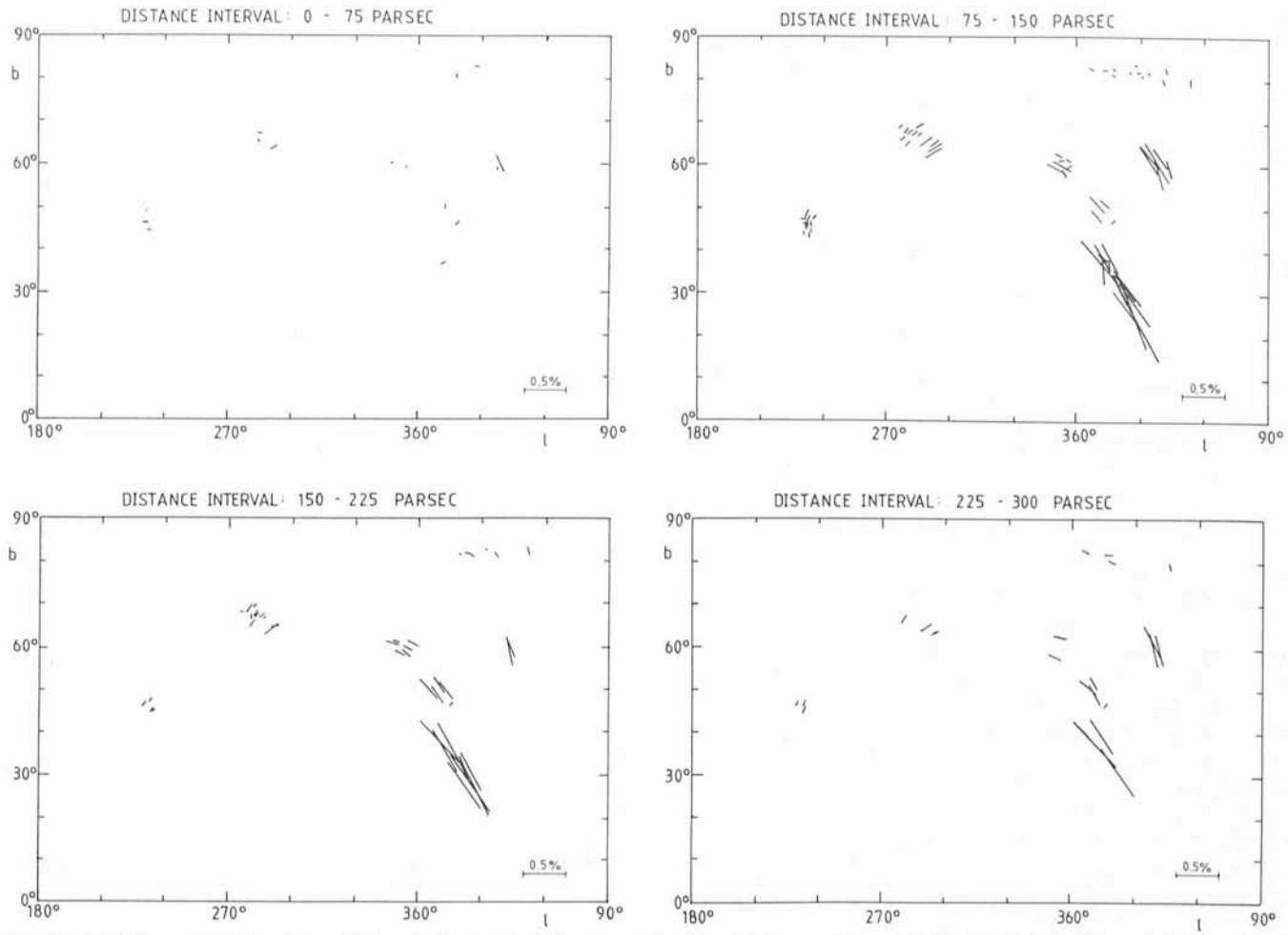

Fig. 4: *Interstellar polarization of A and F Population II stars in 8 areas, plotted in galactic coordinates for different distance intervals. The length of the bars indicates the amount of polarization, their orientation the electric field vectors.*

The polarization measured in 1980 for all A and F Population II stars for which reliable distances were available have been plotted in galactic coordinates (Fig. 4). The length of the line is a measure of the polarization, the orientation is relative to the north galactic pole. For stars closer than 75 parsec, there is no sign of parallel orientation of the E vectors; the interstellar polarization of stars in this group is markedly smaller than for the other distance groups, hence the position angle shows a considerable scatter. The low interstellar polarization suggests a low dust content in this part of space. There are too few stars in this sample to decide whether there is an increase in polarization and hence in dust content at lower galactic latitudes. There is clearly a discontinuity between the interstellar polarization of stars in the first distance group and those at distances larger than 75 parsec; but one cannot tell from the present material *where* the discontinuity sets in. For stars at distances larger than 75 parsec the orientation of the E vector is approximately the same in each area and distance group. There are no clear signs that interstellar polarization increases with distance. There is a clear indication of increasing interstellar polarization when moving towards the galactic plane, but this could, in part, be explained by local effects.

The observations of the interstellar polarization in the southern sky will be continued in November 1984. Further planned work includes e.g. simultaneous multicolour polarimetry and photometry of magnetic compact binaries (AM Her-type). These objects have a white dwarf component whose field ($B > 10^7$ Gauss) controls the accretion flow onto the magnetic poles. Optical cyclotron radiation is emitted from the fast electrons moving in the magnetic field. This results in high circular polarization (10–30 %) of the observed light, varying with the phase of the orbital period, as the angle between the line of sight and the magnetic field changes. Simultaneous observations in different colours are essential due to the short periods ($P < 3$ h) and the rapid flarelike activity.

There is considerable interest also in star forming regions and young stellar objects. Polarimetry is an effective tool in monitoring circumstellar dust envelopes and particle size distribution. Work is also being done on later stages of stellar evolution, e.g. rapidly rotating giant stars (FK Comae-type) which probably are the result of the coalescence of the components of a close binary star system.

The project has been supported by the Carlsberg Foundation and the Danish Board for Astronomical Research. We are indebted to Leena Tähtinen, who assisted at the telescope and was of great help in reducing the observations.

References

Appenzeller, I.: 1957, *Astron. Astrophys.* **38,** 313.
Efimov, Y.S., Piirola, V., and Shakhovskoy, N.M.: 1984, *Astron. Astrophys.* (in print).
Hsu, J.C. and Breger, M.: 1982, *Astrophys. J.* **262,** 732.
Knude, J.: 1981, *Astron. Astrophys. Suppl.* **44,** 225.
Markkanen, T.: 1979, *Astron. Astrophys.* **47,** 201.
Mathewson, D.S., Ford, V.L.: 1970, *Mem. Roy. Astron. Soc.* **74,** 139.

Piirola, V.: 1973, *Astron. Astrophys.* **27,** 383.
Piirola, V.: 1975, Ann. Acad. Scient. Fenn. Series A, VI. Phys. 418.
Piirola, V. and Vilhu, O.: 1982, *Astron. Astrophys.* **110,** 351.
Piirola, V., Vilhu, O. and Tuominen, I.: 1983, in Cataclysmic Variables and Related Objects, M. Livio and G. Shaviv (eds.), Proc. IAU Coll. No. 72, **101,** p. 207.
Piirola, V.: 1983, ibid., p. 211.
Serkowski, K.: 1974, in Methods for Experimental Physics, Vol. 12, Astrophysics, Part A, Eds. M.L. Meeks and N.P. Carelton, p. 361, Academic Press, New York.
Serkowski, K., Mathewson, D.S., Ford, V.L.: 1975, *Astrophys. J.* **196,** 262.
Tinbergen, J.: 1979, *Astron. Astrophys. Suppl.* **35,** 325.
Tinbergen, J.: 1982, *Astron. Astrophys.* **105,** 53.
Wilking, B.A., Lebovsky, M.J., Martin, P.G., Rieke, G.H. and Kemp, J.C.: 1980, *Astrophys. J.* **235,** 905.
Wilking, B.A., Lebovsky, M.J. and Rieke, G.H.: 1982, *Astron. J.* **87,** 695.

Chromospheric Modelling in Late-Type Dwarfs: 1. Quiescent Objects

J. Beckman, Instituto de Astrofísica de Canarias
L. Crivellari, Osservatorio Astronomico di Trieste
B. Foing, Observatoire de Meudon and ESO

1. The Purpose of Chromospheric Modelling

Observational facts about chromospheres are now well established. The existence of a layer at a higher temperature than the underlying photosphere in a star like the Sun gives rise to "superthermal" emission features of relatively low excitation which are strong and easily recorded. Nevertheless, there are many unanswered basic questions about chromospheres which still merit the attention of observers and theorists alike. In a recent article in the *Messenger* (No. 35) Pallavicini described some of the observations which go into producing a picture of a typical chromosphere. He dwelled in particular on two types of observations which can be made with the CES (Coudé Echelle Spectrograph) which operates with either the 3.6 m or the CAT at La Silla. These were the use of high spectral resolution to try to derive the rotational velocities of slowly rotating objects via Gray's asymmetry method, and close examination of the cores of the Ca II H and K emission lines. He also picked out X-ray luminosity, measured by the Einstein satellite, as a parameter strongly correlated with rotation, and hence with the existence and strength of chromospheres.

In this article we will be dealing more directly with some of the problems which arise when trying to use observational material to clarify the mechanisms which heat the chromosphere of a late-type star, in order to obtain a clear physical picture of what a chromosphere is like, how it is related to the underlying photosphere, and to the overlying corona. It is usually said that the chromospheres of late-type stars are heated by mechanical deposition of energy from the convective zone of the upper photosphere, or alternatively by magneto-acoustic energy. To what extent can we distinguish in practice between these two mechanisms, and is either of them the same as that which heats coronae? How directly can we translate information given to us in the form of high resolution line profiles of, say, the H and K resonance lines of Ca II, or their Mg II h and k analogues into a semi-empirical model which incorporates energy sources and their distribution with depth. We will illustrate our points with observations taken with the CES and also with the IUE satellite long wavelength spectrograph.

2. Reliable Data and Reliable Interpretation

The cool star observer has an apparently major asset compared with those who are trying to interpret the spectra of other stars, which is his ability to make comparisons with the Sun. This can, however, be misleading, and as an example we can cite our experience with IUE spectra in the h and k resonance lines of Mg II. Thanks to some careful and beautiful balloon-borne solar spectroscopy by Lemaire and Skumanich (*Astronomy and Astrophysics,* **22,** 61), it was clear as early as 1973 that a chromospheric emission line would have a significantly different appearance and strength depending on whether it came from the quiet chromosphere or from a plage "active" region; its strength varies from one chromospheric regime to another, from plages, to supergranular cells, to cell boundaries. To some degree also the shape changes, so that the central self-absorption appears differentially shifted with respect to the chromospheric emission core. Clearly, even from this small sample of information we can see that it will not be easy to interpret the spectra of other stars, which are of course the integrated products of all the regions of their chromospheres. In a star which may have stronger velocity fields than the Sun, it will be hard to take out the line structure imposed by the combination of velocity fields, leaving only the dependence of density, electron density and temperature with height, which must typify the model. In fact the Mg II spectra of G dwarfs taken with IUE, of which four examples are shown in Fig. 1, appear to give striking evidence for the widespread existence of such velocity fields. The central self-absorption is displaced by several km s^{-1} with respect to the emission core, sometimes to the red, sometimes to the blue. Most papers dealing with Mg II until 1983 (with the notable exception of one by Bohm-Vitense) dealt with such line profiles as showing evidence for chromospheric motions, although few attempts were seriously made to provide physical explanations. The values for the red-shifts or blue-shifts were from a few km s^{-1} to ten or even twenty. It is inconceivable that whole chromospheres could be moving outwards or inwards at those kinds of speeds, but one problem was that accurate absolute velocity data with IUE were hard to derive (typical precision was of order $\pm$ 10 km s^{-1}), so it was never wholly clear whether the emission or the self-absorption at the centre was shifted with respect to the photospheric radial velocity. Circumstellar shells, either in expansion, or even in collapse, could be ruled out as the mass-losses or mass accretions implied were orders of magnitude too large. Finally, after several years of effort in improving the wavelength and photometric fidelity of the spectra, it could be ascertained that the whole story was a "red herring" (or a blue herring as the case may be) in that most

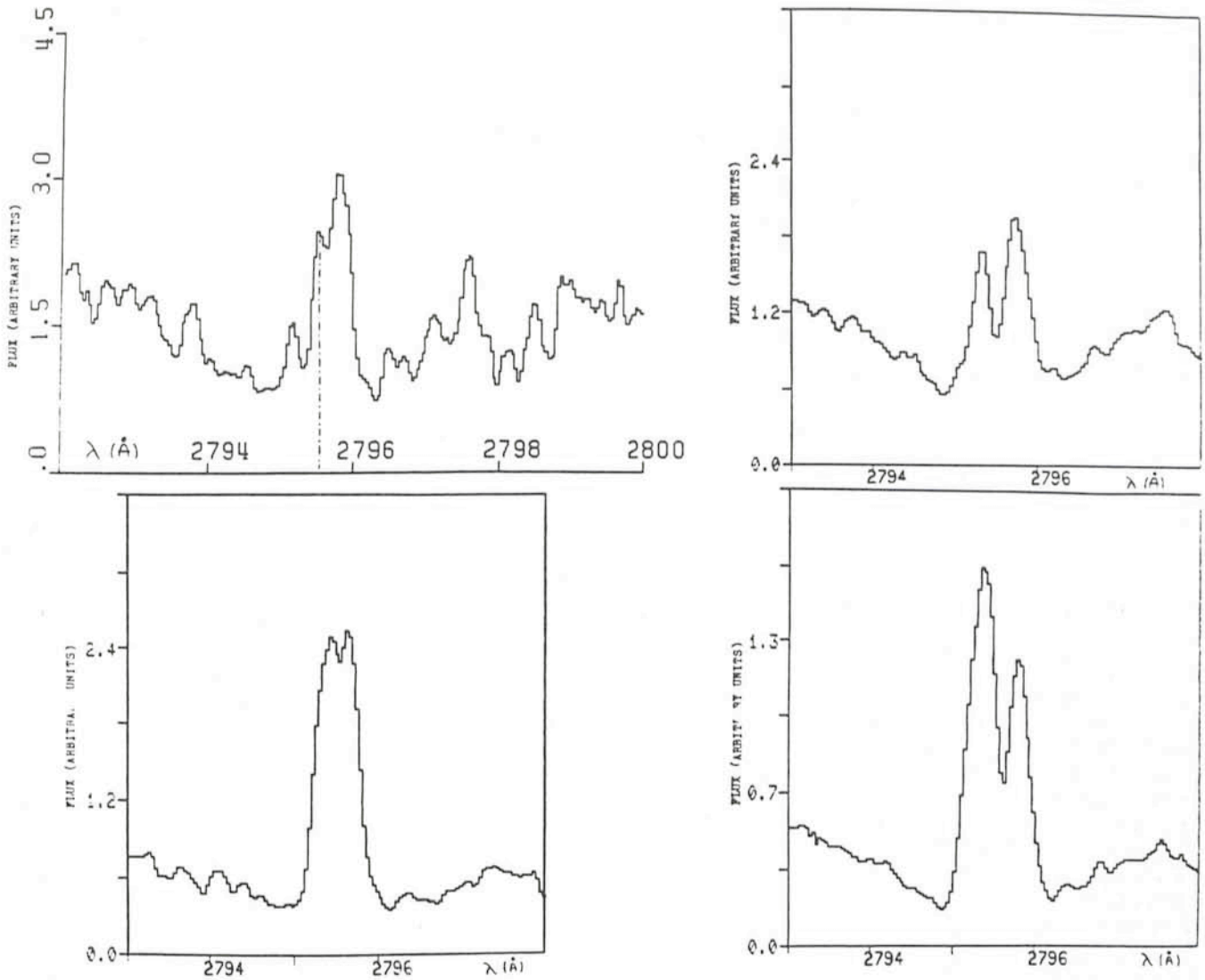

Fig. 1: *Mg II k lines from the chromospheres of four late-type stars: (a) β Hya (G2 IV); (b) ζ Tuc (G2 V); (c) τ Cet (G8 V); (d) δ Pav (G8 IV). The strikingly different central self-absorptions within the chromospheric emission cores are due to the LISM (local interstellar medium).*

of the absorptions could be identified with the local interstellar medium (LISM).

Fig. 2 gives the vital clue to the separation of chromospheric from LISM components. We can see the spectrum of β Hya taken with the CAT+CES compared with an IUE high resolution spectrum, and hence a comparison of Ca II K with Mg II k. The Mg II emission core, as well as exhibiting a different profile, shows two absorption features, while the Ca II core shows only one. With our improved velocity resolution (± 4 km s^{-1}) we were able to identify the blue-shifted feature with a cloud in the ISM, because its velocity coincides with that predicted by Crutcher from Lyα data using Copernicus. We could then go on to identify LISM features in many nearby late-type stars, and thereby map the LISM down to 3 pc from the Sun, so intense are the Mg II absorptions. The reason for the absence of any equivalent features in the Ca II spectra is simply one of lower abundance, and slightly less favourable IS excitation conditions for Ca II. We now know that the best way to avoid LISM effects is either to choose a line of sight where its radial velocity is large enough to take the absorption feature right outside the chromospheric core, or to observe in the direction of a "hole" in the LISM. This work has now brought us to the point where we can make serious use of IUE spectra to examine the effects of both velocity and intensity fields in the chromospheres of stars, with signal-to-noise ratios of the order of 30 : 1 in the h1 and k1 intensity minima.

3. Why Simple Models Cannot Predict Line Shapes

Fig. 3 shows the full panoply of chromospheric lines which we can now use: Hα, Ca II K, and the Ca II infrared triplet, all taken with the CES, and Mg II h and k taken with IUE. These profiles relate to different but overlapping depths in the chromosphere. Can we use them to derive meaningful models? Such models normally comprise the run of temperature and total pressure with depth above a reference level (typically the photospheric level where the optical depth in the continuum at 5000 Å is unity), together with the depth dependence of electron density, and the atomic and ionic densities of the more important components. Once such a model has been established, the problem of providing a consistent set of energy sources as a function of depth becomes much more tractable. Of course, the arguments are going to be somewhat circular, because there is always some degree of model dependence in the allocation of depth to flux within a line profile, and this means that the use of line profiles to predict energy sources and sinks is itself model-dependent. The ideal situation would be that a particular depth in the chromosphere

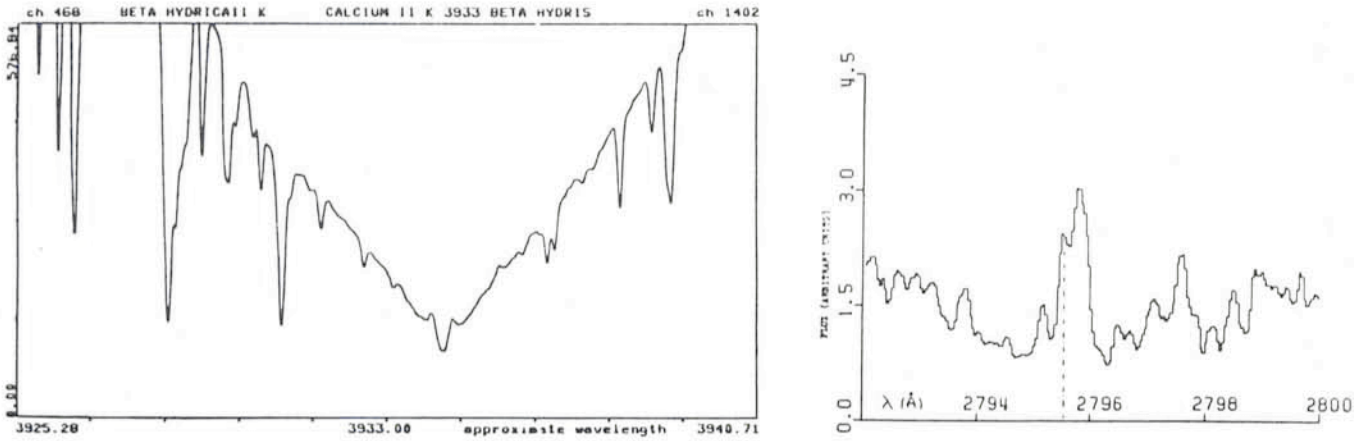

Fig. 2: *Comparison of the K line of Ca II, formed in the chromosphere of β Hya, and measured with the ESO CAT+CES with the k line of Mg II from the same star observed with IUE. Note the extra absorption feature in Mg II which is due to the LISM.*

would be cross-referenced by several different lines, by the wings of the lines in the IR triplet, for example, and by the core of the Mg II doublet, so that a self-consistent model could be built up.

Theoretical progress in relating line profiles to model atmospheres has been considerable, especially since the introduction of the techniques of partial redistribution to the formation of resonance lines in the chromosphere, in the 1960s and 1970s, which has transformed our ability to reproduce profiles from one of near failure to one of near success (the number of excellent theorists involved is too great to single out anyone here. Essentially this type of analysis is an attempt to specify what happens to any and every photon which goes to produce a spectral line in the atmosphere of a star, or indeed in any plasma. In grossly oversimplified terms, the theory attempts to compromise between the case of resonant scattering, in which a photon is absorbed and re-emitted coherently, and the case of complete redistribution in which the photons emerging from a particular layer of the atmosphere preserve no "memory" of those that entered, but are redistributed according to the prevailing temperature in the layer. The detailed dependence of the photon flux at any frequency on angle and on velocity is not yet wholly under the control of the modeller, though within a few years, and with the increasing use of computers, the solution of what can be reduced to a multidimensional set of matrix tranformations becomes imaginable. Of course, chromospheres are far from being in a state of LTE, and are not even in a state of hydrostatic equilibrium, so that line modelling presents more challenges there than in a photosphere.

4. Chromospheric Inhomogeneities

Another set of problems comes from the fact that the atmosphere itself is by no means a set of spherically symmetric static uniform layers. Firstly, there is the obvious fact, as seen on the Sun, that structure exists on many scales: typically on the scale of the granulation (1,000 km in diameter) and the supergranulation (100,000 km in diameter) dictated by magnetic fields. Secondly, there are the well-known phenomena associated with the temperature minimum, and the onset of a positive temperature gradient, and the presence of a rapid transition to the corona, all within 10,000 km of the photospheric surface, and with the presence within that layer of one or more "plateaux" where the temperature does not rise with height. In sum, there is structure both horizontally and vertically. Thirdly, there is the set of phenomena associated with activity, which, on the Sun, means the proportion of the chromospheric disk covered with "plages" which appear brighter in Hα and in Ca II H and K spectroheliograms. Finally there is the less well-known presence of more than one set of temperatures as a function of height, the presence of two co-existing "streams".

5. Two-Stream Modelling

This latter phenomenon might have been recognized as long ago as the early 1970s, when attempts to build reliable chromospheric models by combining data from the UV (both line and continuum), and the submillimetre continuum, which should in theory come from the same layers of the chromosphere, showed strange discrepancies. These could be resolved in principle if it was assumed that we are dealing with two streams of plasma, one much hotter than the other. The submillimetre continuum appears to be coming from the cooler stream, and the UV Lyman continuum and Lyα from the hotter. The observations receive a more or less rational explanation if we assume that the cooler stream occupies a greater fractional area of the disk, and can thus dominate the submillimetre radiation, whereas the hotter stream can dominate the UV because of a "Wien averaging" effect. The two streams could be thought of as occupying the super-granular cells, and the cell boundaries respectively. The difference between these appears to be a greater concentration of magnetic flux tubes along the boundaries.

This apparently dichotomic structure has been interestingly confirmed in recent years by measurements of the different temperature structures implied by different lines. One of the first pieces of deduction possible with a good quality spectrum of a late-type star in either the Ca II or Mg II resonance lines is to derive the temperature minimum, using the residual intensity at K3 or k3 (or their H and h equivalents), the points of minimum intensity in the combined chromospheric-photospheric line. Temperatures derived in this way for the Sun are of order 4,500 K. On the other hand, temperature minima derived from the infrared overtone, and fundamental vibration-rotation systems of carbon monoxide are of order 4,000 K or even lower.

In a recent article (preprint), Ayres has offered a persuasive physical scenario for this two-stream temperature structure. He starts by identifying the principal cooling agents in the hotter upper chromosphere which are in fact the Mg II and Ca II resonance lines, the Ca II infrared triplet, and the chief emission lines of hydrogen. Not only do these lines offer the best diagnostics for measuring the temperature structure via their

profiles, but they also indicate, via their fluxes, the quantities of energy radiated to space, and the "only" remaining problem is to apportion these losses as functions of height.

It is usually assumed that the negative hydrogen ion H^- is a key chromospheric coolant by recombination, but Ayres points out that at temperatures below a critical value of 4,900K, H^- is in fact heating the chromosphere this way. It is very difficult to find alternative cooling agents in the critical height region where the temperature lies between 4,000K and 4,900K. Below 4,000K the CO can act as an effective coolant. Its radiative de-excitation rate is rather small, while collision rates are large, since the molecular vibrational-rotational states are excitable by collisions with neutral atoms and molecules, whereas in the case of ionic or atomic transitions only electron excitation is effective, and these states are far away from LTE in chromospheric conditions; CO can be in LTE at the same place in the chromosphere. The basis of the reasoning is that the cooling (or for that matter the heating) rate in any spectral line is proportional to the factor C/(C+A), where C and A are respectively the collisional and radiative transition probabilities. Where this factor approaches unity, the line can act as a strong net coolant, and at the same time the species will be in a state of LTE, in the sense that the distribution of its members among the possible energy levels available will follow Boltzmann statistics. Above the 4,000K temperature limit, CO can no longer act as a coolant, since it dissociates.

6. How Two Temperature Structures Can Co-Exist

The interesting point about the dual cooling mechanism is that in a good part of the chromosphere, that is to say between the temperature minimum of around 4,000K and a value just below 5,000K where H^- cooling can take over, there is a range which is unstable, in the sense that the higher the temperature the less efficient the cooling. Below 4,000K there is, as we have seen, a most efficient mechanism via CO. It is known that the chromosphere contains many small-scale magnetic structures, the "flux-tubes", and that the rate of deposition of

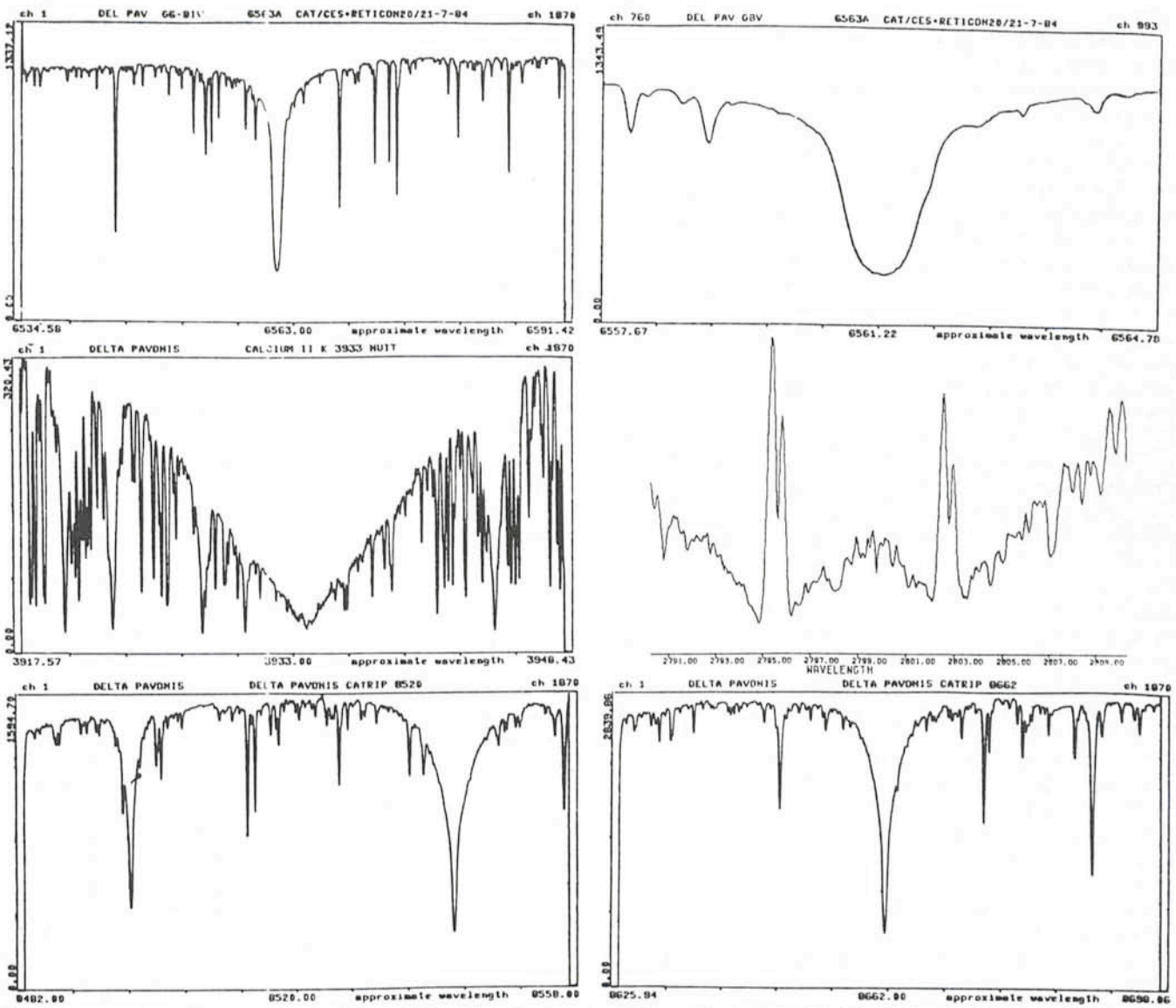

Fig. 3: *A compilation of lines accumulated from δ Pav giving chromospheric diagnostics. The Hα, CaII K and the CaII IR triplet come from the ESO CES; the MgII k is from IUE. Note the considerably different line shapes, implying different strengths and formation regimes, and permitting exploration of the chromosphere in depth. These lines are the most potent in cooling the upper chromosphere, while CO rotation-vibration lines cool the lower regions (see text for details).*

energy within a flux tube should be significantly enhanced compared with the surrounding field-free regions. This would provide a mechanism for a two-stream radiative model, because the flux-tubes would reach the critical temperature of 4,000K, and then tend to higher temperatures, while the surrounding plasma could remain comparatively cool, essentially below 4,000K.

If this mechanism is indeed important, the consequences for those trying to model chromospheric lines either from the Sun itself or from solar-type stars, are certainly significant. As far as the Ca II and Mg II resonance lines are concerned, the part of the line formed in the "chromosphere", which is essentially the emission core, will be diluted by a purely "photospheric" absorption line, essentially the very broad surrounding feature, which in fact comes from the rather large bulk of cool material which co-exists outside the flux tubes but at the same height. The emission cores will come principally from those regions where the flux tubes are most concentrated, which, in the case of the Sun, implies the supergranular boundaries and the plage regions, and the broad absorption wings will come from an entirely different pressure and temperature regime. One way to test the idea on the Sun, is by careful centre-to-limb measurements of the Ca II profiles, since near the limb the cooler more opaque regions will have a greater effect, and the absorption trough should deepen relative to the emission core. Such a test will be necessary before serious attempts to apply two-stream modelling to stars can be contemplated, but solar measurements of this type are not exceptionally difficult.

7. The Use of Observations at High Spectral Resolution

According to the "classical" method of dealing with high resolution profiles, one starts by using the K1 and H1 minima in intensity to determine the stellar chromospheric temperature minima, the widths of the emission core to establish a microturbulence parameter to insert within the model, and the emission fluxes to compute the distribution of heating and cooling rates. A simple combination of the photospheric and chromospheric components (not neglecting the effects of non-LTE and partial redistribution) then sets up the line profile. By combining information from lines formed at different heights, one can then hope for self-consistent models. Now we are faced with a situation in which not only we must take into account the unknown (and almost unknowable) field of microturbulence with height, but also the streaming velocity fields inside the structures that produce the lines. We must take into account the role played by inhomogeneities, which appears to be dominant, and we must be sure that any interstellar effects in the line profile data from the star are well and truly eliminated. We can then begin to apply models which allow for non-LTE and partial redistribution effects. Only at that point can we begin to realize our goal, which is to parametrize those factors which lead to the deposition of energy within chromospheres, before going on to show how they vary with the mass, age, chemical composition, and rotation rate of a star.

CASPEC and IUE: A Perfect Match

I. Appenzeller, G. Klare, O. Stahl, B. Wolf and F.-J. Zickgraf, Landessternwarte Heidelberg

As not all readers of the *Messenger* may be familiar with the lingo of today's astronomers, we shall first try to explain the acronyms used in the title: CASPEC stands for "Cassegrain Echelle Spectrograph", IUE for "International Ultraviolet Explorer". Both are modern and very successful instruments for high resolution spectroscopy of astronomical objects. In both devices the high resolution is achieved using an echelle design, i.e. by dispersing the light with two perpendicularly oriented diffraction gratings, one of which is operated at high ($\sim 10^2$) orders. (For more technical details see the articles by D'Odorico et al. in *Messenger* No. 33 and by Le Luyer et al. in *Messenger* No. 17.) There are also some differences between CASPEC and IUE: CASPEC was developed as an auxiliary instrument for the ESO 3.6 metre telescope at La Silla. It can be used in the spectral range ~3500 Å to 9500 Å. The IUE spectrograph circles the earth as an artificial satellite at a mean distance of about 36,000 km above the equator and is fed by a telescope of only 0.45 metres aperture. As its name implies, IUE is used at UV wavelengths (about 1100 Å to 3200 Å) where ground-based observations are impossible because of the strong UV absorption in the earth's atmosphere.

During the past six years our group has been using IUE for investigations of a variety of different astronomical objects. During this time we found the IUE satellite to be particularly valuable for studies of distant blue supergiant stars. There are several reasons to investigate extreme blue supergiants: First, these stars are at the upper limit of stellar luminosities and their properties allow important insights into the problems of stellar stability. Secondly, because of their extreme brightness such stars are easily observed in nearby extragalactic stellar systems and therefore can be used to probe the physical conditions in other galaxies. The potential of these objects is illustrated by the fact that the absolute brightness of a single extreme blue supergiant typically exceeds that of a globular cluster or even that of a dwarf galaxy containing millions of stars.

IUE is particularly useful for studying blue supergiants as these stars emit most of their radiation just in the IUE spectral range. Hence, these objects can be observed at high spectral resolution even at the distance of the Magellanic Cloud galaxies. In fact, in spite of the much larger telescopes at La Silla, before 1983 we were often unable to match the high resolution of IUE spectrograms of bright Large Magellanic Cloud (LMC) stars with ground-based spectroscopic observations at longer wavelengths. This was unfortunate since at different wavelengths we observe different layers of these objects and only observations over a large spectral range allow to deduce a complete picture of their physical structure: In most cases the UV observations result in information on the dense and hot parts of the expanding envelope, while measurements in the visual and red provide data on the deeper, more static, layers, but also (using forbidden-line profiles) on the rarified outermost regions. CASPEC therefore greatly improved the efficiency of spectroscopic studies of such stars. In the following we shall describe in a few examples how CASPEC and IUE can be combined for obtaining a maximum of physical information.

The "Star" HDE 269599

This object derives its name from its number in the **H**enry **D**raper **E**xtension star catalog, where its position was pub-

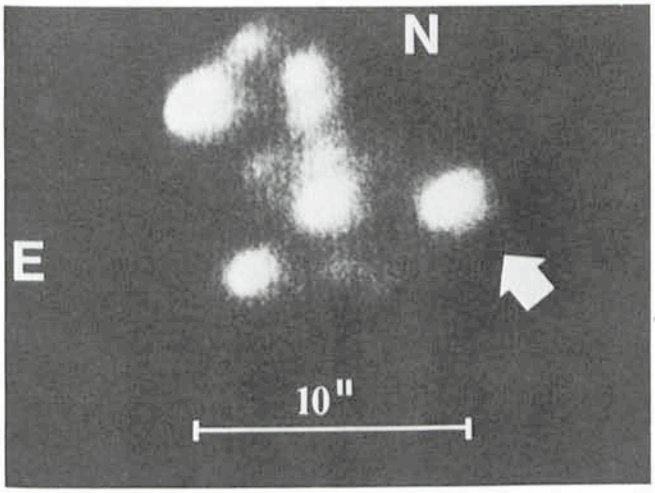

Fig. 1: *The LMC objects HDE 269599. The arrow indicates the emission line component S 111.*

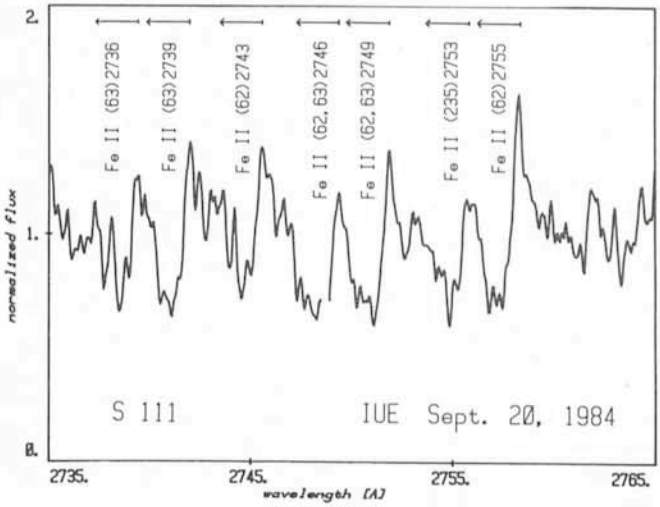

Fig. 2: *Examples of P Cygni profiles in the UV spectrum of S 111.*

lished by Annie J. Cannon in 1936. Cannon gave an approximate magnitude and spectral information based on objective prism plates obtained in 1925 at Chuquicamata, Chile. The spectrum must have looked rather strange, since it is one of the relatively few cases where Cannon did not dare to assign an explicit spectral type. Instead she only stated that the spectrum was "peculiar". In 1956 Karl Henize found HDE 269599 to be an emission line star and gave it the additional catalog designation S 111. The first slit spectrogram of this star was published by Feast, Thackeray, and Wesselink in 1960. From the observed radial velocity they were able to prove that this object was a very bright member of the LMC galaxy. In their (**R**adcliffe Observatory) catalog the star also acquired the additional designation R 105. The Radcliffe spectrogram showed a B-type absorption spectrum without emission lines. However, Feast et al. noted that HDE 269599 was not a single star but a very compact small cluster, which was only partly covered by the spectrograph slit. Further slit spectrograms obtained by A. Ardeberg et al. at ESO (cf. *Astronomy and Astrophysics Suppl.* **6,** 1972) showed that the emission line spectrum was produced by a component at the SW edge of the compact cluster. More recently Shore and Sanduleak (*Astrophysical Journal Suppl.* **55,** 1984) confirmed the emission line character of HDE 269599 = S 111, but stated that this object was not identical with the (B type star?) R 105. On the other hand, on a low resolution IUE spectrogram Shore and Sanduleak found S 111 to have a pure B-type absorption spectrum in the UV.

Although in such cases new observations usually only increase the confusion, we recently obtained additional spectrograms. To understand our results, let us first look at Fig. 1, where we reproduce an image of HDE 269599 as seen by the television camera of the ESO 3.6 m telescope guiding system. Obviously HDE 269599 is a highly compact cluster of at least ten high luminosity stars. Its diameter is about 10 arcseconds, corresponding to 2.5 pc at the distance of the LMC. Our CASPEC observations confirmed that the emission line spectrum is produced by the bright star at the SW edge of the cluster. For clarity henceforth only this component will be called S 111. The second visually bright component of HDE 269599, the star at the NE edge of the object, was found to show a normal B-type absorption spectrum as observed by Feast et al. Therefore we suggest to reserve the designation R 105 for this latter component of HDE 269599.

Observing S 111 (as defined above) with IUE was less easy, as the IUE field camera, which produces 8" pixels, cannot resolve HDE 269599 into its components. Nevertheless, with some tricks and the kind help of the Villafranca IUE observatory controller, Dr. Willem Wamsteker, it was possible to isolate S 111 for obtaining a high resolution UV spectrogram. This spectrogram showed that S 111 is an emission line object in the UV as well.

Apart from its history, S 111 also shows a particularly interesting emission line spectrum: In the UV many spectral lines show pronounced P Cygni profiles, which obviously are produced in a dense expanding envelope. Examples are the moderately strong (non-resonance) Fe II lines reproduced in Fig. 2. Sometimes the blue absorption components seem to show a double structure with a strong low velocity and a weaker high velocity component. However, the signal-to-noise ratio of the IUE spectrogram is too low to clearly establish this structure. On the other hand, this type of line profile becomes obvious on the CASPEC spectrograms, as illustrated e.g. by the H_γ line profile in Fig. 3. But much more interesting is a comparison of these P Cygni profiles with the structure of the forbidden lines, like the [Fe II] λ 4359 in Fig. 3: While the P Cygni lines indicate very high wind velocities of up to 600 km s^{-1}, the forbidden lines, which can be formed only in the rarified outer regions of the envelope, indicate a much lower velocity dispersion. From the unblended strong [O I] λ 6300 line reproduced in Fig. 4 we obtain a velocity range

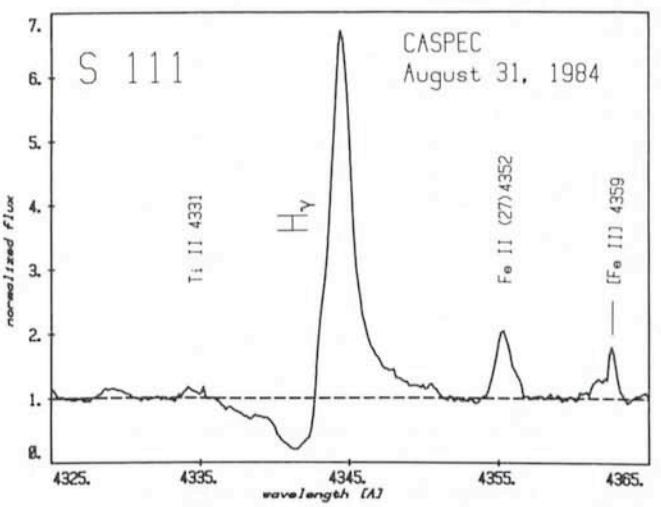

Fig. 3: *The H_γ region of the visual spectrum of S 111.*

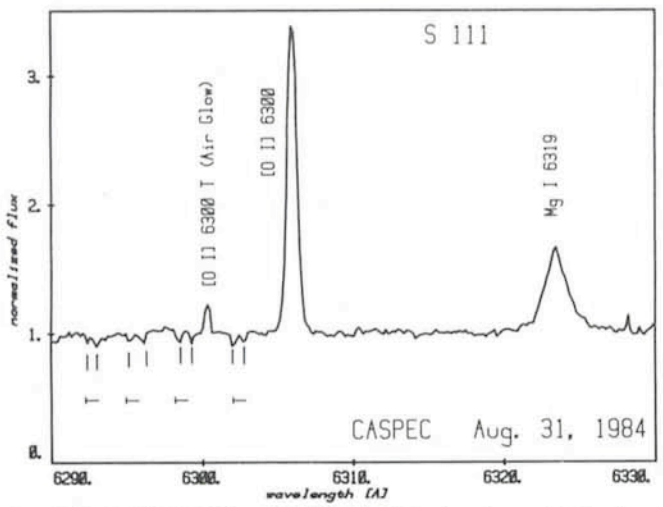

Fig. 4: *The [O I] λ 6300 line of S 111. The "T"s denote spectral features produced by the terrestrial atmosphere. The wavelength shift between the stellar and airglow emission results mainly from the orbital motion of the solar system in our galaxy.*

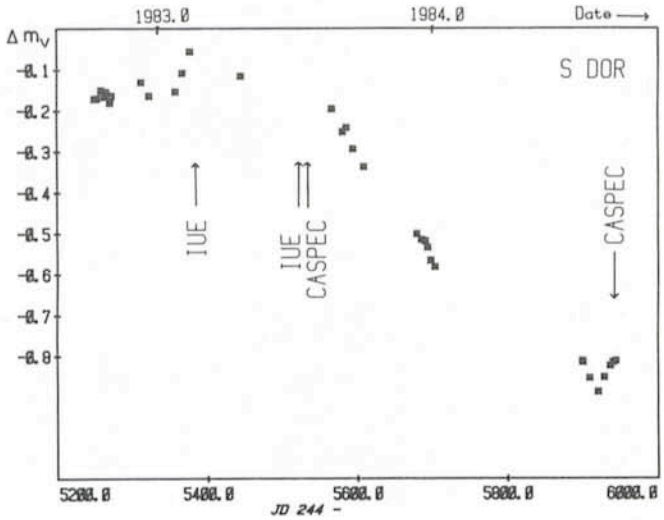

Fig. 6: *The recent brightness evolution of S Dor. This lightcurve is based on the "long-term photometry of variables" programme organized at ESO by Ch. Sterken. Δm_v denotes the visual magnitude difference relative to an (arbitrarily chosen) constant comparison star.*

which is less than 10 % of the expansion velocity derived from permitted lines. In principle there are two possible explanations of this discrepancy: Either the wind is strongly decelerated (which for various reasons appears unlikely) or the stellar wind and circumstellar envelope of this star show a strongly non-spherical geometry, as deduced earlier from similar arguments for the related LMC emission star R 126. (For details see Zickgraf et al., *Astronomy and Astrophysics,* in press.) From a detailed spectral analysis, which has just been started, we expect for S 111, with its rich emission spectrum, firmer and more quantitative conclusions than were possible for R 126.

R 127 and S Doradus

These two variable stars of the "S Dor" or "Hubble-Sandage" class are also members of the LMC galaxy. We now believe that S Dor variables are very hot (typically OB-type) supergiants with variable and sometimes extremely dense and optically thick stellar winds. Although their bolometric luminosity seems to remain essentially constant, the variations of the wind optical depth results in changes of their continuum energy distribution and consequently in variations of the visual brightness. Although this model has been developed from earlier observations of other stars, it gained its strongest support from the discovery of the S Dor nature of R 127. As described by Wolf and Stahl in the *Messenger* No. 33, until

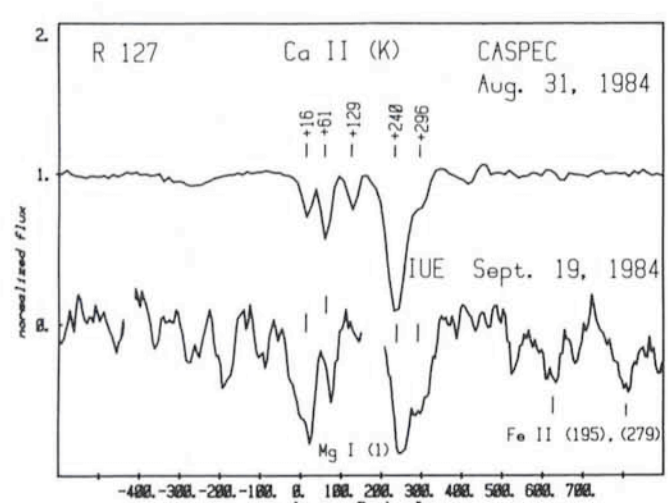

Fig. 5: *A comparison of the velocity structure of the Ca II (K) λ 3934 and the Mg I λ 2852 absorption profiles of R 127. The components are labelled by their heliocentric radial velocity (in km s^{-1}).*

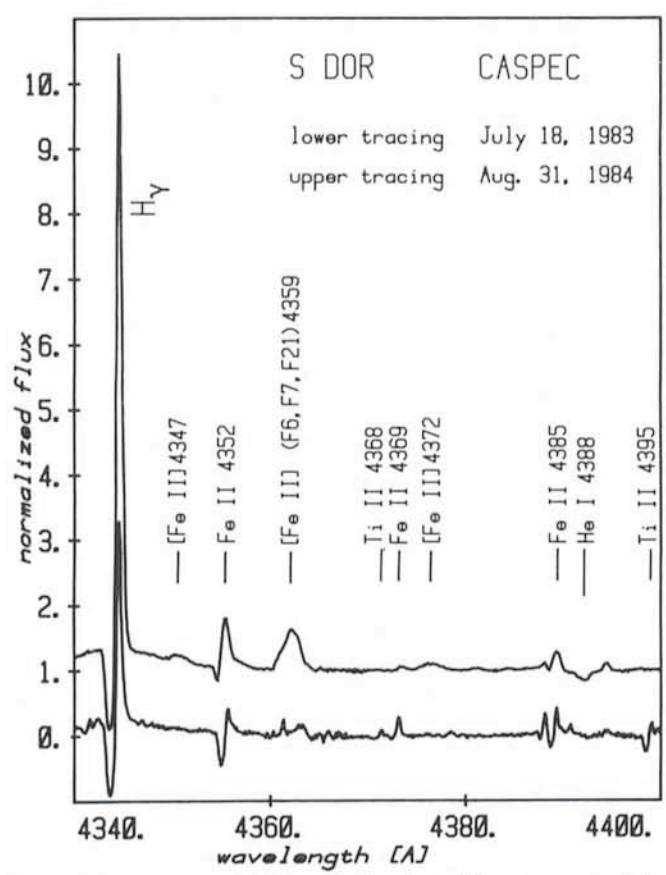

Fig. 7: *Two spectra of S Dor, obtained at different epochs. The ordinate scale refers to the upper tracing. The lower tracing is shifted by one ordinate unit.*

about 1977 R 127 had been a well classified O star. In 1982 it was discovered that R 127 had developed an S Dor type envelope which resulted in a considerably higher visual brightness. During the past two years this envelope has become even more pronounced and R 127 has now become the second brightest star in the LMC. As m_v is still increasing, R 127 may soon become the visually brightest star of this galaxy.

As described by Wolf and Stahl in the article quoted above, on IUE high resolution spectrograms the envelope absorption lines and P Cygni absorption components of R 127 showed a complex multiple structure, indicating discrete mass loss events. As illustrated by Fig. 5 with CASPEC it has now become possible to observe these features also in many additional lines in the visual spectral range. These observations will certainly help to clarify the nature of this phenomenon and the mass loss mechanism of the S Dor stars in general.

A final example of the potential of CASPEC observations is presented in Fig. 7, where we give sections of two CASPEC spectrograms of the star S Doradus itself, obtained at different epochs. During the past 13 years S Dor has been in its maximum state. However, in August 1983 its visual brightness started to decrease again (cf. Fig. 6) and it seems now to be on its way towards its minimum state. Fortunately, just before the star began to dim significantly, a first CASPEC spectrum of S Dor could be obtained while the instrument was still being tested at the telescope. Recently (13 months later and after the star had become fainter by $\Delta m_v \approx 0.8$) the second spectrum was obtained.

As shown by Fig. 7 the brightness changes are accompanied by characteristic spectral changes: With decreasing visual brightness (i.e. decreasing wind density) the (blue-shifted) envelope absorption features decrease rapidly, some envelope lines (like the Ti II lines) simply disappear, while the Balmer emission, the low density forbidden lines, and the unshifted high excitation "photospheric lines" (like He I λ 4388) increase in strength. Although some of this behaviour was known before, only the high spectral resolution and linearity of CASPEC allows to determine these changes without distortions. Even a slight decrease of the resolution would result in a partial fill-in of the deep envelope absorption components of H_γ by the adjacent very strong emission component.

Most of the data described above have been obtained only very recently and this paper resulted from our excitement during a first quick look at the reduced spectrograms. But we are convinced that the usefulness of the combination of high resolution spectrograms obtained with IUE and CASPEC will become even more evident when all our data are fully analyzed. We also note that the potential of such coordinated space and ground-based spectroscopic programmes will become even greater when the Space Telescope and future UV satellites allow high resolution UV observations of astronomical objects which are beyond the limiting magnitude of the IUE.

Catching Carbon Stars in the Baade's Windows

M. Azzopardi, ESO, J. Lequeux and E. Rebeirot, Observatoire de Marseille

Near-infrared objective prism surveys at low dispersion (1700 to 3400 Å mm^{-1}) using Schmidt telescopes have been extensively used to detect M-, S- and C-type stars in the galactic equatorial zone, and in other strategically selected regions of the Milky Way. The detection techniques have been perfected by Nassau and his associates (Nassau and Velghe, 1964, *Astrophysical Journal* **139,** 190) during their survey, at Cleveland, of the northern part of the Milky Way. These techniques are based on the identification of a number of typical molecular bands (TiO, CN, LaO, VO) that fall in the 6800–8800 Å spectral range, and which are used to classify M-, S- and C-type stars (Mavridis, 1967, Coll. on Late Type Stars, p. 420). Using the same method, partial or entire near-infrared surveys of the southern Milky Way have been carried out by Blanco and Münch (1955, *Bol. Obs. Tonantzintla y Tacubaya* **12,** 273) at Tonantzintla, Smith and Smith (1956, *Astronomical Journal* **61,** 273) at Bloemfontein, and later by Westerlund (1971, *Astronomy and Astrophysics Suppl.* **4,** 51; 1978, ibid. 32, 401) with the Uppsala Schmidt telescope at Mount Stromlo Observatory.

These near-infrared, low dispersion spectra surveys allowed the space distribution of the most recognizable red stars to be studied. These stars are essentially all S stars, or M and C stars later than M2 and C2. It is important to note that the observed distributions are affected by biases due to inhomogeneities in the interstellar absorption and to luminosity differences amongst the various types of stars. Also, the limiting magnitude to which the various red stars can be classified, and thus identified, varies according to their type: in particular, C stars can be detected almost to the limiting magnitude of the plates. Because they are rather luminous – all C and S stars and the majority of the M stars are giants – and less affected by the interstellar absorption in the near-infrared, the red giant stars lead to deep surveys of our Galaxy. The study of the distribution of the C stars as a function of the galactic latitude shows that these stars, which are strongly concentrated in the galactic plane, form the coolest component of the galactic disk population. Local variations in the distribution of the carbon stars with galactic longitude are due to known dark clouds. Nevertheless, it is possible to assert that C stars are inclined to cluster and are correlated with the spiral structure. Their number decreases strongly toward the galactic centre while the number of the late-type M stars increases (Westerlund, 1964, IAU Symp. No. 20, 160).

The three fields selected by Baade (1963, *Evolution of Stars and Galaxies,* p. 277) in the Sagittarius Star Cloud as relatively low absorption regions – currently named NGC 6522 ($l = 0^\circ.9$; $b = -3^\circ.9$), Sgr I ($l = 1^\circ.4$; $b = -2^\circ.6$), Sgr II ($l = 4^\circ.2$; $b = -5^\circ.1$) – allow this trend to be confirmed. A first attempt to identify red giant stars in the galactic nuclear bulge, namely in the clear region near the globular cluster NGC 6522, known as Baade's window, was made by Nassau and Blanco (1958, *Astrophysical Journal* **128,** 46). Owing to the unfavourable scale of the Schmidt telescope used to prospect so crowded a region, they found numerous late-type M stars. McCarthy (1983, *Mem. Soc. Astron. Ital.* **54,** 65) reports that a new near-infrared survey of this region was carried out by Blanco and Hoag as early as 1975 with the grism technique (Bowen and Vaughan, 1973, *Publ. Astron. Soc. Pacific* **85,** 174) at the prime focus of the CTIO 4 m telescope. Using this observational material (region of 0.12 square degree) Blanco et al. (1978, IAU Symp. No. 80, p. 33) found about 300 M stars later than M5 and just one C star. More recently, a preliminary survey by McCarthy and Meier (see McCarthy, 1983) of the Sgr I Baade's window

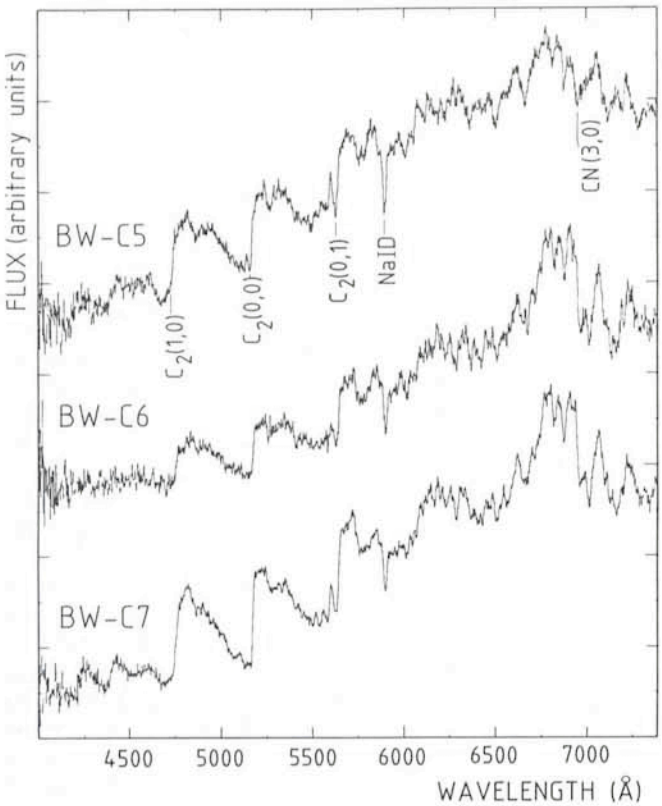

Fig. 1: *Spectra of the three carbon stars identified in the NGC 6522 Baade's window obtained with the ESO 3.6 m telescope using the Boller and Chivens spectrograph and IDS detector. The resolution is 16 Å (FWHM) and the integration time 30 minutes for each.*

resulted in the identification of about 700 late-type M stars and one probable C star in a field of 0.12 square degree, confirming the paucity of carbon stars in the galactic nucleus. In fact, McCarthy (1984, *Bull. Am. Astron. Soc.* **16,** 494) and Blanco et al. (1984, *Astronomical Journal* **89,** 636) now retract the presence of any carbon star in the NGC 6522 and Sgr I Baade's windows.

We have been using for some time another technique for searching for carbon stars: instead of working in the near-infrared spectral range, we use grism and grens devices in the blue-green spectral domain. Carbon stars are identified via their strong Swan bands of the C_2 molecule, mainly those with heads at 4737 Å, 5165 Å and 5635 Å. The greater strength of these bands compared to that of the CN bands in the near-infrared more than compensates for the fainter flux of the C stars, which are very red. From such observations at the 3.6 m telescopes of ESO and CFH Corporation we have discovered many new carbon stars in the Small Magellanic Cloud (SMC) and in nearby spheroidal galaxies, doubling the number of these stars known in the latter objects (Azzopardi and Westerlund, 1984, *The Messenger* **36,** 12). It is important to note that the C stars detected with this method are generally fainter and bluer than those found by the more conventional near-infrared surveys.

Last July we observed the three Baade's windows quoted above, with the CFH 3.6 m telescope using the green grens and the triplet corrector at the prime focus. The dispersion is 2000 Å mm^{-1} and the useful field about 1 square degree. We restricted the spectral range towards the short wavelengths with a Schott GG 435 filter while the range towards the long ones is limited by the cut-off of the hypersensitized IIIa-J emulsion we used (Breysacher and Lequeux, 1983, *The Messenger* **33,** 21). The selected spectral range (4350–5300 Å) makes the C_2 bands at 4737 Å and especially at 5165 Å available for the identification of the C stars. The spectra are very short and thus image overlapping is not a major problem, even in very crowded fields such as those found in the SMC bar or in the galactic centre.

After a careful examination of the plates with a binocular microscope, we discovered 9 C star candidates near NGC 6522, 4 in the Sgr I region and 2 in the Sgr II one as well as other interesting objects whose nature is not yet clear and needs to be found out. Soon after this, we were lucky enough to have an observing run at the ESO 3.6 m telescope with the Boller and Chivens spectrograph and the Image Dissector Scanner (IDS) giving a dispersion of 171 Å mm^{-1}. After some difficulties with bad weather and power failures, we succeeded in observing three candidates during the beginning of the nights of September 26 and 27. All three, located in the NGC 6522 Baade's window, are without doubt carbon stars (Fig. 1). One of these stars (BW-C6) lies in the field studied by Blanco et al. (1984, *Astronomical Journal* **81,** 636). Fig. 2 is an identification chart of star BW-C6. B and V magnitudes as well as B-V colours can be estimated from the IDS spectra. The V magnitudes of the confirmed C stars range between 15.8 and 16.7 and their apparent B-V colours are between 2.0 and 2.5 magnitudes, which is rather blue for carbon stars. The reddening estimate by Arp (1965, *Astrophysical Journal* **141,** 43) for NGC 6522 is E(B-V) = 0.46 mag. ± 0.03 but the interstellar absorption is uneven in Baade's window and the colour excesses of our three C stars might be even larger, making them among the bluest of the known carbon stars. Their luminosity ($M_V \gtrsim -1.5$) is also relatively low.

The interpretation of our discovery is not straightforward. The galactic bulge is a mixture of stellar populations of various ages and metallicities and we do not yet know to which component the newly detected C stars belong. They may also be close binaries in which one of the components has been enriched in carbon transferred from the other, evolved component (see Aaronson and Mould, 1984, Steward Obs. preprint No. 544). Much further work is necessary to get a full understanding of these interesting objects.

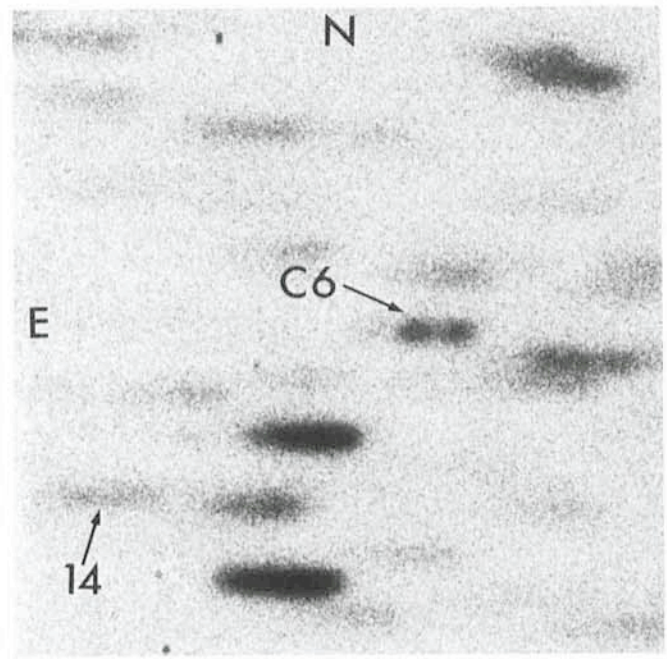

Fig. 2: *Finding chart for carbon star C6 detected in the NGC 6522 Baade's window. The late giant M star No. 14 from Blanco et al. (1984,* Astronomical Journal **89,** *636) is indicated to ease the identification of the discovered C star. Copy of a part of a CFH 3.6 m telescope grens plate (forming gas baked IIIa-J emulsion; 20-minute exposure).*

Light Element Abundances in F Stars and the Chemical Evolution of the Galactic Disk

B. Edvardsson, Uppsala Astronomiska Observatorium
B. Gustafsson, Stockholms Observatorium
P. E. Nissen, Astrofysisk Institut, Aarhus

Summary

A project for investigation of the evolution of the chemical elements in the galactic disk, and in particular of the elements in the third and fourth period of the periodic table, is presented. Chemical abundances of F dwarfs of different ages and of different overall metal abundance are used for this purpose. Preliminary results for 15 stars are reported; they indicate abundance ratios of O, Mg, Si, Ca and Ti relative to iron that are systematically greater than the solar ratio for stars with [Fe/H] < -0.5 and with the excess increasing with decreasing [Fe/H] and decreasing atomic number. An odd-even effect for the sequence Na, Mg, Al, Si is found for the metal-poor disk stars.

Introduction

The history of the chemical elements in our Galaxy is still known only fragmentarily. Man pieces are left to be put into the puzzle, and as yet we can do little but guess what the final picture will look like. More systematic observational investigations are necessary before a number of fundamental questions can be answered (the answers will however have bearings far beyond the problems of the chemical evolution of the Galaxy): In which objects were the first heavy elements formed; massive supernovae of about 25 $M_\odot$, very massive ones (100–300 $M_\odot$, so-called hypernovae), or still heavier supermassive stars? What is the importance in nucleosynthesis of Type I supernovae – do they produce most of the iron-group elements? Which is the role played by infall of intergalactic gas during the disk evolution? Are there bursts of star formation in the disk? Does the initial mass function (IMF) vary significantly with time from the halo phase to the disk phase or even during the disk phase? Is the IMF a function of radial distance from the centre of the Galaxy? And so on.

For the study of the chemical evolution of the galactic disk it would be important to investigate the initial chemical composition of stars of different well-known ages and with different kinematical properties. Thanks to the power of the Strömgren photometric uvbyβ system, the modern coudé scanners, such as the ESO CAT/CES, and the astrophysical properties of F dwarfs, it is possible today to make a first systematic attempt in this direction.

The F dwarfs are suitable for a study of the history of the galactic disk for several reasons: their ages range all the way up to 10^{10} years and these ages may be determined with the uvbyβ photometry, by measuring the effective temperature and the distance of the star from the zero age main sequence. For somewhat evolved stars an accuracy of about 0.2 dex in the age can be achieved in this procedure, with major sources of errors being due to the uncertain mixing length parameter and helium abundance as well as other possible more fundamental errors in the stellar-structure calculations. The chemical composition of the atmospheres of F dwarfs is not thought to be affected by the nuclear reactions in the cores of the stars, nor should it for most stars be affected by gravitational diffusion or selective radiative pressure, since the convective motions in the stellar envelopes should prevent these separation mechanisms from playing any important rôle. Thus, the atmospheres of most F dwarfs may be taken as samples of the chemical composition of the interstellar matter from which the stars were once formed. Furthermore, suitable absorption lines of many chemical elements can be found in F dwarf spectra. The stars are also close enough to the Sun in the HR diagram for making it reasonable that the interpretation of line strengths in terms of chemical abundances relative to solar abundances may be reliable, since the errors in the model atmospheres should cancel to a great extent in a differential study relative to the Sun.

It is of considerable interest to explore the abundance of the elements lighter than iron as a part of a study of the evolution of the Galaxy. The well established overabundance of oxygen in halo stars by about a factor of four relative to iron (as compared to the Sun) was shown by Clegg et al. (1981) to be significant also in the old disk stars – not until the overall metal abundance approached the solar value at a rather late stage in the evolution of the disk the oxygen-to-iron ratio became solar. Twarog and Wheeler (1982) explained the oxygen overabundance as a result of a more efficient oxygen production in the early nucleosynthesis than in the late disk evolution, as compared with the production of iron. In fact, evolutionary calculations for massive pre-supernovae have demonstrated that the outer layers of these objects should be rich in oxygen produced during helium burning (Arnett 1978) and the discovery of several oxygen-rich supernovae remnants has verified this (Trimble 1983, and references given therein). It may be reasonable to assume that such massive supernovae are responsible for the oxygen overabundance of Pop II, and that the oxygen-rich/iron-poor gas produced continued to affect the composition of the early disk due to the continued infall of this halo gas onto the disk. It is of great interest to study the abundances of "α-elements" such as Mg, Si, Ca and Ti, to see whether similar overabundances as a function of metal abundance can be traced for these elements; that would not agree with the predicted smaller relative enhancements in the pre-supernovae models of Woosley and Weaver (1982a, b). The "odd" elements (Na, Al, P, K, Sc) were predicted in some theoretical scenarios (Arnett 1971, Truran and Arnett 1971) to be less abundant, relative to the α-elements, in metal-poor stars. These odd-even effects have been looked for by several investigators with very few definite results. E.g. Tomkin, Lambert and Balachandran (1984) find a considerable scatter in their plot of [Al/Mg] versus [Mg/H] for halo and disk stars. The Al abundance, e.g., relative to the Mg abundance, is important as a measure of the initial composition of the site of nucleosynthesis, since the Al production is controlled by the neutron excess of the parent nuclei.

Most investigations of the evolution of the abundances of the light elements in the Galaxy have been confined to the study of the relations between the abundance of any element X, [X/H] vs. [Fe/H] (the square brackets as usual denoting the logarithmic abundances relative to the Sun), and the iron abundance or the overall metal abundance has been adopted as a measure of time. However, there are several indications that the metal abundance is not a well-defined monotonic function of time in the Galaxy, i.e., the mixing of the interstellar gas is not complete enough for producing a homogeneous

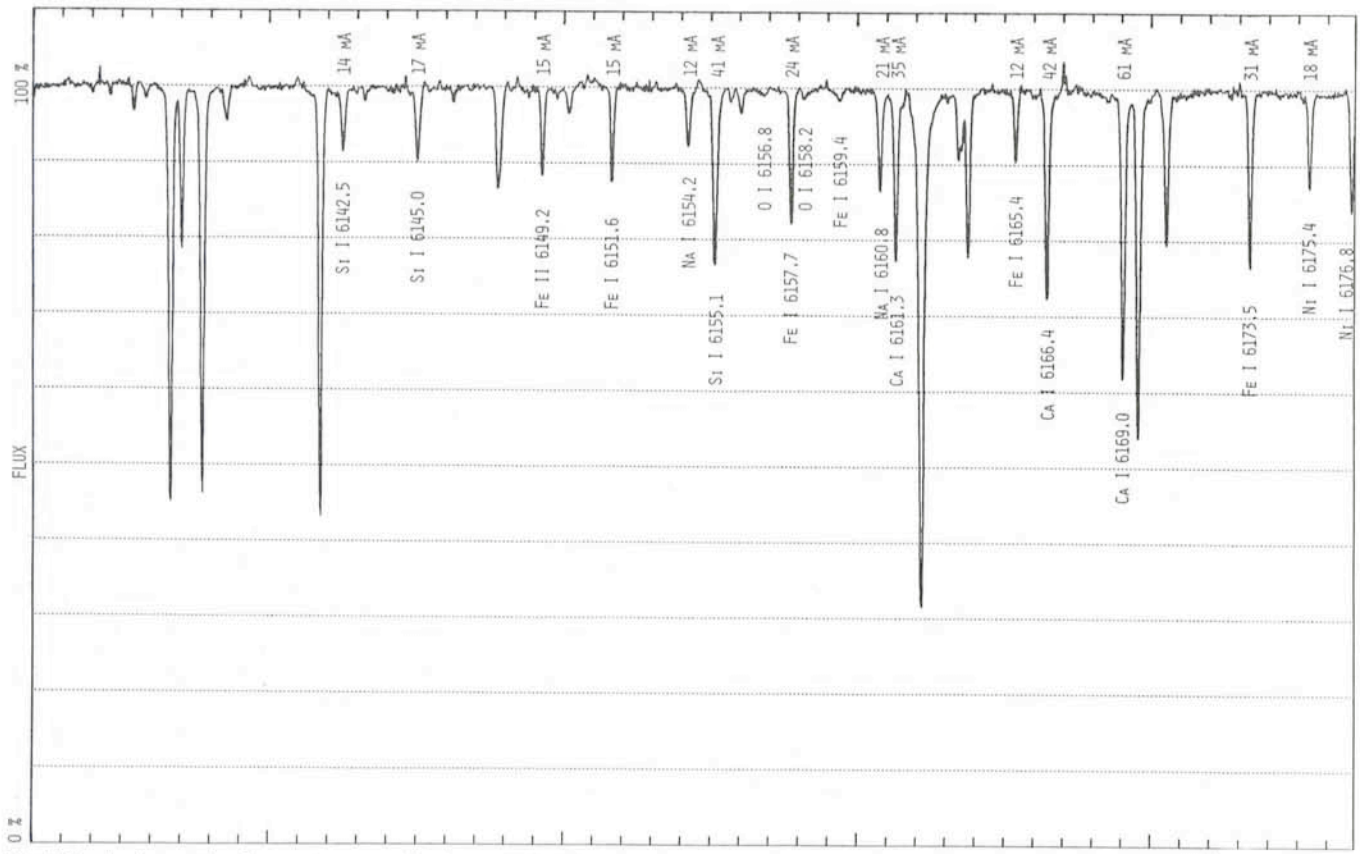

Fig. 1: *Typical example of a spectrum used in the analysis. It is a 45-min. exposure of HR 3018, V = 5.4, in the region 6132–6177 Å. The resolving power is 100,000. The lines used in this region are identified, and the equivalent widths measured and used for this spectrum are indicated.*

interstellar medium at a given time. Traces of chemical gradients and inhomogeneities in the Galaxy can be found in the composition of stars from relatively recent epochs, and we have certainly no good reason to expect these phenomena to be less important in the early epochs of the Galaxy and of its disk. From this point of view it is important to combine the abundance information with independent age information and kinematic information for the stars. Use of this additional information in attempts to study the detailed chemical composition, e.g., as a function of [Fe/H], age or eccentricity of the galactic orbit, requires a well-defined statistical approach and a large sample of stars. The present study is a progress report from a study of this systematic character.

In order to minimize unknown selection effects we have sampled our programme stars from the complete uvbyβ survey catalogue of F stars by Erik Heyn-Olsen (see Olsen 1983). The photometry gives independent information on effective temperatures from the reddening-free β index and the b-y colour (the present stars are within 50 pc and thus practically unreddened), log g from the δc_1 index (and rather good age estimates for stars with $\delta c_1 > 0^m.040$) and [Fe/H] from the δm_1 index. We have subdivided the 13,000 stars in the catalogue into nine sub-groups of δm_1, i.e. according to overall metal abundance, and we shall observe the approximately 30 brightest stars in each group. We have excluded known binaries and peculiar stars, partially guided by the results of a CORAVEL study of all programme stars.

The northern stars are being observed at the McDonald Observatory by D. Lambert and J. Tomkin and the southern stars by the present authors at ESO. The final analysis will be performed jointly by the two groups. The 150 southern stars, observed and analysed in collaboration with J. Andersen, Copenhagen University Observatory, are distributed uniformly over the hemisphere, and are brighter than about $6^m.0$ for the more metal-rich groups. For the most extreme – and rare – metal-poor stars the apparent-magnitude limit is $7^m.0$.

Observations and Reductions

Spectra in five wavelength regions are obtained for each programme star; for the southern stars this is done with the ESO 1.4 m CAT telescope, the Coudé Echelle Spectrograph, and an 1,870 channel RETICON detector. The resolving power is about 80,000 and typically a signal-to-noise ratio of about 100 is obtained for each channel. The channel width is 23 to 37 mÅ, depending of wavelength region, which makes the spectrum oversampled by a factor of about 3. The reductions of the ESO spectra obtained until now have been carried out with the ESO IHAP system in Garching and Uppsala, and the equivalent widths were measured by fitting Gaussians to the line profiles with the convenient PHYS code written at Uppsala by several astronomers. Only lines with equivalent widths between 5 and 100 mÅ are used in order to reduce problems in measuring and with the theoretical damping treatment. The main emphasis is on spectral lines on the linear part of the curve of growth, with equivalent widths less than about 50 mÅ and thus relatively unaffected by microturbulence. For each individual line the Gaussian fit is checked by eye and the line is rejected if the fit is found too poor. In further attempts to avoid erroneous measures the line is also rejected if the FWHM measure is found to be unreasonable compared to those of other lines. The equivalent widths refer to a continuum defined by a number of narrow regions in each spectrum, selected to be free of lines in the Solar and Procyon spectra.

A typical spectrum is shown in Fig. 1 of the star HR 3018, V = 5.4. This star was independently observed by two observers, in two wavelength regions, at two different occasions, with two different RETICON arrays, and the spectra have been inde-

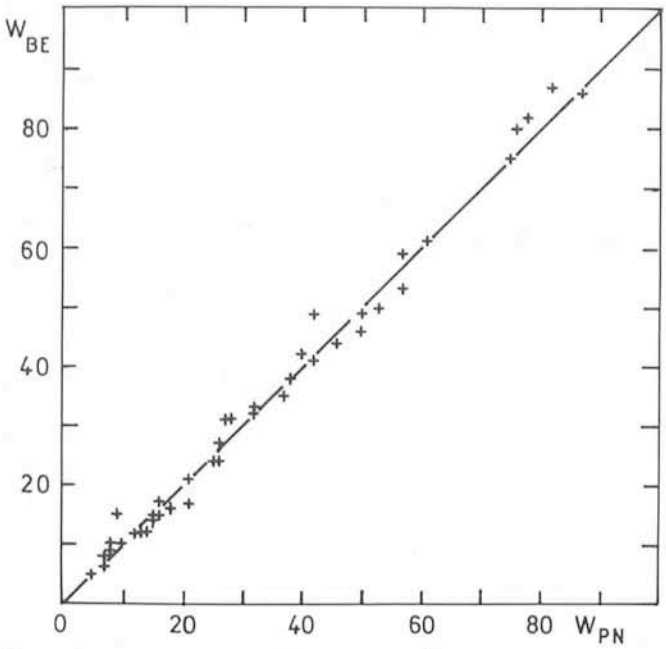

Fig. 2: *Comparison of equivalent widths (in mÅ) obtained from two sets of spectra of HR 3018 (one shown in Fig. 1) taken by two observers, using two different Reticon arrays. The spectra were separately measured and reduced by the two observers. The mean difference is 0.3 mÅ with a standard deviation of 2.6 mÅ for one measure.*

pendently reduced and measured by the two observers. The equivalent widths are compared in Fig. 2, where the lines between 5 and 100 mÅ are compared. The mean difference is 0.3 mÅ with a standard deviation of 2.6 mÅ for a single line. From this we conclude that it is possible to obtain very accurate equivalent widths with the present instrumentation.

Data on the five wavelength regions and on the elements studied in each region are given in Table 1.

Table 1: Wavelength regions

The 5105 Å region is not used here because the present study is made relative to the Sun and no observations of the solar spectrum are yet available for that region with the present equipment. Except for FeII 6149.23 Å and BaII 5853.68 Å all lines measured so far are lines of neutral elements.

Region	Range (Å)	Elements	Comm.
5105	5085–5125	Ti, Cr, Fe, Co, Ni, Y	Not used
5860	5840–5880	Ca, Ti, Fe, Ni, Ba	14 lines
6155	6130–6180	O, Na, Si, Ca, Fe, Ni	18 lines
7772	7740–7805	O, Si, Fe, Ni	12 lines
8746	8715–8780	Mg, Al, Si, Fe	9 lines

The lines are carefully selected to be free from hidden blends; of 101 candidate lines in the four last regions of Table 1 only 53 were finally included in the analysis.

Analysis

The abundance analysis is based on the assumption of LTE; however, the effects of departures from LTE on the abundances are being studied theoretically (cf. Saxner 1984) and observationally (see below). The models used in the analysis are blanketed and convective model atmospheres calculated with an updated version of the programme presented in Gustafsson et al. (1975), cf. Nissen and Gustafsson (1978). The models are individually calculated for each star using model parameters T_{eff}, log g, and overall metal abundance [M/H], derived from Strömgren photometry. The microturbulence parameter was derived as a function of the fundamental parameters in accordance with Nissen (1981). In Table 2 we give identifications, spectral type, V magnitude, model parameters from Strömgren photometry and derived iron abundance for the 15 stars investigated until now.

Table 2: The programme stars

			Parameters obtained from uvbyβ photometry					
HR	Name	Sp. type	V	T_{eff}	log g	[M/H]	ξ_t	[Fe/H]
33	6 Cet	F7V	4.9	6320	4.1	−0.5	1.8	−0.34
1545		F5V	6.3	6550	4.1	−0.4	1.8	−0.34
1983	γ Lep	F6V	3.6	6450	4.3	−0.1	1.6	−0.05
2883		F5V	5.9	6080	4.2	−0.7	1.5	−0.71
2906		F6IV	4.5	6250	4.1	−0.2	1.7	−0.16
2943	α CMi	F5IV-V	0.4	6840	4.1	+0.1	2.0	+0.04
3018		G0V	5.4	5890	4.4	−0.7	1.2	−0.78
3578		F6V	5.9	6060	4.4	−0.7	1.4	−0.82
4540	β Vir	F9V	3.6	6180	4.2	+0.1	1.6	+0.14
4657		F5V	6.1	5940	4.4	−0.7	1.2	−0.95
4989		F7IV	4.9	6400	4.2	−0.4	1.6	−0.24
5019	61 Vir	G6V	4.7	5580	4.3	+0.2	1.3	−0.03
5338	ι Vir	F6III	4.1	6240	4.0	−0.2	1.9	−0.09
6445	ξ Oph	F1III-IV	4.4	7010	4.2	−0.1	1.9	−0.13
HD22879		F9V	6.7	5920	4.3	−0.9	1.3	−0.85

The abundance analysis is made differentially to the Sun, with oscillator strengths determined from the solar flux spectrum, the reflected light of the Sun being observed with the same instrumentation as the one used for the stars.

Systematic errors in the abundances would result from errors in the effective temperature scale, in the surface gravities and in the microturbulence parameters. We estimate that errors in these fundamental parameters could amount to, at most, 100 K (cf. Saxner and Hammarbäck, 1984), 0.2 dex and 0.2 km/s respectively, leading to errors in the abundances relative to hydrogen smaller than 0.05 dex. One exception is the oxygen abundance which is more temperature and gravity sensitive, since it is mostly neutral – the errors on [O/Fe] may well amount to 0.1 dex. Since our only line of barium is fairly strong, the abundance of this element is also sensitive to the microturbulence parameter – an error of 0.2 km/s corresponds to 0.1 in [Ba/Fe].

In a recent study, based on non-LTE calculations, Saxner (1984) has shown that iron is likely to be overionized in the transparent atmospheres of the metal-deficient F stars. If real, such a tendency should show up as a negative slope in Fig. 3a, unless it is masked by some other systematic error. Only for the most metal-deficient star, signs of an overionization may be seen in Fig. 3; a correction of an isolated iron-overionization effect would move it in the direction of the arrow in Fig. 3a. Further theoretical studies of the O, Na, Mg, Al and Si ionization equilibria in F stars are being planned.

The convection zone in the model atmospheres of F stars reaches rather shallow optical depths, and in real stars, the effects of convection are probably more important than the mixing-length recipe in the calculations indicates. A study of the uncertainties caused by convective energy transport, convective motions and convective inhomogeneities on our results must await detailed numerical simulations, similar to those of Nordlund (1978, 1982) for the Sun. In particular one should note the risk for even more pronounced non-local excitation and ionization as a result of thermal inhomogeneities, especially in metal-poor atmospheres. We hope to include a detailed study on possible errors due to convection in our final paper on the present subject.

Tomkin, Lambert and Balachandran (1984, TLB below) have recently determined abundances of light elements for F stars, and they have two stars in common with the present paper.

The resulting abundances relative to hydrogen differ from those obtained by us by less than 0.06 dex, except for [Na/H] and [Al/H] for HR 4540 which deviate by 0.09 and 0.07, respectively.

Results, Discussion and Conclusions

The results presented here for a small number of stars are preliminary and include data from only four of the five selected wavelength regions. In Fig. 3 values of [X/H] are plotted against [Fe/H] for X = O, Na, Mg, Al, Si, Ca, Ti, Ni and Ba in an attempt to trace possible evolutionary trends in the abundances relative to iron. The tendencies found here for the elements O, Mg, Al, Ca, Ti to be overabundant relative to iron for stars with [Fe/H] < -0.5 confirm the results of TLB for F stars and also agree well with those of Luck and Bond (1984) for more evolved stars. It is of interest to decide whether this increase of [X/Fe] with decreasing [Fe/H] is gradual and starts already at [Fe/H] ~ 0.0 (as suggested by the results of Luck and Bond) or whether it sets in more abruptly around [Fe/H] ~ -0.5 for elements heavier than oxygen. Fig. 3 suggests the latter to be the case for Mg and Fe. Thus, disk abundances with roughly solar abundance ratios relative to iron seem to have been established at a rather early epoch in the evolution of the Galaxy. More observations of stars with [Fe/H] ~ -0.5 are necessary to firmly verify this suggestion, which has bearings on when the IMF of the halo phase changed to the present day IMF and on the importance of infall of gas during the early disk evolution.

The slope found in the relations between [X/Fe] and [Fe/H] (Fig. 3) is clearly decreasing with increasing atomic number; the degree to which this is the case has relevance for estimates of the mass of the supernovae that originally produced these elements. The present result suggests a decrease in the slope δ[X/H] / δ[Fe/H] by about a factor of two when X changes from O to Ca, but observations of more stars are necessary before this number can be adopted and applied in further studies.

The general overabundance of light elements is of importance for stellar evolution calculations, since these elements provide a dominating fraction of the total opacity throughout most of the stellar models. Thus, the Z variable should not be uncritically identified with an overall metal abundance, determined from spectroscopic or photometric measures of, predominantly, spectral lines of the iron-peak elements. It is not yet known whether the modifications resulting when these non-solar abundance ratios are included in stellar evolution studies are vital for evolutionary tracks and estimates of stellar ages.

The two "odd" (by atomic number) elements Na and Al show a less marked overabundance, if any, for the metal-poor disk stars (Fig. 3). Since Mg, in contrast to Fe, is thought to be produced in the same astrophysical regions as Na and Al, we have plotted [Na/Mg] and [Al/Mg] versus [Mg/H] in Fig. 4. Obviously, the more metal-poor stars show a more negative [Na/Mg] value and, probably, also a significantly negative [Al/Mg] value. This odd-even effect was predicted by Arnett (1971) and Truran and Arnett (1971) from calculations of explosive carbon burning, and the effect was expected to be the result of explosions in matter with a small neutron excess, such as in Pop II stars. Here, we have traced the effect also for disk population stars. Explosive nucleosynthesis in metal-rich environments should yield smaller odd-even effects, since in these stars the CNO burning has increased the ^{14}N abundance, which controls the neutron excess. Woosley and Weaver (1982 a, b) have calculated the outcome of explosive C and Ne burning for model Pop I and Pop II supernovae, with solar abundances of heavy elements, and one hundredth

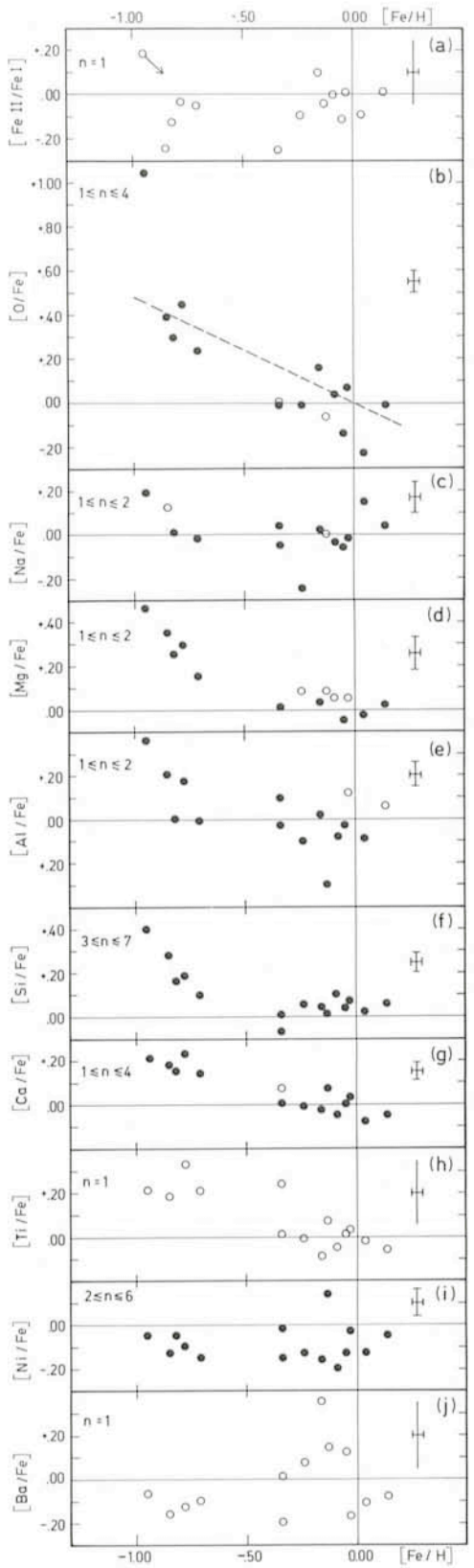

Fig. 3: *Logarithmic abundances relative to the Sun, [X/Fe] = log* $(N_X/N_{FE})_\star - \log(N_X/N_{Fe})_\odot$*, plotted against [Fe/H] in (b)–(j). "n" indicates the number of lines used in each determination. The error bars indicate the mean for all stars of the standard deviations of [X/Fe] and [Fe/H], respectively. Open circles denote stars with n = 1, for which the vertical error bars are not defined. (a) The upper panel displays the ionization balance of iron. If [FeII/FeI] is systematically different from zero this may indicate errors in the fundamental parameters, e.g. the adopted surface gravity, or in the assumption of LTE as discussed in the text. In (b) the dashed line is the relation found for F dwarfs by Clegg et al. (1981).*

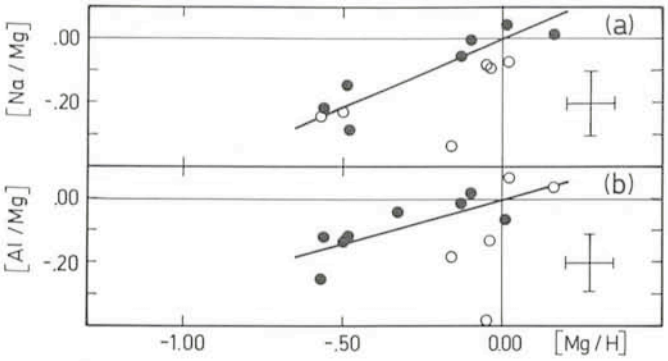

Fig. 4: *(a) Abundance ratio [Na/Mg] as a function of magnesium abundance. The error bar is calculated as in Fig. 3. Open circles denote stars where only one line of either Na or Mg was measured and for which the error bar is not defined. The line is a least squares fit to the points, required to pass through the origin. The points denoted by filled circles were given a weight of two, and those denoted by open circles a weight of one. The slope of the line is [Na/Mg] = (0.43 ± 0.08) · [Mg/H]. (b) [Al/Mg] as a function of [Mg/H]. The symbols are defined in analogy with (a). The slope of the least squares fit is [Al/Mg] = (0.28 ± 0.10) · [Mg/H]. The two panels support the prediction of Arnett (1971) and Truran and Arnett (1971) that elements with odd numbers of nucleons were less abundantly produced relative to even-numbered nuclei in metal-poor stars with low neutron excesses.*

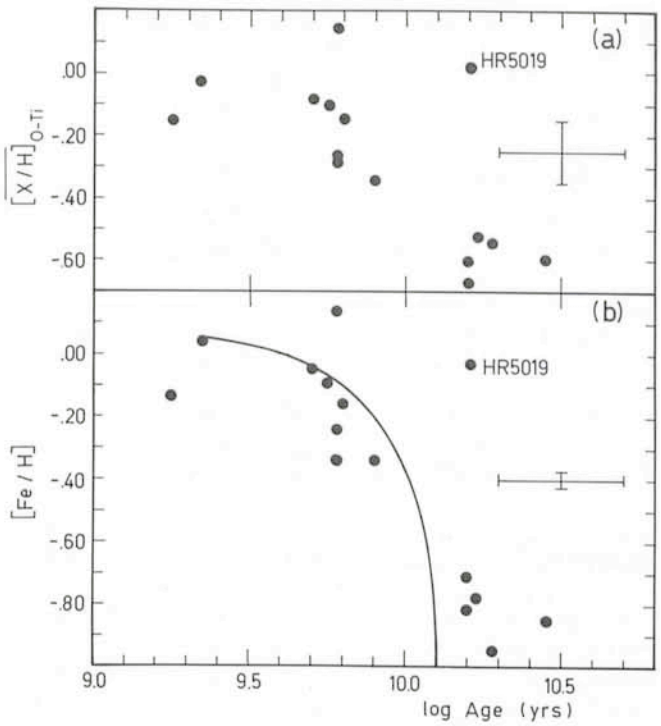

Fig. 5: *Abundances as a function of stellar age, (a) mean value of [X/H] for the "light" elements, X = O, Na, Mg, Al, Si, Ca and Ti; (b) [Fe/H] as a function of age. The curve indicates the time variation of the metal abundance in the solar neighbourhood as derived by Twarog (1980), from uvbyβ photometry of F dwarfs. The position of the star HR 5019 is also indicated.*

thereof, respectively. The slopes in Fig. 4 agree well with these calculations, if we interpolate to intermediate chemical compositions.

The heavy elements represented in the present study, Ni and Ba, seem to follow the iron abundance, with barium, determined from only one Ba II line, showing a relatively large scatter.

In Fig. 3 and 4 the origin denotes the position of the Sun. In all the diagrams it occupies a typical position for stars of similar iron abundances, indicating that the Sun is a typical star as regards its abundance pattern.

The present data are still too meagre to provide a firm basis for studying the build-up of the chemical elements as a function of age in the Galaxy. However, we have tentatively determined ages of the programme stars from the isochrones of Hejlesen (1980). The ages determined from the effective-temperature–luminosity diagrams (using the stellar trigonometric parallaxes for estimating the luminosity) are consistent within 0.2 dex with those obtained from the T_{eff} – log g diagrams (with log g determined photometrically from δc_1). The latter procedure was adopted here. We adopted a value of 2.0 pressure scale-heights for the mixing length, and a value of the hydrogen abundance by mass of X=0.70. The choice of these parameters is not important for the discussion here. We note, however, that a mixing length of 1.5 scale heights should shift the stars to lower ages by typically 0.1 dex. Such a shift would improve the agreement between the Hejlesen solar model and the Sun. The abundances of the lighter elements and the iron-peak elements are plotted as a function of stellar age in Fig. 5a. It is seen that for the present sample of stars the abundances of lighter elements, as well as that of iron and nickel can be represented by monotonic functions decreasing with stellar age. The most noteworthy exception from this is the star HR 5019 (61 Vir). Although this star has a high metal abundance, it is found to be $1.6 \cdot 10^{10}$ years old, both with the photometric method (with δc_1, as a gravity criterion) and the parallax method. It also has a relatively high space velocity, 62 km/s, for being so metal rich. However, this star is significantly cooler than the rest of our stars, and possible systematic errors in the age determinations may affect this star differently as compared with the hotter stars. The star may be worth a closer investigation. The general variation of [Fe/H] with age appears rather consistent with results derived earlier by Twarog (1980) on the basis of uvbyβ photometry for many F dwarfs, see Fig. 5b, in view of the fact that the isochrones used by Twarog were calculated with an assumed mixing length of 1.0 scale heights. When a considerable fraction of the planned sample of stars in the present investigation have been analysed, further conclusions will be possible as regards the age variation of abundances, the uniformity of abundances at any given age in the Galaxy, as well as possible tendencies for star formation to occur in bursts.

ESO Workshop on the Production and Distribution of Carbon, Nitrogen and Oxygen in Stellar Systems

A 3-day workshop to discuss observational and theoretical aspects concerning the presence of carbon, nitrogen and oxygen in stars, clusters and galaxies, will be held at ESO, Garching, 13–15 May, 1985. Contact I. J. Danziger, ESO, for more information.

Acknowledgements

Our thanks are due to the night assistants at La Silla, Señores G. Roman, H. Vega and L. Ramirez, for valuable help during the observations, and to Aina Ekström for drawing the figures 2–5.

References

Ardeberg, A., Lindgren, H. and Nissen, P.E. 1983. *Astron. Astrophys.* **128,** 194.

Arnett, W.D. 1971, *Astrophys. J.* **166,** 153.

Arnett, W.D. 1978, *Astrophys. J.* **219,** 1008.

Clegg, R.E.S., Lambert, D.L. and Tomkin, J. 1981. *Astrophys. J.* **250,** 262.
Gustafsson, B., Bell, R.A., Eriksson, K. and Nordlund, Å. 1975, *Astron. Astrophys.* **42,** 407.
Hejlesen, P.M. 1980, *Astron. Astrophys. Suppl.* **39,** 347.
Luck, R.E. and Bond, H.E. 1984, *Astrophys. J.*, submitted.
Mihalas, D. 1978, Stellar atmospheres, W.A. Freeman & Co., p. 286.
Nissen, P.E. 1981, *Astron. Astrophys.* **97,** 145.
Nissen, P.E. and Gustafsson, B. 1978, Astronomical papers dedicated to Bengt Strömgren, Eds. A. Reiz, T. Andersen, Copenhagen University Observatory, p. 43.
Nordlund, Å. 1978, ibid, p. 95.
Nordlund, Å. 1982, *Astron. Astrophys.* **107,** 1.
Olsen, E.H. 1983, *Astron. Astrophys. Suppl.* **54,** 55.
Saxner, M. 1984, Thesis, Uppsala Astronomical Observatory, and to be submitted to *Astron. Astrophys.*
Saxner, M. and Hammarbäck, G. 1984, submitted to *Astron. Astrophys.*
Tomkin, J., Lambert, D.L. and Balachandran, S. 1984, *Astrophys. J.*, in press. (TLB).
Trimble, V. 1983, *Rev. Mod. Phys.* **55,** 511.
Truran, J.W. and Arnett, W.D. 1971, *Astrophys. Space. Sci.* **11,** 430.
Twarog, B.A. 1980, *Astrophys. J.* **242,** 242.
Twarog, B.A. and Wheeler, J.C. 1982, *Astrophys. J.* **261,** 636.
Woosley, S.E. and Weaver, T.A. 1982a, Essays in nuclear astrophysics, eds. C.A. Barnes, D.D. Clayton, D.N. Schramm, p. 377.
Woosley, S.E. and Weaver, T.A. 1982b, Supernovae: A survey of current research, eds. M.J. Rees and R.J. Stoneham, Reidel, p. 79.

The RPCS Detector

P. R. Christensen, E. Hviid, G. Thomsen, and O. Ulfbeck
Niels Bohr Institute, University of Copenhagen

A one-dimensional dual array linear photon counting device for optical spectroscopy of faint astronomical objects has been developed and tested.

1. Technical Description

The RPCS (**R**eticon **P**hoton **C**ounting **S**ystem) is based on the principles given in its original form by Shectman and Hiltner (1) and utilizes a self-scanning RETICON dual photodiode array model CP 1008 (2 x 936 pixels, each 30 μ x 375 μ). One array is used for the "object", the other for the "sky".

The light amplification system consists of a 3-stage magnetic focused EMI image tube with a UV zinc crown entrance window and a standard S20 photo-cathode followed by a 3-stage electrostatic focused VARO image tube. The output from the EMI tube is optically coupled to the entrance of the VARO tube by an 85 mm f/1 Repro-Nikkor lense.

The light output from the VARO tube is transferred to the diode array through a short fiber-optic.

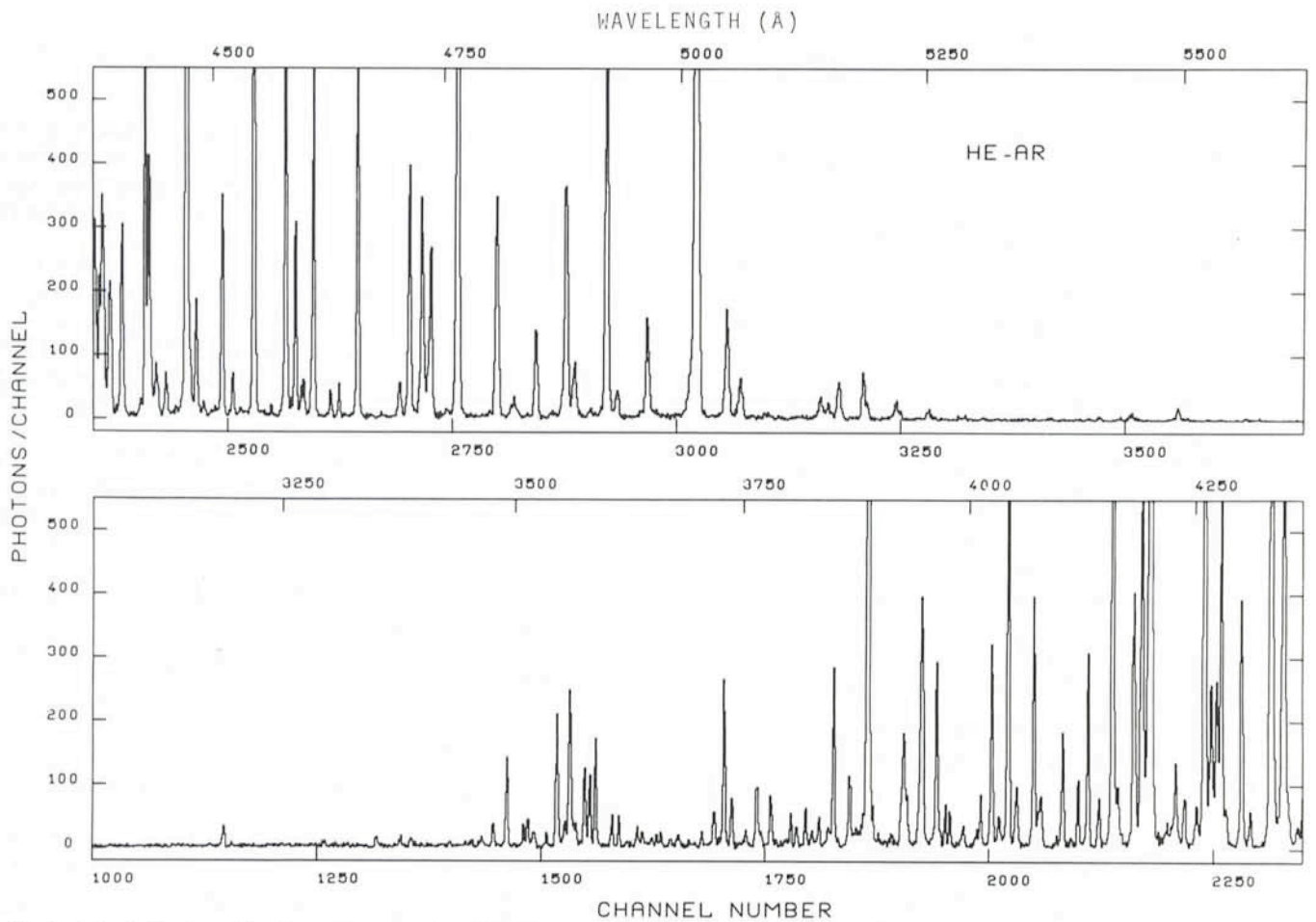

Fig. 1: *A 4 min He-Ar calibration spectrum using a 600 l/mm grating. For details of the measurement, see text. The bottom scale is channel numbers, and each channel is shown. The top scale is the corresponding wavelengths in Å and has been determined by fitting a 3' order polynomial. The ordinate is observed number of photons per channel.*

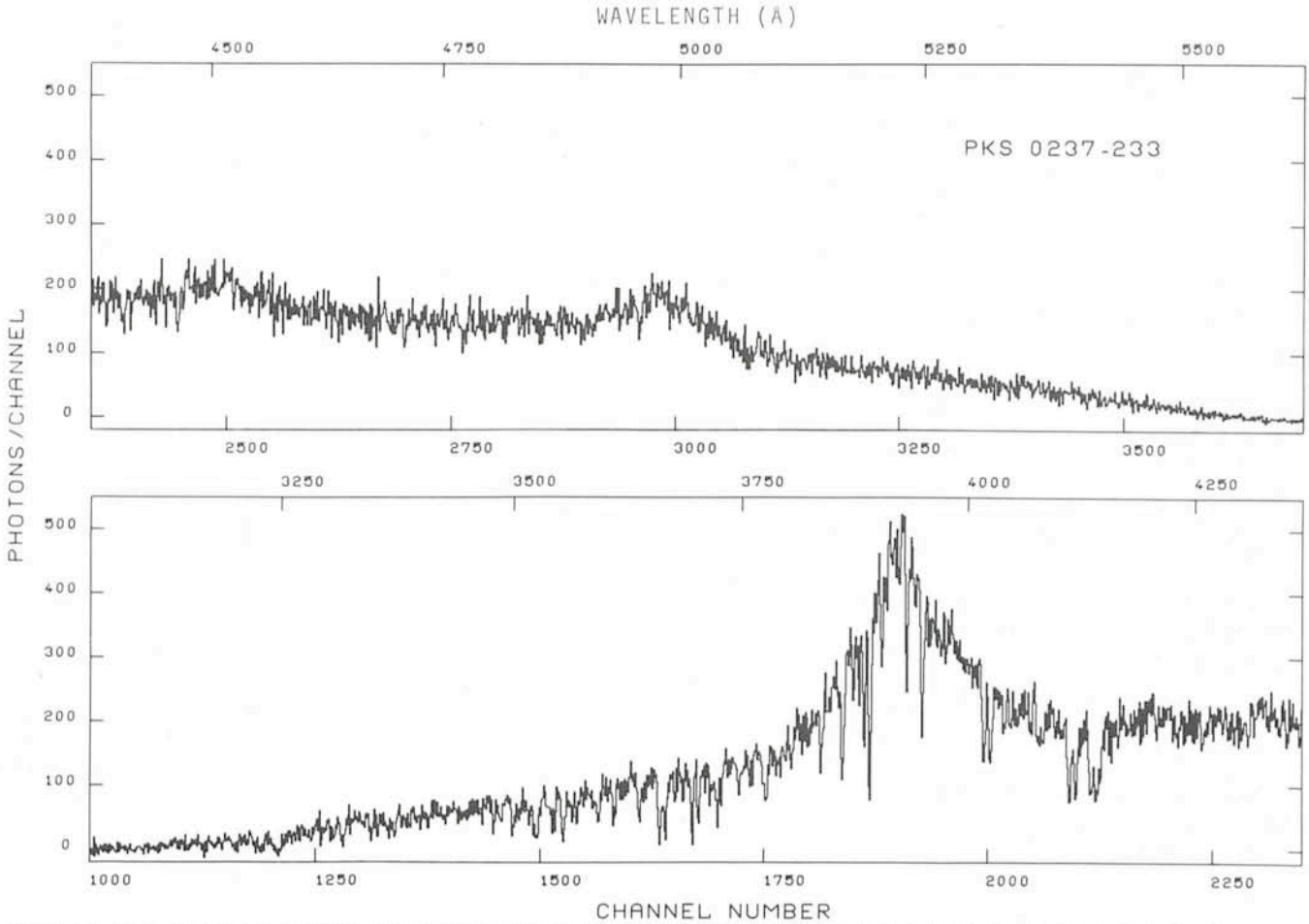

Fig. 2: *A 1 hour exposure of the QSO PKS 0237-233. For details, see text. The calibration is from Fig. 1. The layout is as in Fig. 1.*

The ejection of one photo-electron from the first photocathode (in the EMI tube) results in a "light-spot" on the RETICON array with a diameter (FWHM) $\approx$ 100 μ ($\approx$ 3 pixels) and a time distribution with a rise time of $\approx$ 2.5 msec and a decay time of $\approx$ 10 msec for the first 80 % and a long ($\sim$1 sec) tail for the rest. The total number of photons in this "spot" is of the order of 10^8 photons.

Each diode accumulates photo charge in the interval between successive read-outs of the diode. This period is 3 msec. The basic principle for extraction of the position information from these video-signals is identical to the original idea by Shectman and Hiltner (1), but whereas they essentially use analogue circuits, the present system immediately converts the video signals to digital information, and the information remains digitized.

The system performs a determination of the "light-spot" position (along the diode array) to within 1/4 pixel, which we call a channel, and updates the content of this "address" by one in an external memory.

Each array thus gives rise to 4 x 936 channels (= 3,744 channels) spectra, each channel corresponding to 7.5 μ. For convenience the system is built in such a way that each spectrum is 4k (4,096) channels, with 352 empty channels.

The detector is interfaced with the HP computers at La Silla and is operated through a special segment included in IHAP.

2. Operation and Performance

2.1 Projection

The RPCS detector is used in connection with a Boller and Chivens spectrograph and a Schmidt camera. The projection factor from the entrance slit of the spectrograph to the RETICON array is $\approx$ 6. As the scales for the 3.6 m telescope and the 2.2 m telescope are $\sim$ 140 μ/arcsec and 86 μ/arcsec, respectively, a 1 arcsec slit projects into 23 μ at the 3.6 m telescope and into 14 μ at the 2.2 m telescope.

2.2. Deckers

Two different deckers are available. One is made for the 3.6 m telescope with a set of 2 by 2 arcsec apertures and a set of 4 by 4 arcsec apertures, and one for the 2.2 m telescope, again with a set of 2 by 2 arcsec and 4 by 4 arcsec apertures.

If the "3.6 decker" is used at the 2.2 m telescope, the apertures correspond to 3.3 by 3.3 arcsec and 6.5 by 6.5 arcsec, and if the "2.2 decker" is used at the 3.6 m telescope, the apertures correspond to 1.2 by 1.2 arcsec and 2.4 by 2.4 arcsec.

Due to the fixed distance between the two RETICON diode arrays, the distance between the two decker apertures (corresponding to each array, respectively) is 26.5 arcsec for the 2.2 m telescope and 16.2 arcsec for the 3.6 m telescope.

2.3. Resolution

By narrowing down the slit ($<<$ 1 arcsec) and by careful alignment of the RETICON chip, one can obtain a resolution (FWHM) of $\approx$ 1.5–1.8 channels over approximately half the detector length, and somewhat less ($\sim$ 2.5–3.5 channels) outside this range. This degrading may be due to optical limitations in the B & C spectrograph.

The resolution to be obtained in an actual observation, where it is necessary to open up the slit in order to get enough

light, is essentially determined by the slit width. A slit width of 1 arcsec corresponds to a resolution of ≈ 3.4 channels (≈ 25 μ) at the 3.6 m telescope, and ≈ 2.5 channels (≈ 19 μ) at the 2.2 m telescope.

Fig. 1 shows a He-Ar calibration spectrum using ESO grating No. 7 (600 groves/mm, 114 Å/mm) blazed at 7°30′. The apertures were ~ 1.0 arcsec (slit) by 3.3 arcsec (decker). The spectrum is a sum of 4 spectra, each integrated for 60 sec. Two of the spectra, one from each array, were recorded before a 1 hour measurement at the 2.2 telescope of the QSO PKS 0237-233, and two, also from each array, after the measurement. The resolution is ≃ 2.8 channels (≈ 2.8 Å) in the central region of the detector.

Fig. 2 shows the recorded spectrum of the QSO PKS 0237-233. It is a sum of 6 integrations each 10 min long. The object was switched between the two arrays after each integration. The sky has been subtracted. The spectrum compares well with a similar spectrum of PKS 0237-233 obtained by Young and Sargent (2).

Flexure and drift is not a very serious problem. Actual observations at the 2.2 m telescope show very little drift (≤ 1 channel) during a night, and flexure ≤ 1 channel for positions within 3 hours of the median.

2.4. Dark Current

The EMI tube is presently operated at 8° C, and at this temperature the thermic emission from the first photocathode results in a count rate of 2.4 x 10^{-3} counts/sec/channel in the central region of the detector, and falling off towards the ends.

2.5. Count Rate

Due to the slow component of the VARO exit phosphor and a limited dynamic range of the electronic system, together with some special "shadowing effects" in the optical amplification system, there are some restrictions on the count rate which can be tolerated in order not to distort the spectra. The maximum count rate is 1.2 counts/sec/channel in "any extended region" of the spectra. If one exceeds that, irregular patterns and "cross-talk" can show up in the spectra. The term "any extended region" is to be understood in such a way that if the count rate exceeds the maximum count rate in only very few and very narrow emission lines, only very narrow regions around the emission peaks are distorted, the rest of the spectrum being undistorted.

2.6 Sensitivity

The sensitivity has been determined by observing white dwarfs calibrated by Oke (3). Fig. 3 shows a RPCS spectrum of the DB EG 149 obtained at the 2.2 m telescope. The spectrum is a sum of 2 integrations, one in each array and both 5 minutes long. The sky background has been subtracted and the spectrum flat field corrected. The apertures were 2 arcsec (slit) by 4 arcsec (decker), and the grating was the ESO No. 7 (600 groves/mm), 114 Å/mm) blazed at 7°30′.

The relative photon sensitivity for this configuration is shown in Fig. 4. A sensitivity curve for a 300 groves/mm grating (224 Å/mm, ESO No. 2), blazed at 4°15′ is shown in Fig. 5. Both curves are based on observations of the white dwarf HZ 4 (3).

The count rate to be observed for a given object is dependent on the seeing and the aperture size, and also the efficiency of different gratings may be different. Absolute sensitivity measurements have been performed at the 2.2 m telescope on nights with good seeing (≤ 1 arcsec) and using apertures of 3.3 arcsec by 3.3 arcsec with the two above-mentioned gratings. The results correspond to 1 detected photon/Å/sec for a star of magnitude 14.5 at the peak wave length (see Figs. 4 and 5). The equivalent magnitude at the 3.6 m telescope would be 15.6.

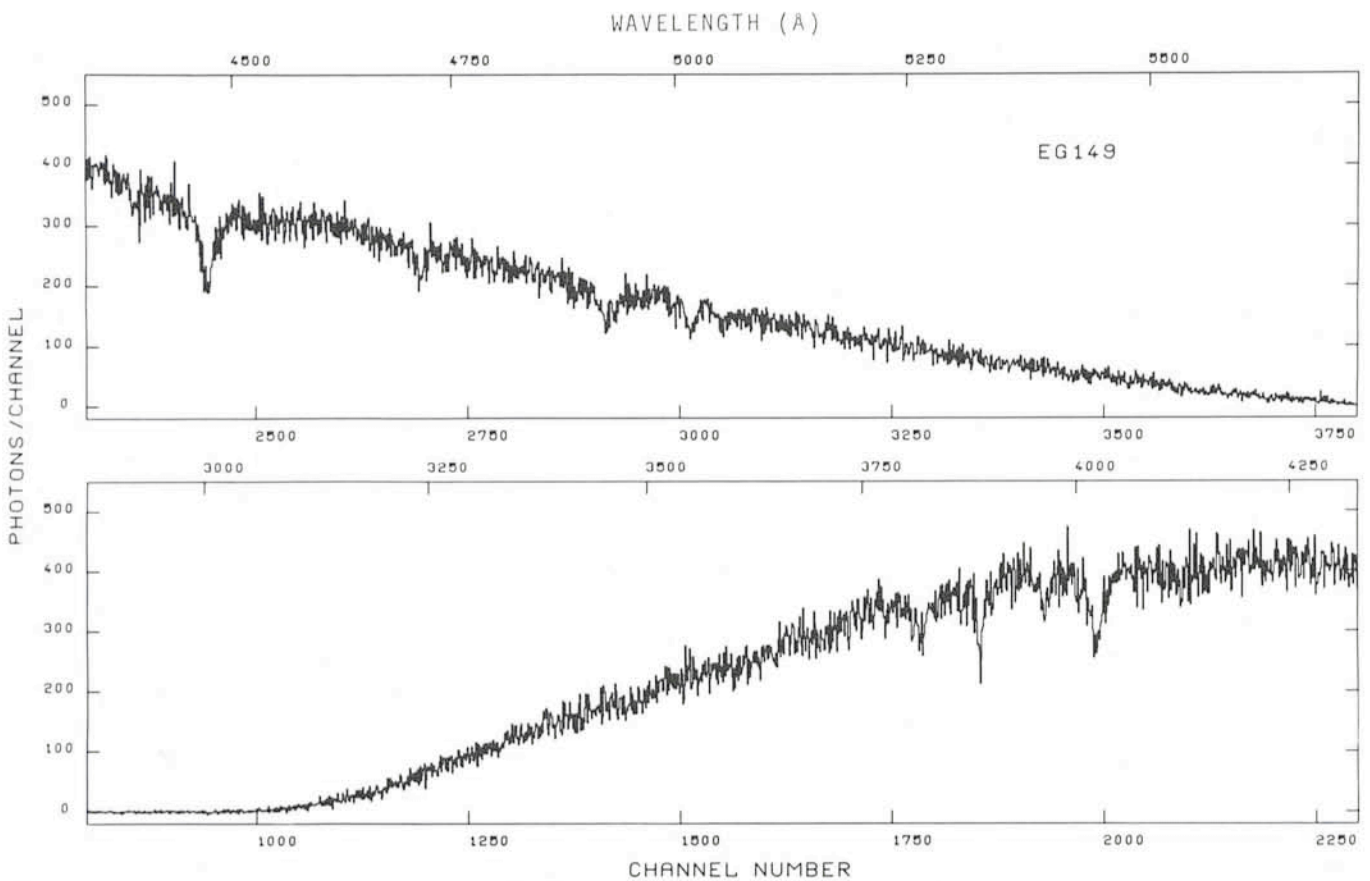

Fig. 3: *A 10-min exposure of the white dwarf EG 149. For details, see text. The layout is as in Fig. 1.*

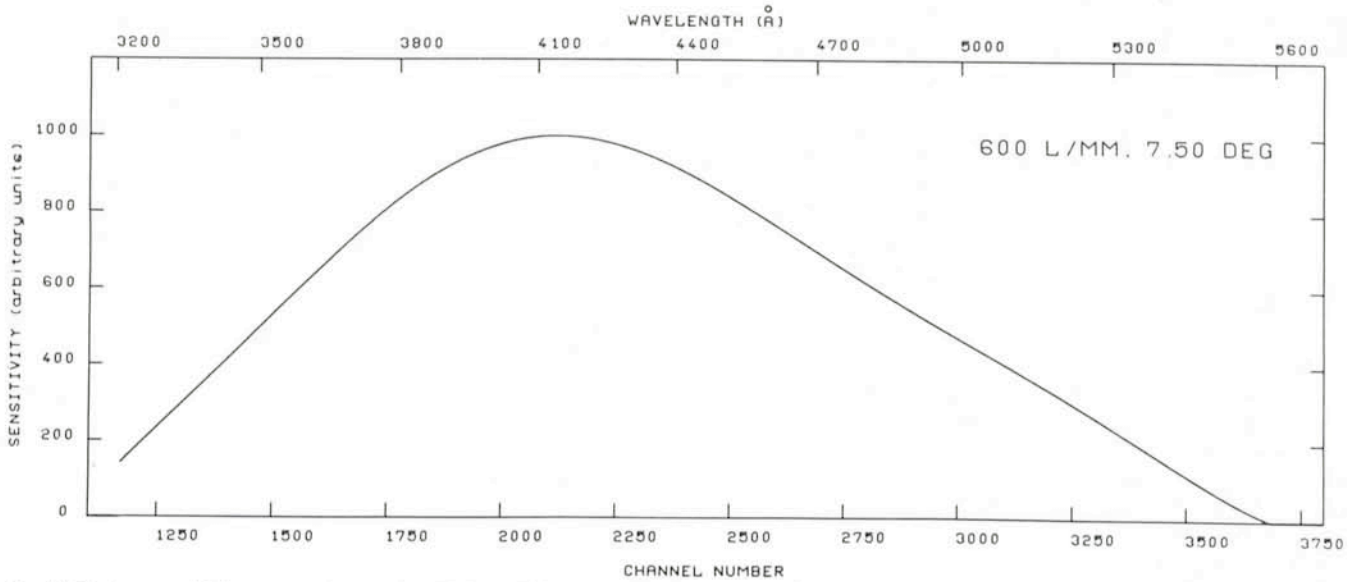

Fig. 4: *Photon-sensitivity curve using grating ESO no. 7 blazed at 7 °30′. For details, see text. The curve was arbitrarily normalized to 1 000 at the maximum.*

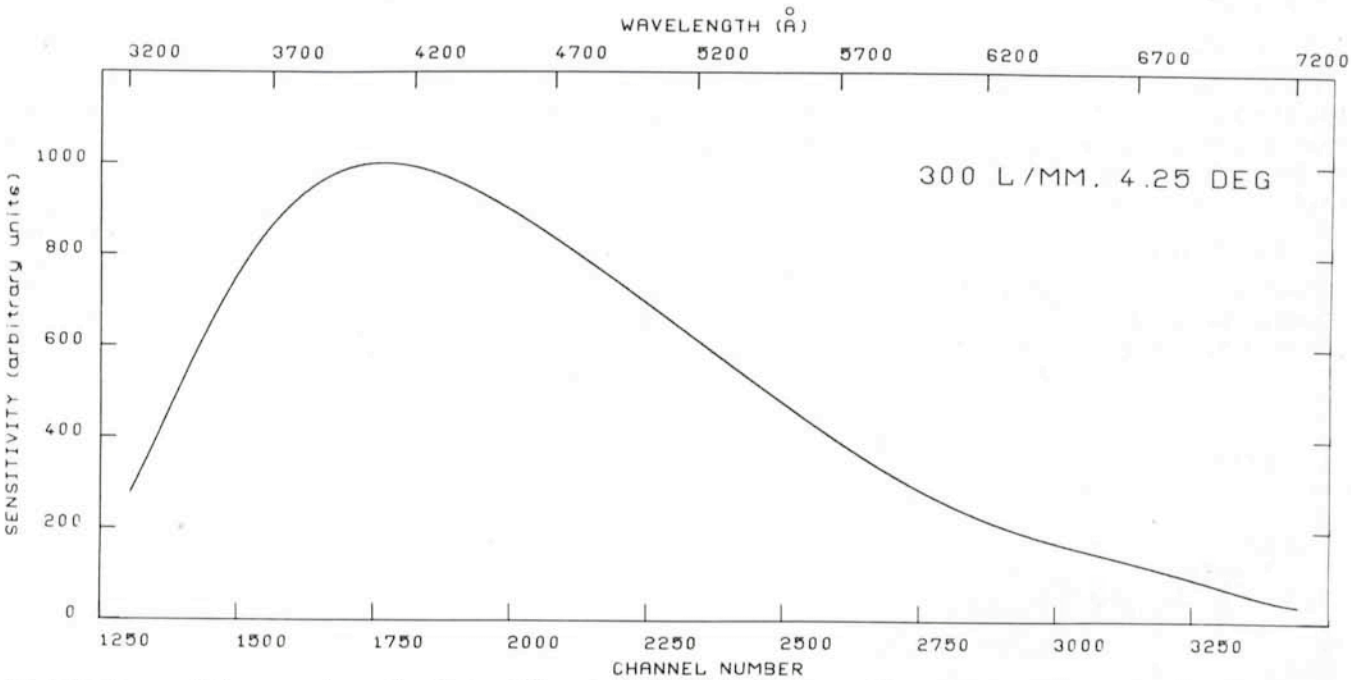

Fig. 5: *Photon-sensitivity curve using grating ESO no. 2 blazed at 4°15′. For details, see text. The curve was arbitrarily normalized to 1 000 at the maximum.*

2.7. Spectrum Pattern

Due to the methods used in the RPCS detector to determine the centre of the light spot to 1/4 of a pixel and to the fact that the odd and even pixels (in each array) are read out by different video-amplifiers, the spectra will show a pattern which repeats itself every eighth channel. The pattern can be interpreted as differences of channel-widths within each 8 channels, corresponding to one odd pixel and one even pixel. A FORTRAN programme, called COR8, which determines the pattern by averaging over the whole spectrum and subsequently transforms it to a spectrum with channels of equal widths, is available at the La Silla VAX 750. The spectra shown in Figs. 2 and 3 have been corrected using this programme.

3. Acknowledgement

The authors gratefully acknowledge the excellent support from the La Silla technical support group and from Martin Cullum, Garching. Very valuable information and diagrams concerning the delicate preamplifier circuits from John Geary, Center for Astrophysics, Mass., as well as preliminary guidance by S.A. Shectman, Caltech, are gratefully acknowledged. We also wish to thank J.H. Bjerregaard, O.B. Rasmussen, O. Christensen and N.J.S. Hansen for their contribution in designing the mechanical and electronic parts. The project was made possible by financial support from the Danish Natural Science Research Foundation and from ESO.

References

(1) S.A. Shectman and W.A. Hiltner, *P.A.S.P.* **88** (1976), 960.
(2) P. Young and W.L.W. Sargent, *Astrophysical Journal Suppl. Series* **48** (1982), 455.
(3) J.B. Oke, *Astrophysical Journal Suppl. Series* **27** (1974) 21.

ESO Photographer Finds New Celestial Object

The production of copies for the ESO/SRC Atlas of the Southern Sky is proceeding at the ESO Sky Atlas Laboratory in Garching. For this atlas 606 blue sensitive plates have been exposed at the UK Schmidt telescopes in Coonabarabran, Australia, and corresponding red sensitive plates are being made with the ESO Schmidt telescope at La Silla, Chile.

The atlas is similar to the Palomar Atlas, which was produced in the 1950s, but it utilizes new materials, resulting in the limiting magnitude being approximately 2 magnitudes fainter than that of the Palomar Sky Survey.

One of the major virtues of the ESO/SRC Atlas of the Southern Sky is that great attention is being paid to the fidelity of the film and glass copies. Much time goes into checking the final product. When it is sent to the more than 200 customers all over the world, it has as few defects as is humanly possible. The photographers at the ESO Sky Atlas Laboratory who are involved in the production of this Atlas spend a substantial part of their time checking the original plates and the copies under microscope.

During this quality control, an ESO photographer, Herbert Zodet, noted a faint patch on a film copy of the field 135 on an ESO red plate. He noticed that there was no corresponding object on the blue plate and suspected a plate fault. However, after further checking it appeared that the object might be real, and he informed one of the ESO astronomers about his discovery. And indeed, there is now little doubt that Mr. Zodet found a hitherto unknown planetary nebula in the Milky Way.

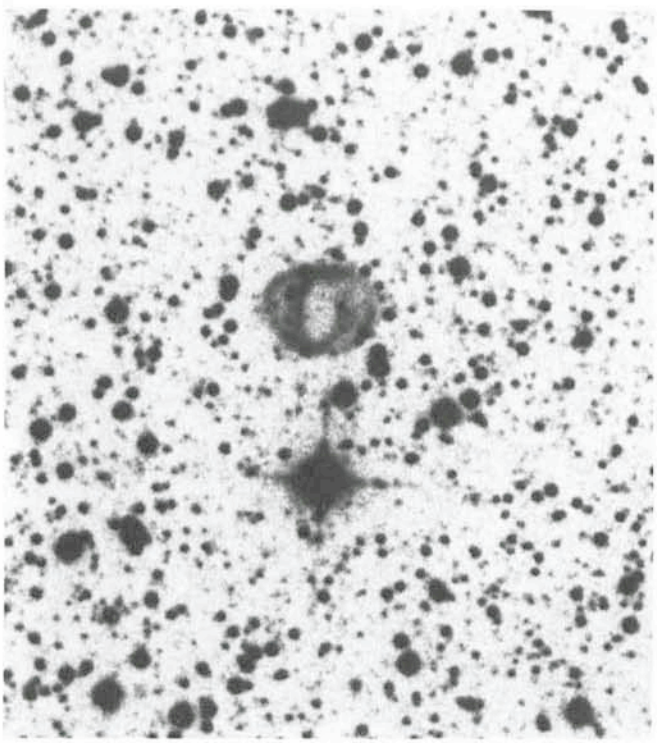

Enhanced image of "Zodet's planetary". Diameter 20".

As can be seen on the picture, it has a double ring structure and, as is sometimes the case in such objects, no central exciting star can be seen neither on the blue nor on the red survey plate. The object, which is located at 15 h 05 m −61° 5, has now been given the designation ESO 135 −PN4. Andris Lauberts has measured the object and assigns B magnitude 17.5 and B−R = 4.2.

Despite its very official name, the object is now better known as "Zodet's planetary" by the staff at ESO Garching.

R. M. West

Nova Sagittarii 1984

On September 26, 1984, W. Liller discovered a possible nova in Sagittarius; the apparent V magnitude was 11.0 (IAU Circ. No. 3995). A prediscovery image was found at magnitude pgm = 13.1 on a plate taken on September 22 at the Maria Mitchell Observatory (IAU Circ. No. 3997). On the evening of October 4, we were observing at La Silla, with the 2.2 m telescope, the Boller and Chivens spectrograph with a grating giving a resolution of 3 Å in the spectral range λλ 6100–7100 Å, and with an RCA CCD detector. The sky was partly cloudy and the seeing rather poor. We took a 10-min exposure of Liller's object. The spectrum shows an extremely strong and broad (FWHM ~2,200 km s^{-1}; total width >3,100 km s^{-1}) Hα emission line as shown on Fig. 1 (the vertical line indicates the rest wavelength of Hα), confirming that this is indeed a nova (IAU Circ. No. 3998).

M.-P. Véron-Cetty and P. Véron

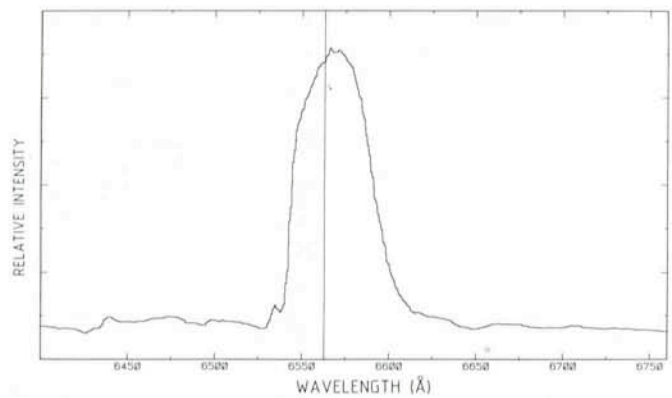

Fig. 1.

List of Preprints Published at ESO Scientific Group

September – November 1984

340. P. Véron and M.-P. Véron-Cetty: Star Formation in Early-Type Galaxies. *Astronomy and Astrophysics.* September 1984.
341. P. Véron, M.-P. Véron-Cetty and M. Tarenghi: The Ultraviolet Absorption Spectrum of NGC 4151. *Astronomy and Astrophysics.* September 1984.
342. G. Contopoulos: Nonlinear Problems in Stellar Dynamics. Proceedings of "ELAF 84". September 1984.
343. R. H. Miller: Flyby: Numerical Experiments on a Galaxy Orbiting Within a Galaxy Cluster. *Astronomy and Astrophysics.* September 1984.
344. P. A. Shaver and J. G. Robertson: The Close QSO Pair Q 1548 + 114A, B. *Monthly Notices of the Royal Astronomical Society.* October 1984.
345. M. Azzopardi, J. Lequeux and B. E. Westerlund: New Carbon Stars in Spheroidal Galaxies: I. Sculptor, Carina, Leo I and Leo II Systems. *Astronomy and Astrophysics.* October 1984.
346. R. E. de Souza, G. Vettolani and G. Chincarini: The Flattening Distribution of Lenticular Galaxies. *Astronomy and Astrophysics.* October 1984.

347. M. Iye and O.-G. Richter: Reddening of Globular Clusters in M31. *Astronomy and Astrophysics.* October 1984.
348. J. Andersen, B. Nordström, A. Ardeberg, W. Benz, M. Imbert, H. Lindgren, N. Martin, E. Maurice, M. Mayor and L. Prévot: Radial Velocities of Southern Stars with the Photoelectric Scanner CORAVEL. III. 790 Late-type Bright Stars. *Astronomy and Astrophysics.* October 1984.
349. A. F. M. Moorwood: Galaxy Photometry in the Infrared. Invited review to appear in the Proceedings of "New Aspects of Galaxy Photometry" (Springer Verlag, "Lectures in Physics" series, ed. J.-L. Nieto): Specialized Colloquium at the Eighth IAU Regional European Meeting, Toulouse, Sept. 1984. October 1984.
350. L. Binette: Photoionisation Models for LINERs: Gas Distribution and Abundances. *Astronomy and Astrophysics.* November 1984.
351. F. Matteucci: Possible Scenarios for the [O/Fe] Ratio in Metal-Poor Stars. To appear in the Proceedings of the Frascati Workshop 1984: "Population II Variables" – *Mem. Soc. Astron. It.* November 1984.
352. G. Vettolani, R. E. de Souza, B. Marano and G. Chincarini: The Distribution of Voids. *Astronomy and Astrophysics.* November 1984.
353. N. Brosch, J. Mayo Greenberg and P. J. Grosbøl: Extragalactic Dust I: NGC 7070A. *Astronomy and Astrophysics.* November 1984.
354. E. M. Sadler and O. E. Gerhard: Dust in Elliptical Galaxies – How Often, How Much? To be published in the Proceedings of "New Aspects of Galaxy Photometry" (Springer Verlag, "Lectures in Physics" series, ed. J.-L. Nieto): Specialized Colloquium at the Eighth IAU Regional European Meeting, Toulouse, Sept. 1984. November 1984.

Departure of Dr. Inge Meinen

Dr. Meinen was employed as Administrator in Chile from 1 April 1975 to 31 August 1984, in which capacity she was responsible for the local administration of the ESO facilities in Chile, i.e. the Observatory on La Silla, office and lodging facilities in La Serena, and the office and Guesthouse in Santiago.

With her excellent linguistic abilities (German, English, French, Spanish) and an exceptional commitment and loyalty Dr. Meinen fulfilled her tasks to the great satisfaction of the Organization.

Her departure, due to health reasons, was very much regretted. We wish her all the best for the future.

VACANCY NOTICE

No. CAS1–10; Grade: 8/9; Code: 109

Astronomer

Education: University degree in astronomy or physics.

Experience and knowledge: Several years of experience in observational astronomical research with emphasis on spectroscopy.

Assignment: Tasks include: (1) Responsibility for the proper functioning of various instruments on La Silla; (2) assisting visiting astronomers in the use of the Observatory facilities; (3) scientific research related to the Observatory activities.

Duty station: La Silla Observatory, Chile. A minimum of 150 days and nights have to be spent at La Silla per year.

Place of residence: La Serena, Chile.

Remuneration: The remuneration will depend on background and family status. For a married non-resident member of the personnel the net tax-free remuneration after deductions for pension and health insurance will not be less than DM 6,200 monthly.

Applications should be submitted **before February 15, 1985.** Application forms and additional information may be obtained from ESO, Personnel Services, Karl-Schwarzschild-Straße 2, D-8046 Garching b. München, Federal Republic of Germany.

PERSONNEL MOVEMENTS

(September – November 1984)

Arrivals

Europe

LUCY, Leon (GB), Astronomer
ZAGO, Lorenzo (I), Engineer/Physicist
VAN MOORSEL, Gustaaf (NL), Scientific Programmer/Analyst, ST/ECF
GATHIER, Roelof (NL), Fellow
DEFERT, Philippe (B), Fellow, ST/ECF

Chile

MONDEREN, Peter (B), Student

Transfers

CRISTIANI, Stefano (I), to Astronomer, Chile
BAADE, Dietrich (D), to Associate ST/ECF
ROSA, Michael (D), to (ESA) staff ST/ECF

ALGUNOS RESUMENES

Visitas del STC a posibles lugares para ubicar el VLT en el Norte de Chile

D. Enard, ESO

El STC (Comité Científico y Técnico) se reunió en La Silla los días 8 y 9 de Octubre. Después de la reunión los miembros del STC emprendieron un viaje de tres días al Norte de Chile para conocer algunos lugares escogidos como potencialmente interesantes por A. Ardeberg durante su estudio exploratorio de 1983/84.

Uno de los lugares más prometedores es Cerro Paranal, ubicado a unos 150 km al sur de Antofagasta y a 15 km de la costa. La altura es de 2.650 m. Este lugar es atractivo debido a su relativamente fácil acceso, su sequedad y calidad fotométrica. Se espera que debido a su proximidad a la costa la atmósfera sea poco perturbada por montañas cercanas, y que, consecuentemente, la visibilidad sea excelente. Como fue notado por algunos miembros del STC el lugar es relativamente angosto, y aunque el espacio disponible sería suficiente para el VLT, habrían muy pocas posibilidades para ubicar otros telescopios. Sin embargo, podrían usarse otras cimas en la vecindad.

También fue visitado otro monte cercano, el cerro Amazonas, con una altura de 3.100 m. Es bastante más extenso pero unos 22 km más hacia el interior que Paranal; podría no prestarse tan bien como Paranal, pero sólo una comparación objetiva podría verificar ésto.

La región cercana a la frontera boliviana, al noroeste de San Pedro de Atacama, es rica en altos volcanes; los valientes miembros del STC cabalgaron durante 3 horas desde San Pedro hacia uno de los pocos volcanes accesibles, el Apagado, a una altura de 5.650 m. Como muestra la fotografía en la pag. 1, (algunos) miembros del STC aun se sentían muy bien, aunque a esa altura ya se notaba cualquier pequeño esfuerzo. Probablemente sería muy aventurero ubicar un observatorio a tal altura, y persiste el problema fundamental que es determinar la calidad de un lugar así con respecto a La Silla y otros tan excelentes como el Mauna Kea.

Hay muchos lugares en Chile que con alturas de aproximadamente 4.000 m ofrecen un buen compromiso entre el deseo de subir a la mayor altura posible y a la vez cumplir con condiciones de trabajo aceptables.

ESO, the European Southern Observatory, was created in 1962 to . . . establish and operate an astronomical observatory in the southern hemisphere, equipped with powerful instruments, with the aim of furthering and organizing collaboration in astronomy . . . It is supported by eight countries: Belgium, Denmark, France, the Federal Republic of Germany, Italy, the Netherlands, Sweden and Switzerland. It operates the La Silla observatory in the Atacama desert, 600 km north of Santiago de Chile, at 2,400 m altitude, where thirteen telescopes with apertures up to 3.6 m are presently in operation. The astronomical observations on La Silla are carried out by visiting astronomers – mainly from the member countries – and, to some extent, by ESO staff astronomers, often in collaboration with the former. The ESO Headquarters in Europe are located in Garching, near Munich.
ESO has about 120 international staff members in Europe and Chile and about 120 local staff members in Santiago and on La Silla. In addition, there are a number of fellows and scientific associates.

The ESO MESSENGER is published four times a year: in March, June, September and December. It is distributed free to ESO personnel and others interested in astronomy.
The text of any article may be reprinted if credit is given to ESO. Copies of most illustrations are available to editors without charge.

Editor: Philippe Véron
Technical editor: Kurt Kjär

EUROPEAN
SOUTHERN OBSERVATORY
Karl-Schwarzschild-Str. 2
D-8046 Garching b. München
Fed. Rep. of Germany
Tel. (089) 32006-0
Telex 5-28282-0 eo d

Printed by Universitätsdruckerei
Dr. C. Wolf & Sohn
Heidemannstraße 166
8000 München 45
Fed. Rep. of Germany

ISSN 0722-6691

La experiencia en Hawai muestra que 4.200 m son aun aceptables desde el punto de vista humano. Lugares así pueden encontrarse en las cercanías de altos volcanes, en la cadena central al occidente de San Pedro y al este de La Silla. Ninguna de aquellas montañas se presenta completamente aislada y su acceso es bastante difícil, pero debería prestárseles atención, especialmente si los lugares menos elevados se presentaran inadecuados ya sea desde el punto de vista de visibilidad o humedad.

Luego de completar la fase inicial del estudio exploratorio hecho por Arne Ardeberg se definirá un programa de investigatión a mayor escala.

Fue designado un grupo de trabajo compuesto por expertos europeos que darán recomendaciones. Ya fueron instaladas estaciones meteorológicas automáticas en Paranal y La Silla; una tercera estación será instalada en un lugar a gran altura en Diciembre. Proporcionarán datos fácilmente procesables que complementarán aquellos ya coleccionados desde Septiembre de 1983. Un balón fijo también permitirá medir las turbulencias y otros parámetros meteorológicos entre 0 y 800 metros sobre las superficies de los lugares. Este equipo es fácilmente transportable y debería permitir una investigación preliminar de las condiciones locales de visibilidad. Equipos más permanentes tales como sensores termales rápidos, radares acústicos y monitores de visibilidad, están previstos para Paranal en 1985 (y en La Silla para permitir a una calibración absoluta con los telescopios existentes).

La importancia de la visibilidad para los nuevos proyectos de los grandes telescopios como también la perspectiva de mejorar la calidad de imágenes a través de correcciones adaptables han fomentado los considerables esfuerzos hechos por varios grupos para lograr entender mejor las causas de las deterioraciones de la visibilidad, y posiblemente encontrar remedios. A pesar de la dificultad de comparar cuantitativamente resultados obtenidos por diferentes métodos en diferentes lugares, se espera que dentro de 2 a 3 años se pueda llegar a un acuerdo sobre algunas preguntas vitales como per ej. "¿qué hace un lugar ser verdaderamente adecuado?", o "¿cuán importante es ubicar un telescopio en un lugar a gran altura?". Por cierto que estas preguntas son de gran importancia para el VLT de ESO.

Término de las actividades de la Sra. Dr. Inge Meinen

La Sra. Meinen estuvo empleada como administradora en Chile desde el 1° de Abril de 1975 hasta el 31 de Agosto de 1984, siendo responsable por la administración local de los servicios de ESO en Chile, siendo éstos el Observatorio en La Silla, oficina y casas para los empleados en La Serena, como también oficinas y Casa de Huéspedes en Santiago.

Con sus excelentes habilidades linguísticas (alemán, inglés, francés, castellano) y su excepcional dedicación y lealtad la Sra. Meinen cumplió sus tareas a la entera satisfacción de la Organización.

El término de sus actividades, debido a razones de salud, fue muy lamentado. Le deseamos todo lo mejor para el futuro.

Contents